Montana State University

Task Report 1-Literature Review

Development of *p-y* Curves for Analysis of Laterally Loaded Piles in Montana

By:

Shahriar Khorami, PhD Student

Mohammad Khosravi, Assistant Professor

Prepared for:

Montana Department of Transportation

August 1st, 2023

TABLE OF CONTENTS

LIST OF FIGURES

LIST OF TABLES

CHAPTER 1: INTRODUCTION

Problem Statement

The response of a laterally loaded pile depends on the lateral stiffness of the soil, the pile stiffness, and the interaction between the pile and the surrounding soil. A laterally loaded pile can be analyzed using different methods; among which, the *p-y* method, a method of intermediate complexity and reasonable accuracy, has been widely accepted by the geotechnical engineering community. In the *p-y* method, the soil reaction is replaced with a series of independent nonlinear springs, and the nonlinear behavior of the soil is represented by the *p-y* curves and relating the soil reaction and pile deflection at points along the pile length. The *p-y* curves are developed based on a relatively small amount of data in specific soil conditions; therefore, their accuracy depends on the data from which the curve was developed which may or may not correlate well with soils in Montana. Consequently, the applicability of these procedures to different soil conditions is uncertain and may lead to unconservative or overconservative designs.

Background and Significance of Work

Pile foundations supporting highway bridges are subjected to lateral loads as well as vertical, gravity loads. Thus, both lateral and vertical loads must be considered in the design of the pile to prevent failure or excessive lateral deflections.

There are several approaches for evaluating pile response to lateral loading, varying from the simplest, limit equilibrium approach, to more complicated ones such as finite element analysis in continuum approach. The lateral response of a pile depends on multiple factors, such as pile-head fixity, pile shape and stiffness, and soil reaction to horizontal deflection. Therefore, the design method for laterally loaded piles should be sophisticated enough to account for all aspects, and not too complicated to be applicable to engineering problems.

Among all the methods, the discrete load transfer method, or *p-y* curve analysis, has been accepted as an accurate and reliable method to evaluate the response of a single pile subjected to lateral loads. As shown in Figure 1, the nonlinear reaction of the soil along the depth of the pile is modeled using a series of nonlinear discrete springs, called the *p-y* curves (McClelland & Focht, 1956). *p-y* curves for a soil-pile system can be developed using different methods. Studies have been developing *p-y* curve using full-scale field tests on instrumented piles (Matlock, 1970; Reese et al., 1974, 1975; Reese & Welch, 1975), laboratory-scale centrifuge tests (Barton et al., 1983; Brandenberg et al., 2013; Choo & Kim, 2016; Haouari & Bouafia, 2020; Lee et al., 2019), in-situ tests (Ariannia, 2015; Briaud et al., 1983; Li et al., 2018; Robertson et al., 1989), and numerical simulations (Brandenberg et al., 2013; Brown & Shie, 1990; Choobbasti & Zahmatkesh, 2016; G. Yu et al., 2019).

While there are several studies pertaining to *p-y* curve analysis of laterally loaded piles that will be beneficial in the development of this study, there is a lack of information on the applicability of existing *p-y* curve criteria to Montana soil conditions. The proposed research project will investigate the applicability of the available *p-y* curves to soil conditions encountered in Montana. The results from a series of model-scale, instrumented centrifuge experiments on piles embedded in prioritized soils

collected from different regions of Montana are coupled with numerical simulations to understand the behavior of a single pile laterally loaded in different prioritized soil conditions. The results will be used to develop *p-y* curves for analysis of laterally loaded piles in Montana.

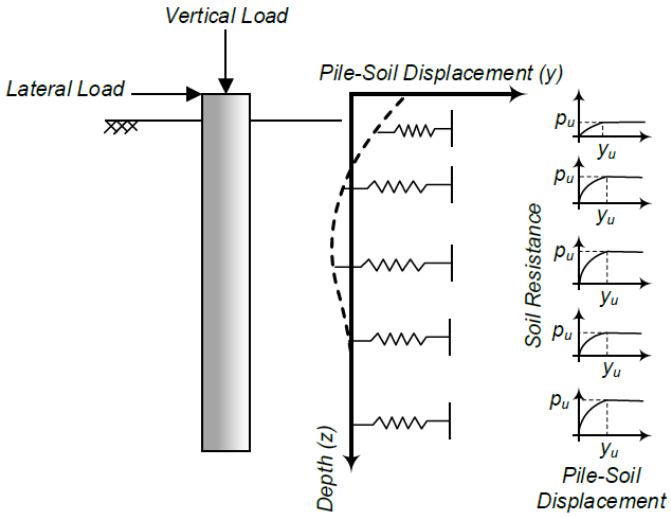

Figure 1. p-y curve analysis

Objectives

The general purpose of the research proposed here is to identify available methods for the development of *p-y* curves and to evaluate their applicability to soil conditions encountered in Montana. The results of this research lead to more accurate prediction of pile response and less conservative design of pile foundation and improve the economy of pile foundations without compromising safety. The research proposed here will be accomplished with the following steps: 1) review the current methods for analysis of laterally loaded piles, from the most common methods (e.g., *p-y* method) to the most complex; 2) review and prioritize soil conditions in Montana for which laterally loaded pile behavior is not well known, and evaluate the applicability of *p-y* curves to Montana soil conditions; 3) perform a series of model-scale, instrumented centrifuge experiments on piles embedded in prioritized soils collected from different regions of Montana in the centrifuge facility at the University of New Hampshire to develop a data set capable of gaining insight into the characteristics of *p-y* resistance in Montana soil conditions; 4) couple the experimental results with numerical simulations to understand the behavior of a single pile laterally loaded in different prioritized soil conditions and develop *p-y* curves for analysis of laterally loaded piles in Montana; 5) use the findings from previous tasks in this research to re-evaluate the performance of a laterally loaded pile from a project site located on Interstate 15 in Lewis and Clark County, MT and validate the findings of the new research.

Research Plan

The progress of this research can be divided into six main steps:

1. A comprehensive literature review and classification of all current design methods for laterally loaded piles.
2. Review and prioritization of soil conditions in Montana for which laterally loaded pile behavior is not well known and evaluation of the applicability of *p-y* curves to Montana soil conditions.
3. Development of a data set of soil characteristics by conducting a series of model-scale centrifuge experiments on embedded pile in prioritized soils.
4. Coupling the experimental results with numerical analysis to understand the behavior of a single pile laterally loaded in different prioritized soil conditions and development of *p-y* curves for analysis the laterally loaded piles in Montana.
5. Development of a framework, based on the results of previous steps, to predict *p-y* curves for prioritized soil conditions.
6. Validation of the framework with laterally loaded pile data in Montana.

CHAPTER 2: DESIGN METHODS FOR LATERALLY LOADED PILES

Introduction

Pile foundations supporting highway bridges and offshore structures experience bending moments, lateral loads, and axial loads. The analysis of laterally loaded piles involves the interactions between the soil and the pile. This means that the pattern and magnitude of pile deflections depend on the characteristics of surrounding soil, and the soil reaction along the pile is affected by the pile's properties, such as head restraint, flexural rigidity, and installation method. The behavior of laterally loaded piles is significantly influenced by certain key soil characteristics, including elastic modulus, bearing capacity, and stress-strain curve. These characteristics are influenced by various soil parameters, such as the internal friction angle, state parameter, undrained shear strength, Poisson's ratio, etc.

Table 1 provides a summary of the design methods for laterally loaded piles in technical literature, along with their respective advantages and limitations. As summarized in Table 1, these methods are divided into four main categories: ultimate limit state (ULS) methods, discrete load-transfer approach, strain wedge (SW) models, and continuum approach. The subsequent sections provide detailed introductions to each design approach and the methods associated with them.

Ultimate Limit State (ULS) Methods

Ultimate Limit State (ULS) methods are employed to predict the ultimate bearing capacity of the soil-pile system, encompassing both the loads and dimensions at failure. Therefore, the governing design factor in this approach is the failure of either the soil or the pile. ULS methods are widely used in practice due to their simplicity and quick outcomes, making them suitable for obtaining preliminary designs of laterally loaded piles. However, these methods usually do not provide an estimation of the pile's deflections at working loads, which is, in fact, a more realistic design factor. In the following section, the most common ULS methods are described, along with their advantages and limitations.

Conventional Static Approach

Poulos and Davis (1980) proposed that the simplest approach to estimate the ultimate lateral resistance of a free-head single pile is to consider the statics of the pile. As illustrated in Figure 2, the pile is subjected to three separate forces, a horizontal force acting on top of the pile (H), a moment (M), and soil pressure at any depth (z) equal to the soil ultimate resistance (p_u). The limiting combination of H and M (i.e., H_u and M_u) mobilizes the ultimate soil resistance along the pile. It should be noted that the pile is considered to be rigid in this approach, and the pile rotation point is at the depth z_r.

Table 1. Summary of the design methods for laterally loaded piles

Method	Source	Approach	Soil Type(s)	Pile Type(s)	Pile-Head Restraint	Serviceability Limit State	Remarks
Conventional Static Solution	Poulos and Davis (1980)	ULS	All Soils	Rigid	Free	No	- Simplest method to calculate the ultimate load and moment of the pile
Blum	Blum (1932)	ULS	Cohesionless	Rigid	Free	No	- Passive soil wedge failure - Not applicable for layered soil - Suitable for short piles in sand - Fixed rotation point
Brinch-Hansen	Hansen (1961)	ULS	Cohesive Cohesionless	Rigid	Free	No	- Varying rotation point - Failure due to both active and passive earth pressures - Applicable for layered soil
Broms	Broms (1964a); (Broms, 1964b)	ULS	Cohesive Cohesionless	Rigid Flexible	Fixed Free	Yes	- Incorporating different types of soil, piles, and pile-head restraint - Unreliable predictions of pile deflections
Linear Subgrade Reaction	Winkler (1867)	Discrete Load-Transfer	All Soils	Flexible	Free	Yes	- Basis of *p-y* curve method - Linear soil behavior
p-y Curve	First developed by Matlock (1970)	Discrete Load-Transfer	All Soils	Rigid Flexible	Fixed Free	Yes	- Incorporating the nonlinearity in soil behavior - Euler-Bernoulli beam - Nonlinear uncoupled springs as soil medium - Most common method in practice
Strain Wedge (Uniform Soil)	Norris (1986)	Strain Wedge	Cohesive Cohesionless	Flexible	Free	Yes	- relating three-dimensional passive soil wedge parameters to *p-y* behavior
Strain Wedge (Layered Soil)	Ashour et al. (1998)	Strain Wedge	Cohesive Cohesionless	Flexible	Free	Yes	- Modified SW for multi-layered soil profiles - Hyperbolic strain development curve
Continuum Models	-	Continuum	All Soils	Rigid Flexible	Fixed Free	Yes	- Most accurate predictions of laterally loaded pile behavior - High computational cost

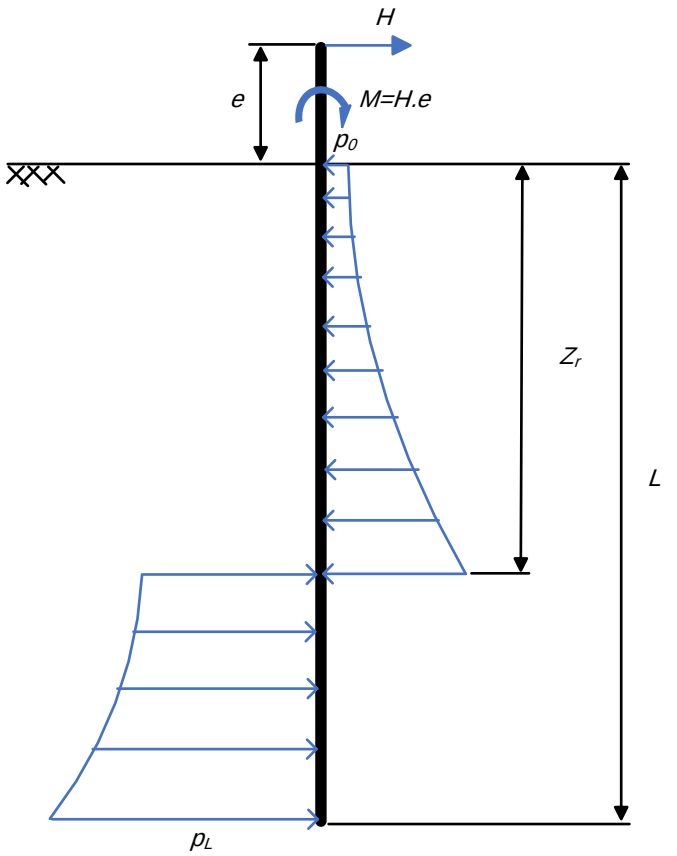

Figure 2. Unrestrained Laterally Loaded Pile, after Poulos and Davis (1980)

If the soil reaction along the pile would be uniform and equal to p_u, z_r, H_u, and M_u can be calculated using the following equations:

$$z_r = \frac{1}{2}\left(\frac{H_u}{p_u d} + L\right)$$

$$\frac{H_u}{p_u dL} = \left[\left(1 + \frac{2e}{L}\right)^2 + 1\right]^{0.5} - \left(1 + \frac{2e}{L}\right)$$

$$\frac{H_u}{p_u dL^2} = \frac{1}{4}\left[1 - \left(\frac{2H_u}{p_u dL}\right) - \left(\frac{H_u}{p_u dL}\right)^2\right]$$

And if the soil reaction along the pile would distribute linearly from p_0 at ground surface to p_L at the tip of the pile, the following equations may be derived:

$$4\left(\frac{z_r}{L}\right)^3 + \left[6\left(\frac{z_r}{L}\right)^2\right]\left[\frac{e}{L} + \frac{p_0}{p_L - p_0}\right] + \left(\frac{12p_0}{p_L - p_0}\right)\left(\frac{e}{L}\right)\left(\frac{z_r}{L}\right) - \left(3\frac{e}{L}\right)\left(\frac{p_0 + p_L}{p_L - p_0}\right) - \left(\frac{p_0 + p_L}{p_L - p_0}\right) = 0$$

$$\frac{H_u}{p_u dL} = \left(1 - \frac{p_0}{p_L}\right)\left(\frac{z_r}{L}\right)^2 + \left(2\frac{p_0}{p_L}\right)\left(\frac{z_r}{L}\right) - \frac{1}{2}\left(1 + \frac{p_0}{p_L}\right)$$

Figure 3 depicts the variation of the normalized ultimate lateral load, $H_u/p_u dL$, versus e/L, for uniform and linear distribution of soil reaction along the pile.

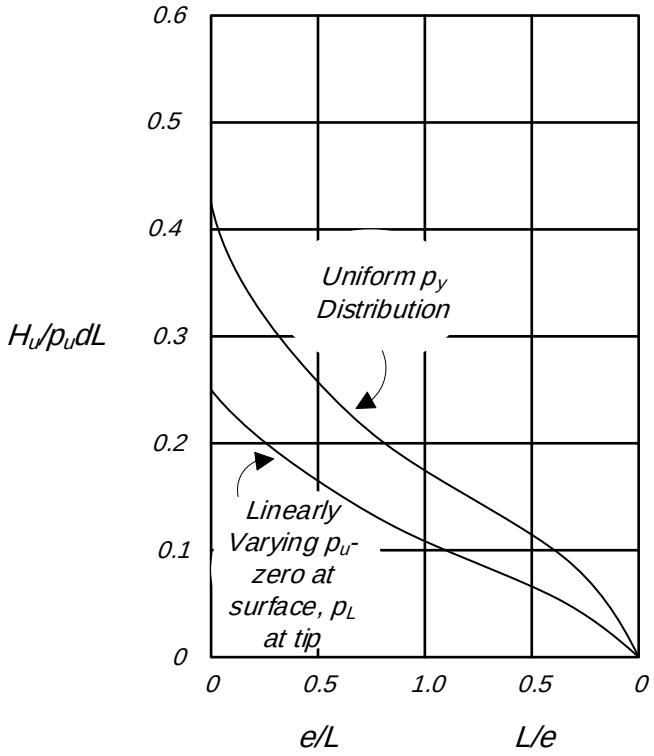

Figure 3. Ultimate lateral resistance of unrestrained rigid piles, after Poulos and Davis (1980)

Blum

The method developed by Blum (1932) is one of the most widely used methods for predicting the lateral bearing capacity of piles at ultimate limit state. This method uses an "ideal loading" condition for its calculations. Using Blum method, one can either calculate the maximum loads that a pile with known dimensions can resist or calculate the minimum dimensions for known load values. It should be noted that this method is not considered as an accurate and reliable method to design laterally loaded piles, but rather a fast and simple tool for a preliminary estimation of the final design.

The list below contains the assumptions of Blum's model:

1. The surrounding soil mobilizes the full passive resistance through a soil wedge, which is pushed upwards by lateral deflections of the pile (Figure 4).
2. The pile has a theoretical penetration depth (t_0). Moments are assumed to be zero at this depth.
3. The pile is fixed against deflections at the theoretical penetration depth.

4. A lateral force is applied to the pile at $z = t_0$ if the pile length is taken to be $1.2t_0$.

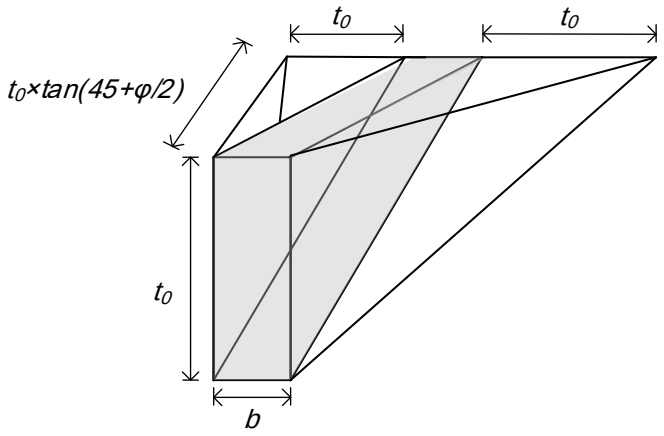

Figure 4. Soil wedge pressing on the pile, after Ruigrok (2010)

Figure 5 shows the diagrams attributed to Blum method. The "Pole" diagram contains the general layout of the loads acting on the pile and the important points. The "Loading" and "Moment" diagrams are the distributions of shear force and moment along the pile, respectively. The "Ideal Loading" diagram shows all the forces acting on the pile at limit equilibrium. In this context, the pile has a theoretical penetration depth (t_0). E_p and $E_{p\prime}$ represent the equivalent forces of the middle and side parts weight of the soil wedge, respectively. Finally, the "deflection" diagram depicts the deflected pile with d and d' values at ground level and pile top, respectively. Table 2 summarizes the model's parameters.

Table 2. Blum's model parameters

Parameter	Description
P	Horizontal force at static loading [kN]
d	Deflection at pile's top [m]
d'	Deflection at ground level [m]
f_w	Soil resistance [kN/m^3]
γ	Soil unit weight above the water table [kN/m^3]
γ_0	Soil unit weight below the water table [kN/m^3]
h	The height where load P is applied [m]
b	Width of the pile perpendicular to the force direction [m]
x_m	Location of M_{max} below surface [m]
t_0	Theoretical penetration depth [m]
t	Actual penetration depth=$1.2t_0$ [m]
I	Modulus of inertia in the P direction [m^4]
W	Section modulus in the P direction [m^3]
E	Modulus of elasticity [kN/m^2]
M_{max}	Maximum moment in ideal loading situation [$kN.m$]

The horizontal equilibrium of the soil wedge will yield the forces E_p and $E_{p'}$ (Figure 6):

$$E_p = G_1 tan\,(45 + {}^{\varphi}/_{2})$$

$$E_{p'} = G_2 tan\,(45 + {}^{\varphi}/_{2})$$

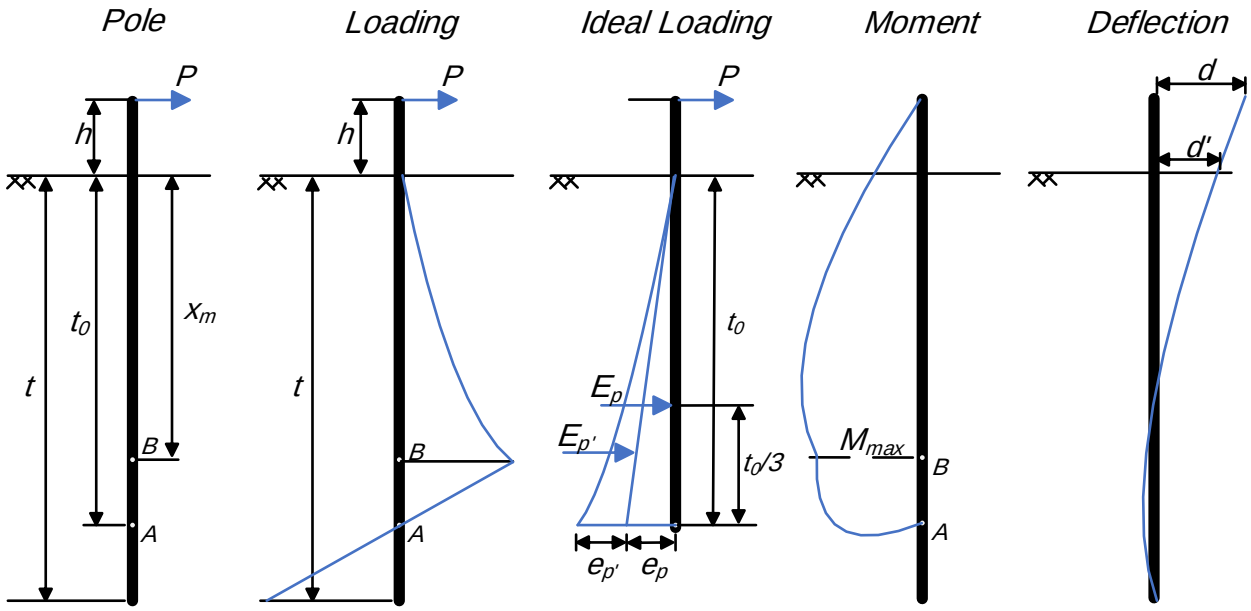

Figure 5. Blum' model layout, after Ruigrok (2010)

Where G_1 and G_2 are the middle and side weighs of the soil wedge, respectively, and can be calculated using the following equations:

$$G_1 = \frac{\gamma b t_0^2 tan\,(45 + {}^{\varphi}/_{2})}{2}$$

$$G_2 = \frac{\gamma b t_0^3 tan\,(45 + {}^{\varphi}/_{2})}{6}$$

The free-body diagram of the passive soil wedge in Blum model is shown in Figure 6.

The maximum bending moment can be calculated by following equations, by implementing the moments equilibrium:

$$M_{max} = \frac{f_w}{24} x_m^2 (3x_m^2 + x_m(4h + 8b) + 12bh)$$

Also, the maximum force would be:

$$P_{max} = \frac{f_w}{6} x_m^2 (x_m + 3b)$$

where:

$$f_w = \gamma \tan^2(45 + {}^{\varphi}/_{2})$$

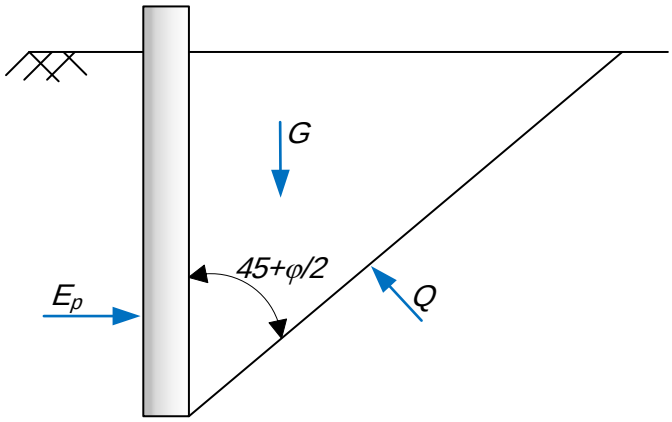

Figure 6. Soil wedge free body diagram in Blum method, after Ruigrok (2010)

If the loads are known, the deflections can be calculated using the following equations:

$$d = \frac{P(h+t_0)^3}{3EI} - \frac{f_w {t_0}^4}{360EI}(2.5{t_0}^2 + t_0(3h+12b) + 15bh)$$

$$d' = \frac{Pht_0{}^2}{2EI} + \frac{Pt_0{}^3}{3EI} - \frac{f_w}{EI}(\frac{t_0{}^6}{144} + \frac{bt_0{}^5}{30})$$

As mentioned earlier, the Blum method is a simple and fast approach to obtain an early estimation of the pile design. However, this model has several limitations and is not an accurate and reliable design method for laterally loaded piles. The following are some of the main shortcomings of this model:

1. The model is not capable of predicting the pile behavior at serviceability loads.
2. Soil cohesion is not considered in the model formulation.
3. The model cannot be used in layered soils.
4. Non-linearity of the soil behavior is not considered.
5. Only suitable for short and rigid piles in sandy soils.

Brinch-Hansen

Brinch-Hansen is another well-known method that employs the ULS approach for designing laterally loaded piles (Hansen, 1961). This method mobilizes the ultimate resistance of the soil through both active and passive earth pressures.

Figure 7 illustrates the schematics of the Brinch-Hansen model. Unlike the Blum method, Brinch-Hansen does not fix the rotation point (point B in Figure 7) and considers the depth of the rotation

point as a variable (D_r). The model also takes soil cohesion into account. Nevertheless, the pile is assumed to be rigid and square, and the calculation of pile deflections is not offered.

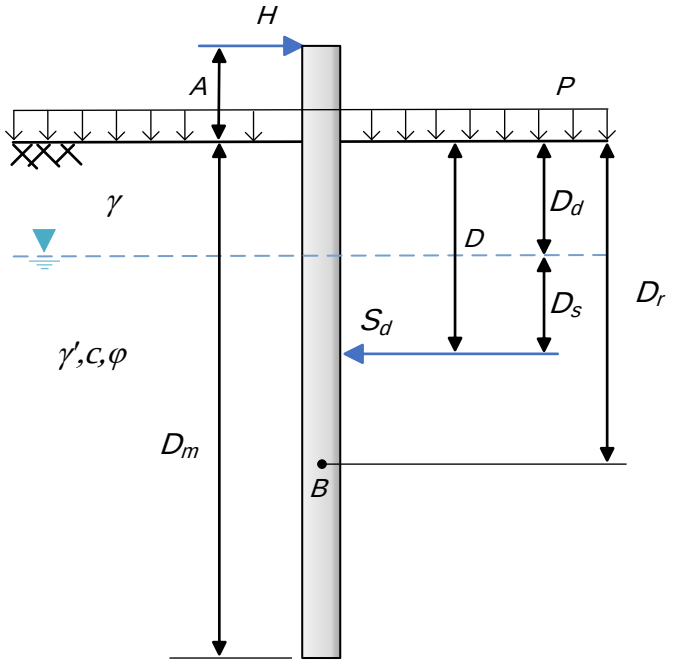

Figure 7. Schematic representation of Brinch-Hansen's method, after Ruigrok (2010)

The following equation is the general formula of the Brinch-Hansen method:

$$e^D = qK_q^D + cK_c^D$$

Where e^D is the net earth pressure acting on the pile, q is the effective overburden pressure, K_q^D is the earth pressure coefficient related to q, c is the soil cohesion, and K_c^D is the earth pressure coefficient related to c.

By considering two limit conditions ($D = 0$ and $D = \infty$), the earth pressure coefficients can be determined using the following equations:

$$K_q^D = \frac{K_q^0 + K_q^\infty \alpha_q (\frac{D}{B})}{1 + \alpha_q (\frac{D}{B})}$$

$$K_c^D = \frac{K_c^0 + K_c^\infty \alpha_c (\frac{D}{B})}{1 + \alpha_c (\frac{D}{B})}$$

where:

$$\alpha_q = \frac{K_q^0 K_0 \sin(\varphi)}{(K_q^\infty - K_q^0)\sin(\pi/4 + \varphi/2)}$$

$$\alpha_q = \frac{2K_c^0 \sin(\pi/4 + \varphi/2)}{(K_c^\infty - K_c^0)}$$

In the equations above, K_q^0 , K_q^∞, K_c^0, and K_c^∞ are the effective stress and cohesion earth pressure coefficients at ground level ($D = 0$) and great depth ($D = \infty$), respectively. These coefficients can be obtained using the following equations:

$$K_q^0 = exp\left[\left(\pi/2 + \varphi\right)\tan(\varphi)\right]\cos(\varphi)\tan\left(\pi/4 + \varphi/2\right) - exp\left[\left(-\pi/2 + \varphi\right)\tan(\varphi)\right]\cos(\varphi)\tan\left(\pi/4 - \varphi/2\right)$$

$$K_c^0 = \left(exp\left[\left(\pi/2 + \varphi\right)\tan(\varphi)\right]\cos(\varphi)\tan\left(\pi/4 + \varphi/2\right) - 1\right)\cot(\varphi)$$

$$K_c^\infty = N_c d_c^\infty$$

$$K_q^\infty = K_c^\infty K_0 \tan(\varphi)$$

where:

$$N_c = \left(\exp[\pi\tan(\varphi)]\tan^2\left(\pi/4 + \varphi/2\right) - 1\right)\cot(\varphi)$$

$$d_c^\infty = 1.58 + 4.09\tan^4(\varphi)$$

Using the model formulation, one can either determine the maximum lateral load and pile rotation point with known lateral load location, pile width, and penetration depth, or determine the minimum penetration depth and rotation point with known value and location of the lateral load. After the soil reaction profile is determined, other desired variables can be calculated using simple equilibrium equations and iteration process.

The Brinch-Hansen method overcame some of the shortcomings of the Blum method, such as including the cohesion component. Also, the model formulation is configured in a way that makes it possible to use them for layered soil profiles. However, the Brinch-Hansen model has its own limitations. The main limitation of this method is the lack of the calculation of pile lateral deflections. Since the model has only one boundary condition (zero deflection at D_r), the pile deflections cannot be obtained by double integration of the bending moment function.

Broms

Broms method can be considered the most inclusive among the traditional ultimate limit state (ULS) methods as it accommodates cohesive and cohesionless soil types, both free and fixed pile-head restraints, as well as rigid and flexible piles (Broms, 1964a, 1964b). In this method, the ultimate limit state is obtained by assuming passive earth pressure failure of surrounding soil for short and rigid piles, and yield resistance of the pile for long piles. Figure 8 and Figure 9 indicate

the failure modes of soil-pile system in Broms method for rigid and flexible piles, respectively. Based on these two failure modes and pile-head fixity condition, Broms presented four sets of dimensionless graphs to estimate the ultimate lateral resistance of piles. In some cases, it is difficult to determine whether a pile is short or long. In this instance, the method recommends that the ultimate resistance is the minimum value of the two conditions.

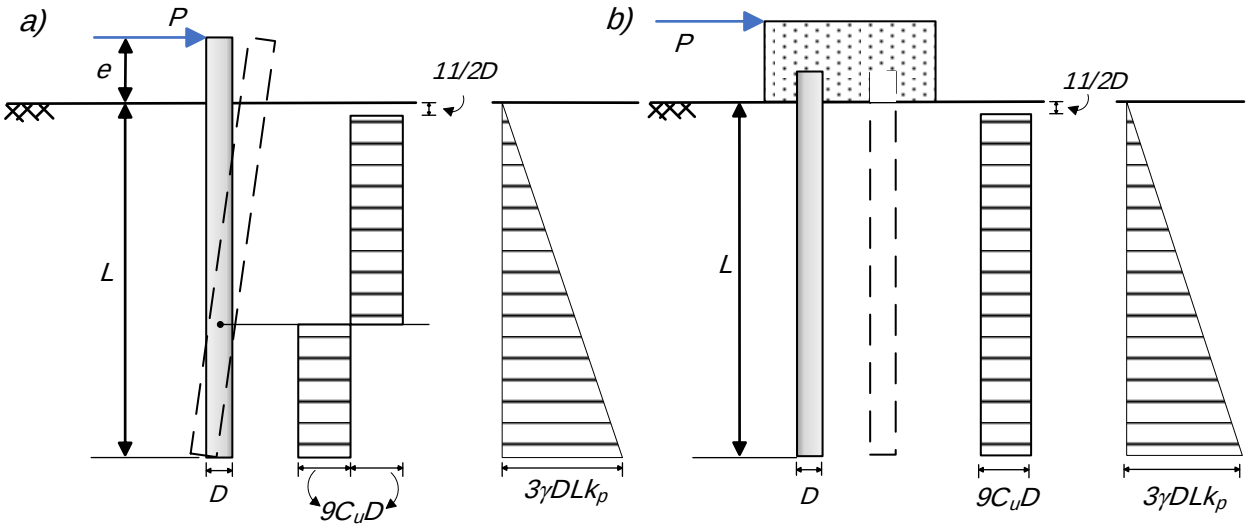

Figure 8. Failure modes of the rigid piles in Broms method, a) free head and b) fixed head, after Broms (1964a) and Broms (1964b)

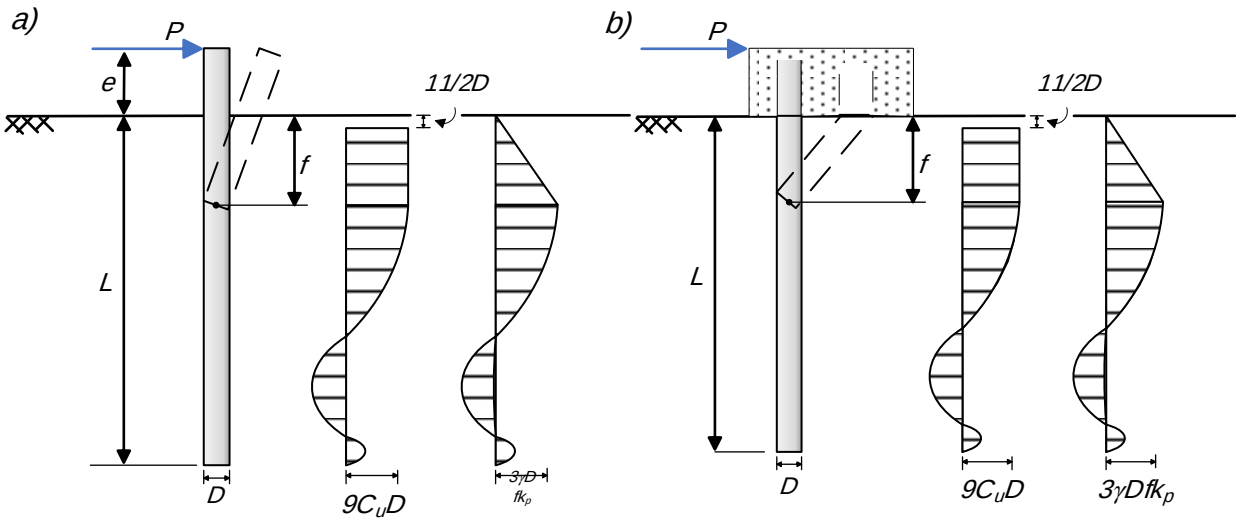

Figure 9. Failure modes of the flexible piles in Broms method, a) free head and b) fixed head, after Broms (1964a) and Broms (1964b)

Using the soil's subgrade reaction modulus, Broms also proposed a method to estimate the lateral deflections of the pile at ground surface level at working loads. In this method, the working loads

are assumed to be 0.3 to 0.5 of the ultimate resistance, and the deflections can be calculated using the following equation:

$$p = k_h y$$

where p is the unit soil reaction, and k_h is the modulus of subgrade reaction. Broms stated that for cohesive soils, the subgrade reaction modulus is constant with depth and can be obtained using the proposed dimensionless graphs. Broms also stated that for cohesionless soils, k_h increases linearly with depth, following the bellow equation:

$$k_h = \frac{n_h}{D} z$$

where n_h is a coefficient that depends on the relative density of the soil. Like cohesive soils, k_h can be found using dimensionless graphs.

Broms method was validated with several field test data. For cohesionless soil, calculated deflections were compared to 19 cases, including single piles, pile groups, restrained piles, and free-head piles. The results of this comparison showed that for almost all cases, the calculated values were noticeably larger than the measured values. For the ultimate lateral resistance in cohesionless soil, the method was validated for 7 cases, where the average of measured values exceeded the calculated values by more than 50%.

For cohesive soil, comparison between the calculated and the measured deflections in 5 cases showed that the measured values were 0.5 to 3.0 times the calculated values. Additionally, the estimated values of ultimate lateral resistance in cohesive soil were compared with three different cases, and the outcome of this comparison demonstrated good agreement between the measured and calculated moments.

The method developed by Broms is fast and simple to use, and it is applicable to both cohesive and cohesionless soil types, different pile flexural rigidities, and various pile-head fixity conditions, making it a more comprehensive model than Blum and Brinch-Hansen models. However, the validation of the method indicates that it is not reliable in most cases, especially for estimating the lateral deflections.

Discrete Load-Transfer Approach

As mentioned earlier, the problem of laterally loaded piles is a soil-structure interaction problem, meaning that the lateral capacity of the soil and the deflections of the pile are interdependent variables. In other words, the soil resistance which is a function of soil properties affects the pile's response and the pile deflections mobilizes the soil resistance (Ariannia, 2015). The common goal of every method developed for the analysis of laterally loaded pile is the attempt to capture the aspects of the soil-pile interactions as accurately as possible.

In the discrete load-transfer approach, it is assumed that the pile behaves as a beam, and the soil medium is discretized into a series of independent linear/nonlinear springs. Each spring is

characterized as a force-deformation function, known as *p-y* curves. To understand the application of *p-y* curves, it is crucial to review the theory of linear subgrade reaction.

Linear Subgrade Reaction Theory

The concept of linear subgrade reaction in applied soil mechanics was first introduced by Winkler (1867), also known as Winkler's beam on elastic foundation (BEF) problem. This theory includes an infinite elastic foundation modeled as linear uncoupled springs (Figure 10) each possessing a linear vertical pressure, *q*, and a vertical deflection, *w*, with the relationship shown in the following equation:

$$\frac{q}{w} = k_0 \text{ or } \frac{qb}{w} = k$$

where k_0 is the subgrade modulus (*force/L*^{3}), *b* is the beam width, and *k* is the subgrade modulus of the beam (*force/L*^{2}).

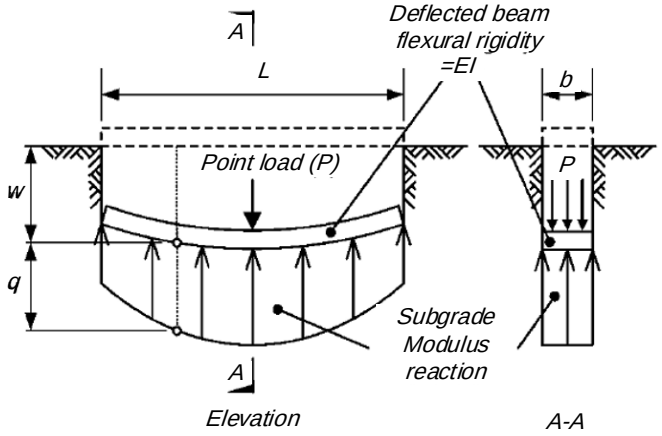

Figure 10. Beam-on-elastic-foundation problem (Ariannia, 2015)

In terms of laterally loaded piles, the relationship between the soil reaction (*p*) and the pile deflections (*y*) at a given depth can be expressed as follows:

$$p = k_h.y$$

or

$$P = K.y$$

where *K* is the subgrade modulus, $K=k_h.b$. It should be noted that the soil's subgrade modulus is not a property of soil but rather a property of the soil-pile system, which takes into account factors such as pile geometry, flexural rigidity of pile, pile head condition, and soil properties.

p-y Curve Models

As discussed in the previous section, Winkler's BEF theory simplifies the analysis of an elastic transversely loaded beam on an infinite elastic foundation by modeling the soil medium as

independent linear springs. The *p-y* curve method follows the same concept but takes a more advanced approach for the soil response. The *p-y* curve method incorporates the nonlinearity of the soil by establishing a relationship between the soil lateral resistance (*p*) and the pile deflection (*y*) at various depths. This is achieved by modeling the surrounding soil as a series of uncoupled nonlinear springs (Figure 1). The *p-y* curves typically consist of three portions. The first portion is a straight line (or has a tangent line) with a slope that represents the soil behavior within the range of elastic deformations. The second portion is a transition curve from the elastic region to the ultimate resistance, expressed as a function of the soil's ultimate resistance and pile deflections beyond the soil's yielding strains. Lastly, the third portion is a horizontal line with the ordinate equal to the soil's ultimate lateral resistance.

The *p-y* curve method is considered to be the most practical method in geotechnical engineering due to its simplicity and accurate results. However, *p-y* curves are usually developed using empirical/semi-empirical methods, such as field tests, laboratory experiments, and in-situ tests. These lead to unique and site-specific curves, which may not be applicable to all soil-pile conditions. Additionally, since the soil medium is modeled as independent springs, the continuum nature of the soil medium (i.e., the shear stresses between the soil's horizontal planes) is not fully captured. A detailed description of the *p*-y curve method is presented in Chapter 3.

Strain Wedge (SW) Models

The strain wedge (SW) method was first developed by (Norris, 1986) to predict the response of a single flexible pile subjected to lateral load embedded in uniform soil (sand/clay). This method uses a three-dimensional passive soil wedge to solve the Winkler's BEF problem. Ashour et al. (1998) modified the original SW model to be applicable for piles embedded in layered soil profiles.

By employing the concept of passive earth pressure, the SW models use an ultimate limit state factor to assess the nonlinear *p-y* response of laterally loaded piles. In other words, the SW method relates the characteristics of an envisioned three-dimensional passive soil wedge in front of a laterally loaded pile to the characteristics of the BEF problem. According to Ashour et al. (1998), the relationship between the BEF problem and the SW models include the following interdependencies:

1. The horizontal soil strain (ε) in the passive wedge to the deflection pattern versus depth (y-z).
2. The change in horizontal stress ($\Delta\sigma_h$) in the passive wedge to the soil's reaction along the pile (p).
3. The nonlinear variation in the soil Young's modulus ($E = \Delta\sigma_h / \varepsilon$) to the nonlinear variation of the subgrade reaction modulus ($E_s = p/y$).

Figure 11 illustrates the geometry of the passive soil wedge in the SW model and its characteristics. The characteristics associated with the SW model include the base angles, Θ_m and β_m, the current depth of the wedge, h, the wedge fan dispersion angle, φ_m, the horizontal stress change at the face of the wedge, $\Delta\sigma_h$, and the mobilized shear stress on the pile sides, τ.

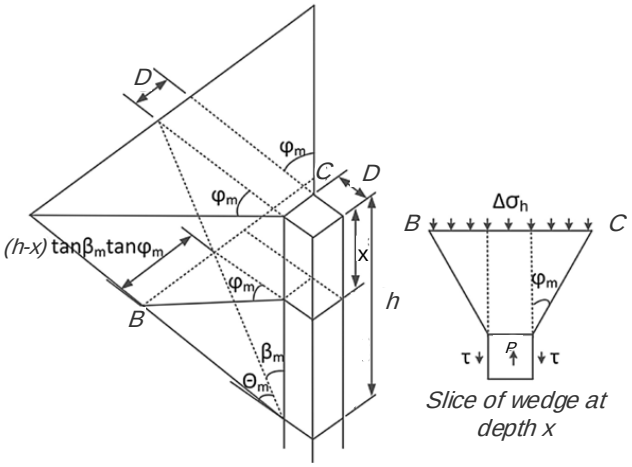

Figure 11. Strain wedge model in uniform soil (Xu et al., 2013)

The angles Θ_m and β_m, and $\overline{BC}$, the width of the wedge face at a given depth, *z*, are given by the following equations:

$$\Theta_m = 45 - \frac{\varphi_m}{2}$$

$$\beta_m = 45 + \frac{\varphi_m}{2}$$

$$\overline{BC} = D + 2(h - z)\tan\beta_m \tan\varphi_m$$

The deflection pattern of the pile from the pile top to the base of the wedge is assumed to be linear with the angle δ (Figure 12). This assumption allows the model to assess the uniform horizontal and vertical soil stresses.

Strain Wedge Model in Layered Soil

One of the main advantages of the Strain Wedge Method is its capability in predicting the response of laterally loaded piles embedded in layered soil profiles. The modified SW model by Ashour et al. (1998) uses an approach, called the multi-sublayer technique, to handle the problem of laterally loaded pile embedded in multiple soil type profiles. Based on this technique, the pile and the soil profile are divided into segments and sublayers with constant thickness (Figure 13). Each of the sublayers has its own properties based on the soil type and the location of the sublayer in the compound wedge.

The base angles and the width of the wedge face for each soil wedge can be obtained from the following equations:

$$(\Theta_m)_i = 45 - \frac{(\varphi_m)_i}{2}$$

$$(\beta_m)_i = 45 + \frac{(\varphi_m)_i}{2}$$

$$\overline{(BC)}_i = D + 2(h - z_i)\tan(\beta_m)_i \tan(\varphi_m)_i$$

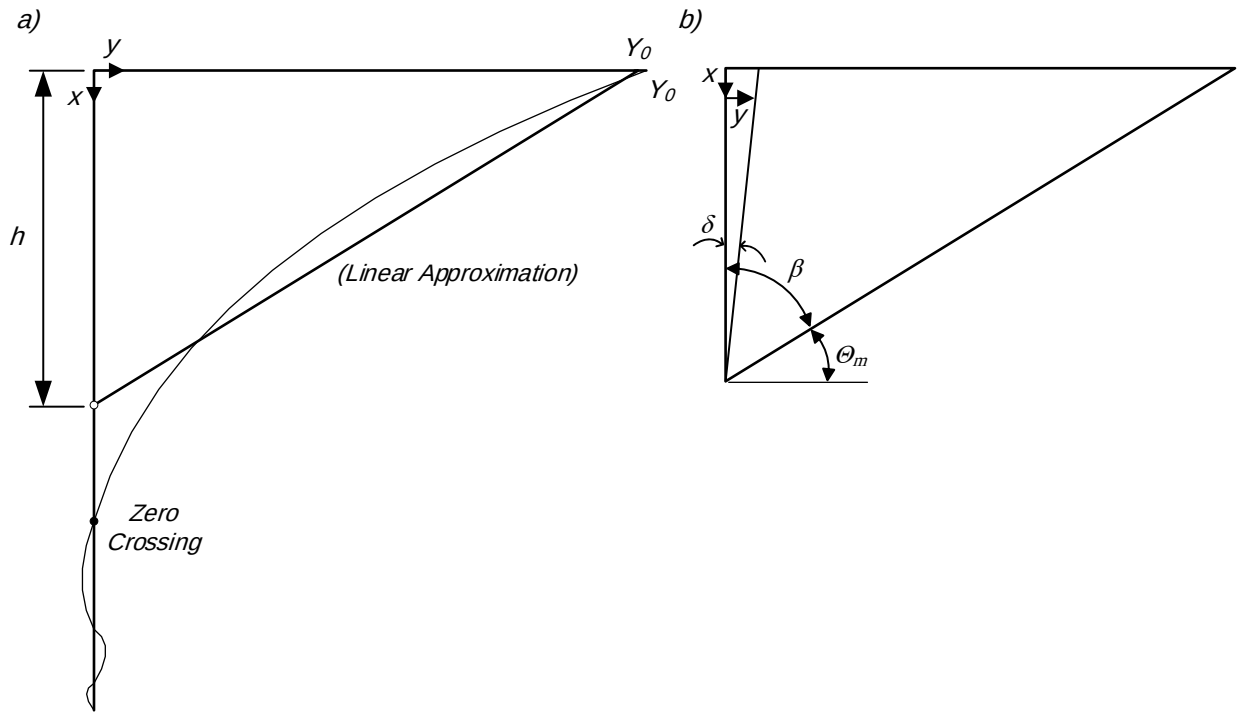

Figure 12. Deflection pattern of laterally loaded flexible pile in the SW model, a) Linear approximation of the pile deflection along the current soil wedge depth, b) side view of the soil wedge and pile linear deflection, after Ashour et al. (1998)

Some of the most important assumptions of the multisublayer technique are as follows:

- The deflection pattern of the pile is continuous regardless of the soil type variation.
- As shown in the last equation, the geometry of each soil wedge depends on the depth of the compound wedge, *h*, as well as the properties of the soil type in the corresponding layer.
- The geometry of the compound wedge depends on the properties and the number of sublayers, and the global equilibrium of the soil-pile system.
- To satisfy the equilibrium between the pile's deflection pattern and the passive soil wedge strains, an iterative calculation is required.

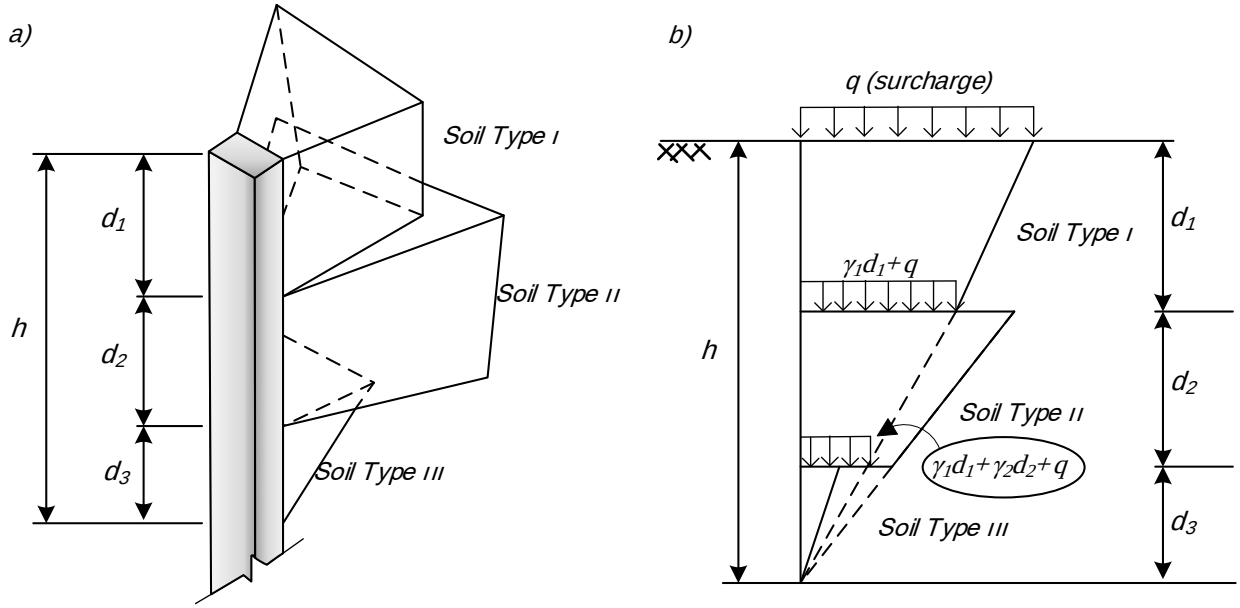

Figure 13. The geometry of the sublayers and compound passive soil wedges, a) three-dimensional soil wedges, b) side view of multi-layered strain wedge model, after Ashour et al. (1998)

Soil Stress-Strain Relationships in Strain Wedge Model

Calculations in the SW model are based on effective stress analysis in both sand and clay. The results of the isotropic consolidated drained (for sand) and undrained (for clay) triaxial tests can be used to define the stress-strain relationships as follows:

- The deviatoric stress change in triaxial test is equivalent to the horizontal stress change ($\Delta\sigma_h$) in the SW model.
- The change in vertical and perpendicular-horizontal stresses are equal to zero, similar to the constant confining pressure in standard triaxial compression test.
- The initial horizontal effective stress (after the pile installation and before loading) is considered equal to the vertical effective stress, similar to the isotropic state in the triaxial test.
- The relationship between the horizontal stress change ($\Delta\sigma_h$) and horizontal strain (ε) is related to the secant Young's modulus in the triaxial test.
- Vertical and perpendicular-horizontal stress strains are given by: $\varepsilon_v = \varepsilon_{ph} = -\nu\varepsilon_h$

Soil's shear strain and stress level (SL) can be drawn from the soil element Mohr's circle.

The SW model uses a hyperbolic strain development curve to obtain the stress level at each sublayer (Figure 14).

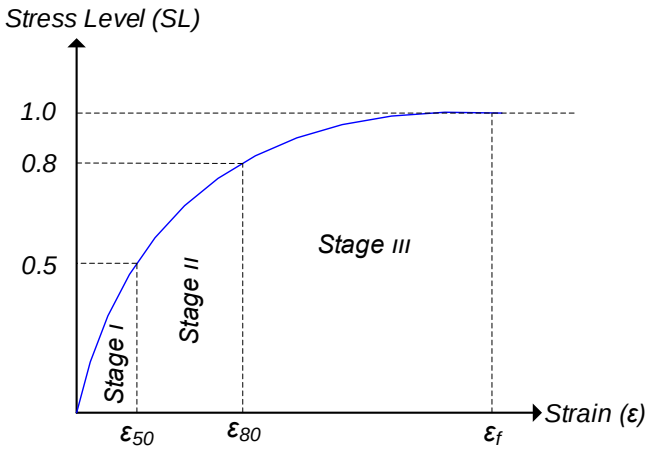

Figure 14. Developed hyperbolic stress-strain relationship in soil, after Ashour et al. (1998)

As shown in Figure 14, the variation of the stress level versus the horizontal strain consists of three stages of strain range, $\varepsilon \leq \varepsilon_{50}$, $\varepsilon_{80} \leq \varepsilon \leq \varepsilon_{80}$, and $\varepsilon \geq \varepsilon_{80}$. Here ε_{50} and ε_{80} are the horizontal strains associated with 50 and 80 percent of the stress level, respectively.

Lastly, the shear stress developed on the sides of the pile can be obtained based on the soil type. For sand, it is simply a function of the vertical effective stress and mobilized contact friction angle. For clay, the side shear stress depends on the undrained shear strength (S_u). The side shear stress level is defined as a function of pile deflection (y). The Coyle and Reese (1966) shear stress transfer curves are used to determine the side shear stress from the pile lateral deflection.

Soil Properties in Strain Wedge Model

The soil profile in the SW model is divided into one/two-foot sublayers, where each sublayer has its properties. These properties include the effective unit weight, void ratio, internal friction angle, and soil strain at 50% of stress level for sand, and effective unit weight, effective friction angle, plasticity index, undrained shear strength, and soil strain at 50% of stress level for clay.

An effective stress analysis on the results of standard triaxial tests may be applied to obtain the required properties for the SW model.

Correlation between Winkler's Beam on Elastic Foundation Problem and the Strain Wedge Models

The subgrade reaction modulus (E_s) in the BEF problem is correlated to the soil Young's modulus in the SW models by means of two linking parameters, A and Ψ_s. The first parameter, A, is a multiplier that yields the sublayer reaction to the pile, p_i, when applied in the following equation:

$$p_i = A_i \times D \times E_i \times \varepsilon$$

where D is the pile width, and E is the Young's modulus of a given sublayer.

The second linking parameter, Ψ_s, is related to the compound wedge geometry and correlates the subgrade reaction modulus to the SW model characteristics. Ψ_s can be obtained from the following equation:

$$\Psi_s = \frac{2}{(1+\nu) \times \sin(2\theta_m)}$$

Using both linking parameters, the relationship for the subgrade reaction modulus of each sublayer in the SW model can be expressed as follows:

$$(E_s)_i = \frac{A_i}{h - x_i} D \times \Psi_s \times E_i$$

Conclusions

The strain wedge method was initially developed to solve the Winkler's BEF problem by using an envisioned three-dimensional passive soil wedge. This method was further modified to account for multi-layer soil profiles. The main aspect of the SW models is related to the soil strain development, hence the name strain wedge. In this method, it is assumed that the deflection of the pile along the depth of the passive wedge is linear. Therefore, the pile deflection at any sublayer can be obtained by multiplying the thickness of the sublayer to the deflection pattern angle. Consequently, the pile head deflection is equal to the summation of all sublayer deflections.

The capability of the SW models in predicting the response of laterally loaded piles in layered soil profiles is the main advantage of this method over the *p-y* models. However, assuming a rigid pattern of deflection for a flexible pile may produce unrealistic results.

Continuum Approach

Although the *p-y* curve models are widely used in practice, they fail to capture all the aspects of the interactions between a laterally loaded pile and its surrounding soil. This limitation mainly arises from the fact that *p-y* curves are typically derived from empirical methods and are site-specific. Also, the coupling shear resistance between the springs is neglected in the *p-y* curve method.

Continuum-based methods, which rely on numerical solutions, such as finite element (FE), finite difference (FD), and boundary element (BE) analysis, overcome this limitation due to their versatility in the applied soil and pile conditions. The soil medium in continuum models can be modeled using elastic/elastoplastic, linear/nonlinear constitutive models in uniform/layered soil profiles. These models typically include three-dimensional FE analysis (Brown et al., 1989; Randolph, 1981; Trochanis et al., 1991), three-dimensional FD analysis (Ng & Zhang, 2001; Verruijt & Kooijman, 1989), and three-dimensional BE analysis (Banerjee & Davies, 1978; Budhu & Davies, 1988). The BE continuum models incorporate the interactions of the soil-pile system by discretizing the pile into strips and numerical integration of Mindlin's equations (Mindlin, 1936).

As a result of a more complex analysis, continuum-based models lead to more accurate and realistic predictions of laterally loaded pile behavior. However, this accuracy comes with a high

computational cost. While continuum methods are conceptually more appealing, they are not applicable to common engineering problems.

Studies have attempted to reduce the computational effort of continuum-based analysis by applying simplified assumptions and principles like virtual work and minimum potential energy (Basu et al., 2009; Gupta & Basu, 2020). Basu et al. (2009) used the principle of minimum potential energy of the soil-pile system to obtain the governing equations for pile deflections in layered soil. They implemented a linear-elastic isotropic constitutive model for the soil medium and assumed a Euler-Bernoulli beam as the pile. Neglecting the nonlinearity of the soil behavior and using the principle of minimum potential energy led to reduced computational effort in their study. Gupta and Basu (2020) used the virtual work principle to generate the pile deflection and soil displacement equations and solve the equations using one-dimensional FD analysis. They have stated that the use of elastoplastic constitutive models for the analysis of laterally loaded piles behavior is unnecessary, since laterally loaded piles are often designed for serviceability limit states and only generate small to medium strains.

While the continuum approach is the most accurate method for analyzing the behavior of laterally loaded piles and it is capable of capturing important aspects of soil-pile interactions, the complexity and computational effort of these methods remain a barrier for their practical appeal. The application of continuum models in *the p-y* curve method is discussed in Chapter 3.

Summary

In this chapter, all the common and well-known methods for the design of laterally loaded piles were described. These methods were categorized based on their main approach to the laterally loaded pile problem and include: 1) the ultimate limit state (ULS) methods, which typically use an ultimate soil/pile capacity criterion to predict the response of the pile and do not offer the pile deflections in the range of serviceability loads, 2) the discrete load-transfer (*p-y*) models, which usually assume the pile as a Euler-Bernoulli beam and model the surrounding soil as a series of linear/nonlinear independent springs with characteristics dependent on the soil-pile system properties, 3) the strain wedge (SW) models, which use a three-dimensional passive soil wedge to correlate the *p-y* characteristics to the soil wedge stress-strain development, and 4) the continuum-based models, which are based on three-dimensional numerical analysis of the soil-pile interactions.

The methodology, advantages, and limitations of each approach were described. The ULS methods are mostly used for early designs and do not offer realistic predictions due to their over-simplified assumptions. The *p-y* curve methods offer fairly accurate results with minimum effort, and therefore, are widely used in practice. The continuum methods are capable of capturing the most important aspects of the soil-pile interactions and yield the most accurate outcomes. Nevertheless, these methods require complex numerical analysis and high computational effort, and consequently, are rarely used in engineering problems.

In the next chapter, the *p-y* curve method, which is the focus of this study, is thoroughly described. The chapter includes the different methods for developing *p-y* curves, and the available *p-y* models in technical literature.

CHAPTER 3: p-y CURVE METHOD

Introduction

The *p-y* curve is a method for the analysis of the response of laterally loaded piles based on Winkler's beam on elastic foundation theory. In this method, the interactions between the pile and the surrounding soil are captured through a series of uncoupled nonlinear horizontal springs along the pile (Figure 1). Based on the characteristics of the springs, the relationship between the pile deflection (*y*) and the soil resistance (*p*), called the *p-y* curve, at any given depth can be obtained. Different methods have been utilized to develop the *p-y* for a pile-soil system. These methods can be divided into four main categories, including full-scale field tests, model-scale laboratory experiments, in-situ tests, and numerical models.

Since the characteristics of *p-y* curves are heavily dependent on both the soil type and the pile properties, *p-y* curves are naturally unique to specific soil-pile system. Therefore, lateral loading test on full-scale instrumented piles can be considered as the most reliable method to develop the *p-y* curves. However, the execution of this method can be expensive and time-consuming, and thus, might not be feasible for all purposes. The second method, model-scale laboratory experiments, typically contains the construction of physical models of the soil-pile system in relatively small scales to simulate the soil-pile properties and the loading condition of the prototype. Two types of model-scale experiments are used for developing *p-y* curves, including 1g model-scale experiments (i.e., lateral loading of soil-pile physical models in 1g gravitational field) and centrifuge experiments (i.e., in-flight lateral loading of soil-pile physical models at higher gravitational accelerations in centrifuge device). The main purpose of using centrifuge devices is to accurately simulate the stress state caused by the soil mass. The third method, in-situ *p-y* curves, includes developed frameworks to derive the *p-y* curves directly from in-situ test data, such as cone penetration test (CPT), pressuremeter test (PMT), and dilatometer test (DMT). Depending on the soil condition and the in-situ test results, these methods can yield fast and reliable *p-y* curves at low costs. The last method, numerical modeling, refers to the *p-y* curves derived from numerical models, which are typically developed based on three-dimensional finite element (FE), finite difference (FD), and discrete element (DE) methods. The application of numerical analysis in predicting the response of laterally loaded piles was discussed in chapter 2. *p-y* curves can be obtained from the output results of numerical analysis, such as pile deflections and local strains. However, these methods usually entail high computational effort and may not be consistent with the practical nature of the *p-y* curve method.

The objective of this study is to develop *p-y* curves for the analysis of laterally loaded piles in Montana. The methodology of the study is to develop the *p-y* curves from the results of a series of model-scale centrifuge experiments coupled with numerical analysis of the models. In the following chapter, the different methods for developing the *p-y* curves and the available studies associated with each method are described. Table 3 includes a summary of the methods for development of the *p-y* curves in technical literature. Then, the procedure of obtaining a *p-y* curve from acquired experimental data is explained. Eventually, the available *p-y* models in LPILE software, as a popular software for designing laterally loaded piles, are explained.

Table 3. Summary of the methods for p-y curve development

Model	Method	Soil Type(s)	Pile Type(s)	Loading Condition	*p-y* Curve	Remarks
Matlock (1970)	Full-scale field test	Soft clay	Steel pipe	Static Cyclic	Parabola	- First *p-y* model - Suggested by API
Reese et al. (1975)	Full-scale field test	Stiff clay	Open-ended steel pipe	Static Cyclic	Multi-portion Straight lines and parabolas	- First *p-y* model for stiff clay - Represents the brittle response of stiff clay - Suggested by API
Reese et al. (1974)	Full-scale field test	Sand	Open-ended steel pipe	Static Cyclic	Three straight lines and one parabola	- First *p-y* model for sand - Suggested by API
Mokwa et al. (2000)	Full-scale field test	*c-φ* soils	Drilled shafts	Static	Parabola	- PYPILE spreadsheet for *p-y* curve development - Used experimental data from Helmers (1997)
H. Yu et al. (2019)	Full-scale field test	Gravel	Reinforced concrete	Static	Three-portion *p-y* curve	- Evaluation of the lateral response of a single RC pile embedded in sloping gravelly ground
Barton et al. (1983)	Centrifuge	Sand	Large diameter single pipe	Cyclic	-	- Compared experimental *p-y* curves with API recommendation - Initial stiffness of the curves vary as the square root of depth rather than linearly - Ultimate resistances from API method are underestimated near the ground surface and overestimated at depth - Generally good agreement between the experimental *p-y* curves and API-recommended *p-y* curves
Lee et al. (2019)	Centrifuge	Sand	Monopile	Static Cyclic	Backbone hyperbola	- Higher initial slope with increase in loading cycles and magnitude, and depth
Choo and Kim (2016)	Centrifuge	Dense sand	Copper Steel	Lateral load Overturning moment	-	- Comparison between centrifuge and field test results - Softer *p-y* curves that the ones proposed by API due to large diameter effects

Haouari and Bouafia (2020)	Centrifuge	Dense sand	Rigid Semi-rigid	Monotonic	Cubic hyperbola	- Comparison of centrifuge and numerical results - Incorporating the effects pile flexural rigidity
Brandenberg et al. (2013)	FEM modeling Centrifuge	Liquefiable sand	Single- 2 ×3 pile group	Cyclic	-	- Comparison of the experimental *p-y* response of centrifuge single pile and six-pile group models in level and sloping liquefied sand, respectively -incorporating the effects of cyclic mobility (liquefaction and lateral spreading) in FEM material model
Tokimatsu and Suzuki (2004)	1g model-scale	Liquefiable sand	2 × 2 Steel pipe	Cyclic (Shaking table)	-	- Study of the effects of liquefaction potential on *p-y* response of pile groups
Tak Kim et al. (2004)	1g model-scale	Sand	Pre-installed Driven	Monotonic	Cubic hyperbola	- Study of the effects of installation method, relative density, and pile-head restraint on the *p-y* behavior
P. K. Robertson et al. (1985)	PMT	Cohesive Cohesionless	-	-	Modified pressuremeter curve	- Applied reduction factor to the pressure component of the PMT curve
Robertson et al. (1989)	DMT	Cohesive Cohesionless	-	-	Matlock's parabola	- p_u obtained from DMT results
Briaud et al. (1983)	PMT	Sand Clay	-	-	Modified pressuremeter curve	- *p-y* curve consisted of two frontal and side resistance curves
Li et al. (2018)	CPTu	Clay	-	-	Matlock's parabola	- Equations are proposed for p_u and E_s based on CPTu results
Ariannia (2015)	CPT	Sand Clay Intermediate	-	Static	*PySimple3 p-y* curve	- Input parameters of *PySimple3* are formulated based on CPT data
Brown and Shie (1990)	3D-FE	Sand Clay	Euler-Bernoulli	Monotonic	-	- Comparison of FE derived *p-y* curves and empirical ones

Choobbasti and Zahmatkesh (2016)	3D-FE	Liquefiable sand	Euler-Bernoulli	Cyclic	Backbone *p-y* curve	- Computed reduction factors for the backbone *p-y* curve in liquefiable sands
G. Yu et al. (2019)	3D-FE	Cement-improved gravel	Euler-Bernoulli	Static	Hyperbola	- New equations for p_u and k are proposed

Development of p-y Curves

A typical *p-y* curve consists of three main portions (Figure 15). The first portion is a straight line (or has a sloped tangent) which represents the relationship between the soil lateral reaction (*p*) and the pile lateral displacement (*y*) for small deformations. The slope of this line is usually related to the subgrade reaction modulus, E_s, described in chapter 2. The second portion is a transitional curve between the *p* versus *y* variations at small deformations (elastic range) and the ultimate lateral resistance, p_u, representing the plastic deformations of the soil- pile system. The shape of the transitional curve can be characterized using appropriate mathematical functions, such as parabolic or hyperbolic functions. The third portion of a typical *p-y* curve is a horizontal line with the ordinate value equal to the ultimate lateral resistance of the soil- pile system. The ultimate resistance is governed by the soil's ultimate lateral capacity for rigid (short) piles, and by the pile's failure resistance for flexible (long) piles.

The methods for the development of *p-y* carves are divided into four categories in this report. These categories include full-scale field tests, model-scale laboratory experiments, in-situ tests, and numerical models. In the following section, some of the most outlined studies in each category are briefly discussed to gain insight into the development of *p-y* curves.

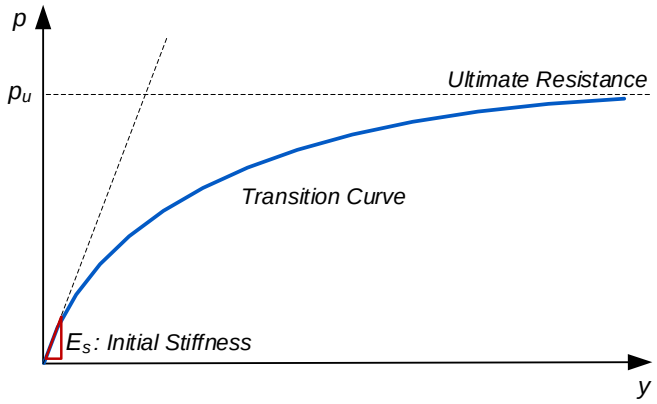

Figure 15. Typical p-y curve

Full-Scale Field Test

Full-scale field tests on instrumented laterally loaded piles are the most accurate method for the development and the assessment of *p-y* curves. The study conducted by McClelland and Focht (1956) was the first significant attempt to handle the nonlinear response of the soil to a laterally loaded piles. Based on the analysis of filed test data, they proposed a linear conversion of the scales for nonlinear laboratory stress-strain curves of undisturbed clay samples to develop p-y curves. Matlock (1970), Reese et al. (1975), and Reese et al. (1974) are considered as the pioneer studies in the development of *p-y* curve models based on full-scale field tests for soft clay, stiff clay, and sand, respectively. Revised versions of their proposed models are suggested by API (American Petroleum Institute) as design codes for laterally loaded piles in soft/stiff clay and sand.

Matlock (1970) performed a series of field tests on steel piles embedded in soft normally consolidated marine clay. He loaded the instrumented pile in three loading conditions, including short-time static loading, cyclic loading, and subsequent loading with forces less than the previous maximum values. The proposed model for static *p-y* curve in soft clay consists of a parabolic curve for the relationship between the soil reaction, *p*, and the pile deflection, *y*, ending in a horizontal line, representative of the ultimate resistance (Figure 16). The following equations are presented for the soil's ultimate resistance and the parabolic *p-y* curve for static loading condition:

$$p_u = N_p c d$$

and

$$p/p_u = 0.5\left(\frac{y}{y_c}\right)^{1/3}$$

where c is the soil strength, d is the pile diameter, N_p is the non-dimensional ultimate resistance coefficient which varies from 3.0 at ground surface to 9.0 at the reduced resistance depth of the pile, y_c is the pile deflection corresponding to 50% of the ultimate soil strength and is expressed as:

$$y_c = 2.5\varepsilon_c d$$

In the equation above, the parameter ε_c is the strain corresponding to the stress equal to 50% of the soil ultimate stress in stress-strain curve, which can be obtained from laboratory/in-situ test results. This parameter (sometimes expressed as ε_{50}) is used widely in empirical *p-y* models.

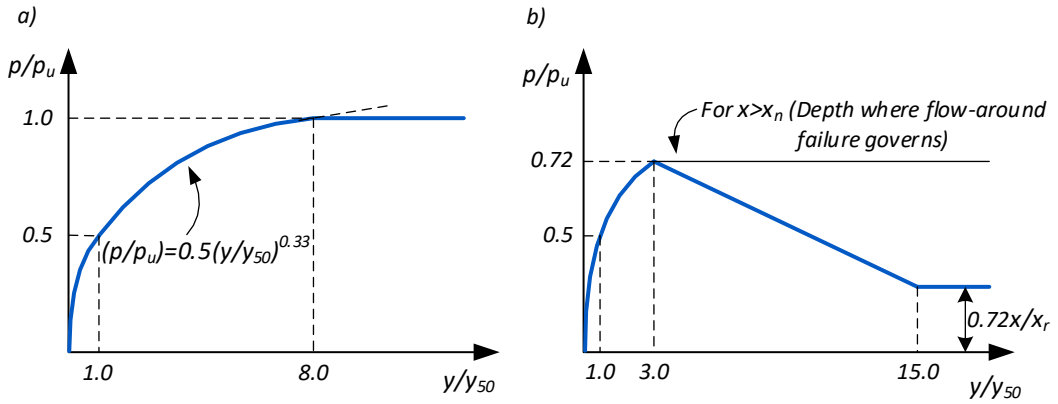

Figure 16. p-y curve characteristics for soft clays, a) short-term (static) loading, b) cyclic loading, adopted from Matlock (1970)

Reese et al. (1975) proposed multi-portion *p-y* curves for static and cyclic loading conditions acting on laterally loaded piles embedded in stiff clays. Their *p-y* models consist of multiple straight lines and parabolas, which represent the brittle behavior of stiff clays (Figure 17). The proposed models shown in Figure 17 were developed based on a series of field test data from full-scale open-ended steel pipe piles embedded in stiff pre-consolidated marine clay. The water table in their tests was

maintained at the ground surface level and strain gauges, deflection gauges, and load cells were installed on the piles to capture the experimental data. As shown in Figure 17a, the proposed *p-y* curve model for static loading consists of three straight lines and two parabolas. The initial line represents the soil response to small pile deflections in pre-plastic ranges. The slope of this line is expressed as follows:

$$E_{si} = k_s x$$

where E_{si} is defined as the soil modulus, which varies linearly with depth, x, with the rate of variation equal to k_s.

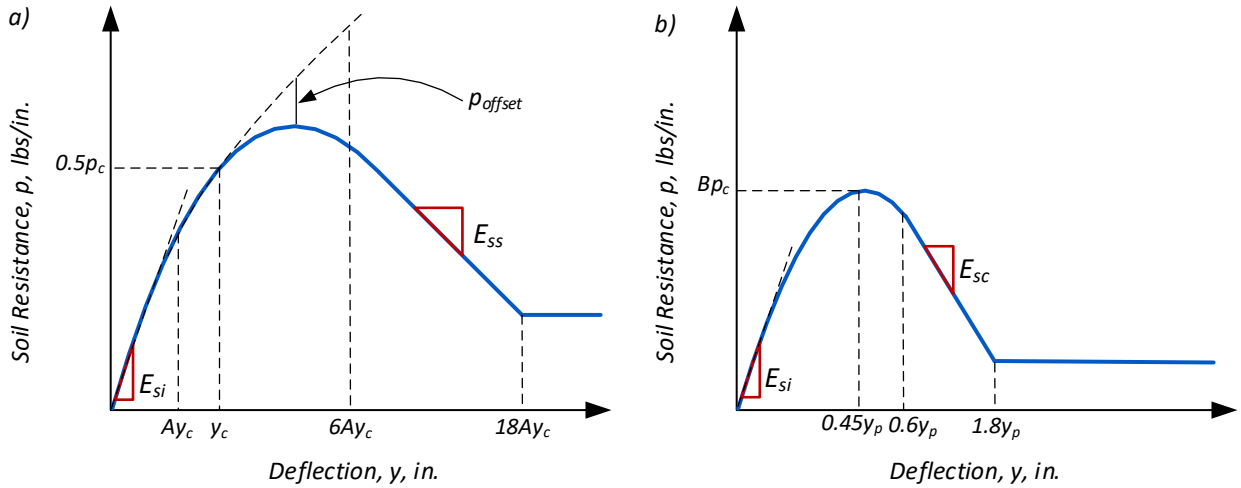

Figure 17. p-y curve models for stiff clay, a) static loading, b) cyclic loading, after Reese et al. (1975)

The second portion of the static *p-y* curve is assumed to begin at the intersection of the initial straight line and the parabola, as expressed in the following equation:

$$p = 0.5 p_u \left(\frac{y}{y_c}\right)^{0.5}$$

where y_c is defined as $\varepsilon_c b$ and p_u represents the ultimate resistance, which is obtained based on the concept of passive soil wedge failure and modified by the empirical factor, A. The third portion of the curve begins at $y_2 = A y_c$ and follows parabolic equation:

$$p = 0.5 p_u \left(\frac{y}{y_c}\right)^{0.5} - 0.055 p_u \left(\frac{y - A y_c}{A y_c}\right)^{1.25}$$

The curve continues as a straight line after point 3 with $y_3 = 6A y_c$ with a slope equal to E_{ss} expressed as follows:

$$E_{ss} = -\frac{0.0625 p_u}{y_c}$$

Eventually, the *p-y* curve merges to a horizontal line when *y* is equal to $18Ay_c$. The development of the *p-y* curve model for cyclic loading condition proposed by Reese et al. (1975) follow similar steps to the static curve, with altered equations and empirical coefficients (Figure 17b).

Reese et al. (1974) also performed static/cyclic load tests on similar piles to those (Reese et al., 1975), which were embedded in clean fine sands with the water table above the groundline. Their proposed *p-y* curve model for sand consists of three straight lines and one parabola (Figure 18). The initial portion of the curve is defined as identical to their model for stiff clay. The ultimate resistance of the soil is determined separately for near the ground depths and considerable depths. For shallow depths, a passive soil wedge was assumed to obtain p_u, and for deeper layers, a failure model based on horizontal soil flow was assumed. The two mentioned methods for obtaining the ultimate soil resistance coincide in the intersection depth, expressed as x_t. To match the computed values with the measured ones, the obtained ultimate resistance values were modified by empirical factors, A_s and A_c for static and cyclic loading conditions, respectively.

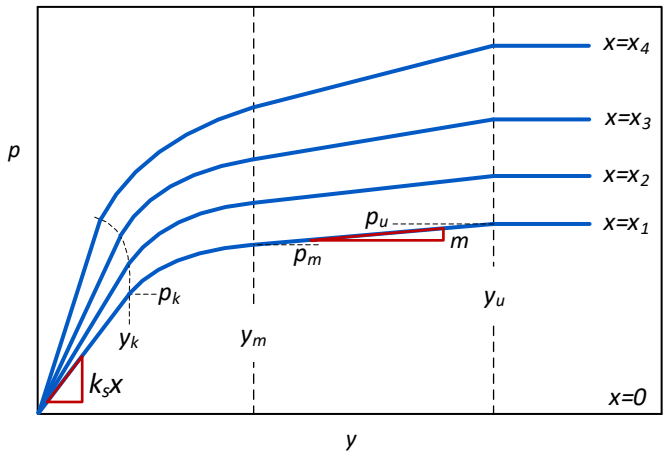

Figure 18. p-y curve models for sand, after Reese et al. (1974)

The parabolic portion follows the equation below:

$$p = Cy^{\frac{1}{n}}$$

where:

$$C = \frac{p_m}{y_m^{\frac{1}{n}}}$$

and,

$$n = \frac{p_m}{my_m}$$

With the obtained value for p_u and the defined values for y_m and y_u, the values of p_m and p_k can be calculated.

Mokwa et al. (2000) developed a spreadsheet, called PYPILE, to generate *p-y* curves for soils with both friction and cohesion (*c-φ* soils), using EVANS JR (1982) formulations. The spreadsheet was developed based on a series of field tests on 20 drilled shafts embedded in partially saturated silts and clays, performed by Helmers (1997). The ultimate resistance, p_u, is determined based on modified values of Brinch-Hansen's formulations. The relationship between the soil reaction (*p*) and the pile deflection (*y*) follows a cubic parabola, similar to Matlock (1970) model, expressed as follows:

$$p = 0.5 p_u \left(\frac{y}{A\varepsilon_{50} b}\right)^{0.33}$$

where *A* is the stress-strain coefficient (EVANS JR, 1982), which is determined by matching the computed deflections with the measured ones. Mokwa et al. (2000) also compared the results with the *p-y* curves for *c-φ* soils in *LPILE Plus 3.0*. As a result of this comparison, they reported that LPILE underestimates the contribution of cohesion which leads to lower ultimate capacities and higher deflections than the measured values, as reported by H. Yu et al. (2019).

In one of the few studies related to the force-deflection behavior of laterally loaded piles in gravelly soils, H. Yu et al. (2019) investigated the behavior of laterally loaded reinforced concrete piles in sloping ground, consisted mainly from gravel. As reported by H. Yu et al. (2019), the pile-head deflection variations versus lateral load in all slope gradients follows the same typical three-portion *p-y* curve, described in previous section, including an initial straight line representing the linear-elastic deflections, an elastic-plastic curve, and a limiting value corresponding to the failure capacity of the soil-pile system.

Model-Scale Laboratory Experiments

While being the most reliable method to develop *p-y* curves, full-scale field tests are extremely expensive and time consuming and may not be feasible for all projects and research purposes. To reduce the cost and the time of investigating *p-y* behavior, researchers have been developing model-scale experiments on laterally loaded piles. The laboratory experiments can be divided into two groups: 1g model-scale experiments, and centrifuge modeling.

1g Models

Tokimatsu and Suzuki (2004) investigated the effects of soil density and pore-water pressure response on the *p-y* behavior of liquifiable sand by conducting three model-scale shaking table tests on 2 × 2 steel pipe pile groups. The liquifiable sand layer of the soil profile in their experiments included three portions of loose, medium, and dense sands. Their results indicated that the pore-water pressure experienced significant reductions with an increase in lateral load in the dense layer, resulting in larger soil reactions to pile deflections (i.e., stress-hardening *p-y* behavior). In contrast, the sand in the loose layer showed minor reduction in pore-water pressure and small soil reactions to pile deflections (i.e., stress-softening *p-y* behavior). The reduction of

pore-water pressure was attributed to the dilative tendencies in dense sands with smaller void ratio than critical void ratio.

Tak Kim et al. (2004) conducted a series of monotonic loading tests on preinstalled and driven single piles embedded in a steel box container of sand to investigate the effects of installation method, pile head restraint, and soil relative density on the *p-y* response of laterally loaded piles. The model's scaling factor for the pile was 34, and the soil modulus was not scaled. Based on the obtained *p-y* curves from experimental data, Tak Kim et al. (2004) proposed a hyperbolic *p-y* curve, which takes into account the effects of pile head restraint, installation method, and relative density.

$$p = \frac{y}{\frac{1}{k_i} + \frac{y}{p_u}}$$

where k_i is the initial slope of the hyperbolic curve and is expressed as the following equation:

$$k_i = F_1 \eta_h z$$

In the above equation, F_1 is the initial stiffness modifying factor, which is established to be 1.0 for preinstalled piles, and 1.5, 2.0, and 2.5 for driven piles with 0.5 *J*, 1.0 *J*, and 1.5 *J* of driving energy, respectively. Note that the driving energy of a pile increases with an increase in relative density. Additionally, η_h is the subgrade modulus that controls the variation rate of k_i with depth, *z*, with average values of 21.1 and 32.5 MN/m_3, respectively for medium and medium dense sands. Furthermore, the following equation has been proposed to calculate the soil-pile ultimate resistance, p_u:

$$p_u = F_2 K_p D \gamma' z^n$$

where *D* is the pile diameter, γ' is the soil's effective unit weight, K_p is the coefficient of passive earth pressure, *n* is a constant with average values of 0.4 and 0.7 for free and fixed head conditions, successively, and F_2 is the ultimate resistance modifying factor that is established to be 1.0 for preinstalled piles, and 2.0, 3.0, and 4.0 for driven piles with 0.5 *J*, 1.0 *J*, and 1.5 *J* of driving energy, respectively. The main assumption of the load-transfer approach is that layers of the soil (i.e., springs) do not interact with each other. Therefore, the pile-head fixity condition should not affect the response of the subsequent layers below the ground surface. The results of the Tak Kim et al. (2004) study indicated that the soil response along the pile is affected by the pile-head restraint.

Centrifuge Models

Centrifuge modeling has been employed by several researchers to investigate the behavior of deep foundations (Barton et al., 1983; Brandenberg et al., 2005; Brant & Ling, 2007; Choo & Kim, 2016; Ghayoomi et al., 2018; González et al., 2009; Haouari & Bouafia, 2020; Lee et al., 2019; Wilson et al., 1997). The main advantage of using the centrifuge apparatus in performing lateral loading tests on model-scale piles is the possibility of scaling the stress-state of the actual soil mass in smaller-scale models relative to 1g models, along with other properties of the soil-pile system.

This advantage is achieved by increasing the gravitational acceleration during the centrifugation of the model and using larger scaling factors (i.e., smaller models) compared to 1g models.

The instrumentation of the centrifuge soil-pile models typically includes strain gauges attached to the pile for capturing the bending strains along the pile, displacement sensors (LVDT) installed to the pile head, and pore-water pressure transducers inserted in the soil around the pile for measuring the pore-water pressure variations in fully/partially saturated experiments.

Due to the smaller dimensions of the centrifuge models and faster test procedures compared to other experimental methods, centrifuge models are more favorable for conducting parametric studies of the effects of different soil/pile properties, such as the pile-head restraint, diameter effect, material and geometry, and soil compressibility and state parameter, on the lateral response of the pile. Another advantage of centrifuge modeling is the ability to perform in-flight miniature cone penetration tests to obtain soil properties after centrifugation. In-flight CPTs were conducted by Price (2018) to investigate the behavior of low plasticity silt-clay mixtures. Figure 19 illustrates the schematics of the setup used by Price (2018).

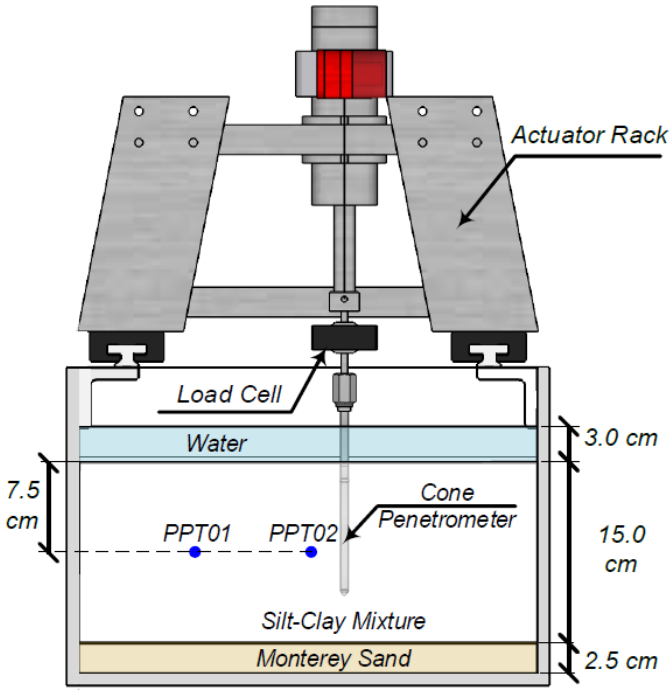

Figure 19. Schematic of the in-flight cone penetration sounding with sensor locations (Price, 2018)

p-y curves for a laterally loaded model pile can be derived from the experimental results of the centrifuge tests through a simple mathematical procedure discussed later in the present chapter.

Barton et al. (1983) conducted a series of cyclic lateral loading tests in the Cambridge University's geotechnical centrifuge to evaluate the API recommendations for *p-y* curves of single large diameter monopoles of offshore structures in sand. The model soil-pile used in this study included a single aluminum tube pile embedded in saturated fine sand with 80% relative density. Drained

triaxial compression test with the confining pressure equal to 200 *kPa* resulted in an internal friction angle of 40.5°. The applied lateral load, pile head bending moment and displacement, and bending moments along the pile were measure at the peak value of 20 load cycles in each test. Barton et al. (1983) observed that during the first half of the load cycles, the soil in front of the pile near the ground surface experiences shearing and failure, and the soil behind separates from the pile, and therefore, a gap forms. In the presence of the free water, the failed soil particles liquefy and fill the gap. Eventually, the soil particles falling into the gap will densify during the reversal of the loading direction. The described procedure results in stiffer lateral responses of the pile with increasing loading cycles until a steady state is reached. In all experiments, an eroded elliptical zone has been observed around the pile head with the major axis extending to 1.5-2.0 times of the pile diameter in the loading direction and down to half of the pile diameter in depth. Below the eroded zone, plastic deformations happened in the surrounding soil, and at great depths, the deformations were small and the soil response fell mostly in elastic ranges. Barton et al. (1983) compared the experimental *p-y* curves with the API-recommended version. They reported that the variation of the initial stiffness of the curves is proportional to the square root of the depth rather than a linear relationship. Also, the ultimate resistances of the API method were reported conservative near the ground surface and overestimated at great depths. However, good agreements were reported between the shape of the API *p-y* curves and the measured ones.

Lee et al. (2019) conducted a series of centrifuge static and cyclic lateral loading tests on a model-scale monopile embedded in sand. Two different soil boxes were designed for the one-direction static and two-direction cyclic loading tests to account for the soil's boundary effects. The gravitational acceleration was 92.4g. They observed that by increasing the depth, the number of cycles, and the magnitude of cyclic load the slope of the cyclic *p-y* curves increases. This behavior is attributed to the densification of the surrounding sand due to the back and forth displacement of the pile. Lee et al. (2019) used the experimental data to propose the backbone *p-y* curve for large diameter monopiles in sand. The backbone *p-y* curve is constructed from the maximum values in cyclic *p-y* curves. The proposed *p-y* relationship is a hyperbolic function similar to the one proposed by Tak Kim et al. (2004) but with adjusted values for fitting parameters. Similar study was conducted by Yoo et al. (2013) and the following equations were proposed for determining the ultimate resistance, p_u, and the initial slope, k_i, for loose and dense dry sands:

$$p_u = 13.3DK_p\gamma' z^{1.02} \qquad ; dense\ dry\ sand$$

$$p_u = 12.5DK_p\gamma' z^{0.90} \qquad ; loose\ dry\ sand$$

and,

$$k_i = \frac{Kp_u}{p_u - K\frac{D}{100}}$$

where *K* is the subgrade reaction modulus and is defied based on the equation proposed by Janbu (1963).

One of the main applications of laterally loaded piles is large diameter monopiles as the foundation of offshore wind turbines. The accuracy of the *p-y* relationships in sands suggested by API and Reese methods (API, 2011; Reese et al., 1974) for large diameter monopiles has been questioned by several researchers (Achmus et al., 2005; Choo & Kim, 2016; Dyson & Randolph, 2001; Haiderali et al., 2013; Klinkvort et al., 2010) . For instance, Choo and Kim (2016) compared experimental *p-y* curves obtained from 60 and 75*g* centrifuge tests with existing conventional *p-y* models. They performed a series of lateral load and overturning moment tests on copper and steel piles representing prototype monopiles with 6 *m of* outer diameter. The experimental curves indicated softer *p-y* variations than those suggested by API and Reese methods. This behavior is attributed to the effects of pile diameter, since the mentioned conventional models were developed based on field tests on piles with relatively small diameters.

Haouari and Bouafia (2020) proposed equations for the initial stiffness and the ultimate resistance in the hyperbolic *p-y* curve, taking into account the effects of the pile's flexural rigidity. They used the results of a series of centrifuge model tests coupled with three-dimensional finite element analysis for obtaining the *p-y* curves for rigid and semi-rigid piles embedded in very dense sand (D_r=92%). Figure 20 indicates the *p-y* model proposed by Haouari and Bouafia (2020).

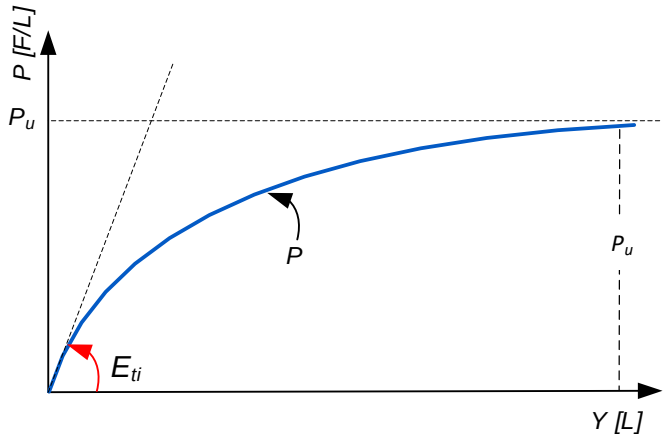

Figure 20. p-y curve model for rigid and semi-rigid piles, after Haouari and Bouafia (2020)

The initial stiffness of the curve, E_{ti}, varies linearly with depth with the average value of 9.0 as its slope. Moreover, they presented the following equation was presented for the ultimate resistance, P_u:

$$P_u = aK_p^2\gamma_d B(z+b)$$

where a and b are coefficients of the ultimate soil-pile resistance which depend on the pile's flexural rigidity.

Brandenberg et al. (2013) formulated a dynamic liquefiable soil-structure interaction material model called PyLiq1and implemented in *OpenSees*. They compared the resulted measurements of two centrifuge test models of single pile in level liquefiable sand and 2 × 3 group pile in laterally spreading liquefiable sand performed by Wilson et al. (1997) and Brandenberg et al. (2005). The

schematics of the two centrifuge models are illustrated in Figure 21 and Figure 22. The material model used in this study follows the same formulation as the PySimple1 model, which has been implemented in *OpenSees* in a number of dynamic analysis studies such as McKenna et al. (2010). The only difference is that the PyLiq1 incorporates the effects of cyclic liquefaction by correlating the material's capacity in a degrading manner to the mean effective stress. Accordingly, the ultimate capacity of the material degrades as the mean effective stress is reduced to a minimum value, known as the residual resistance, at zero mean effective stress. Figure 23 illustrates the concept of the PyLiq1 material model.

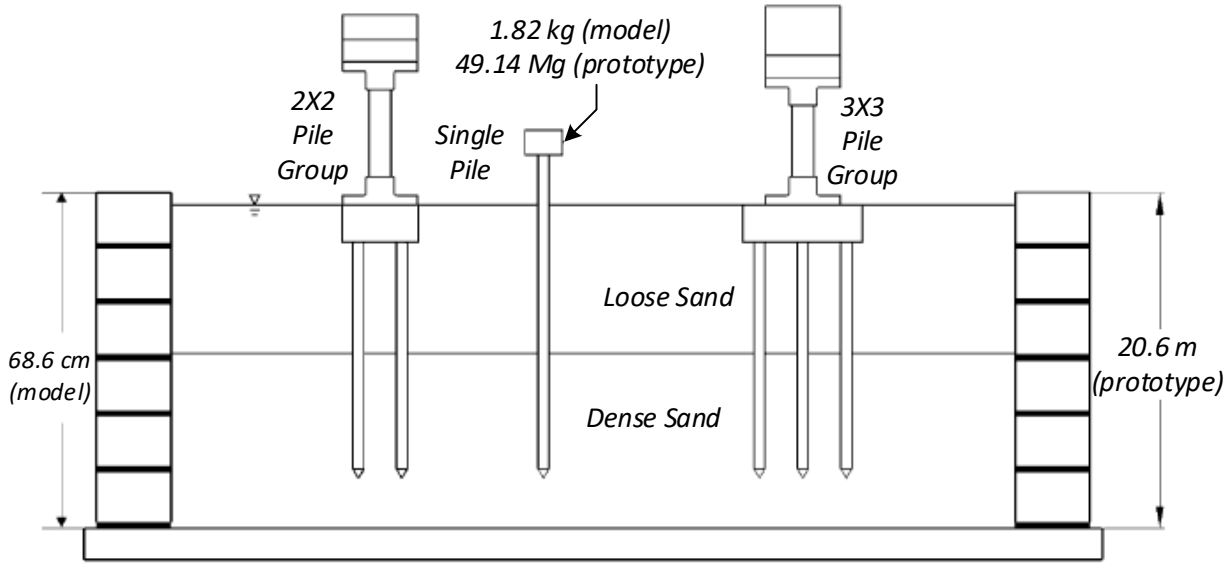

Figure 21. Model sketch for centrifuge tests of piles in level liquefiable sand (Brandenberg et al., 2013)

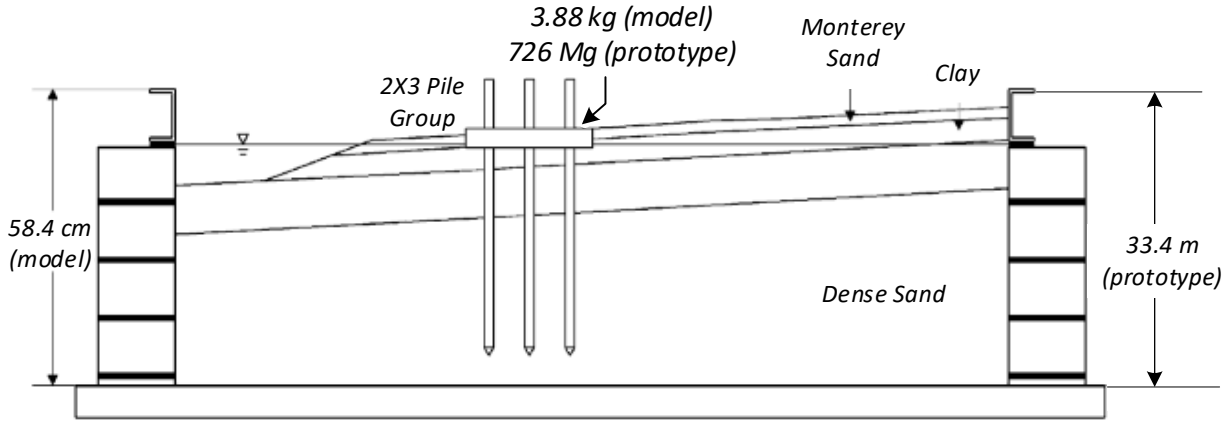

Figure 22. Model sketch for centrifuge tests of piles in sloping liquefiable sand layer with lateral spreading (Brandenberg et al., 2013)

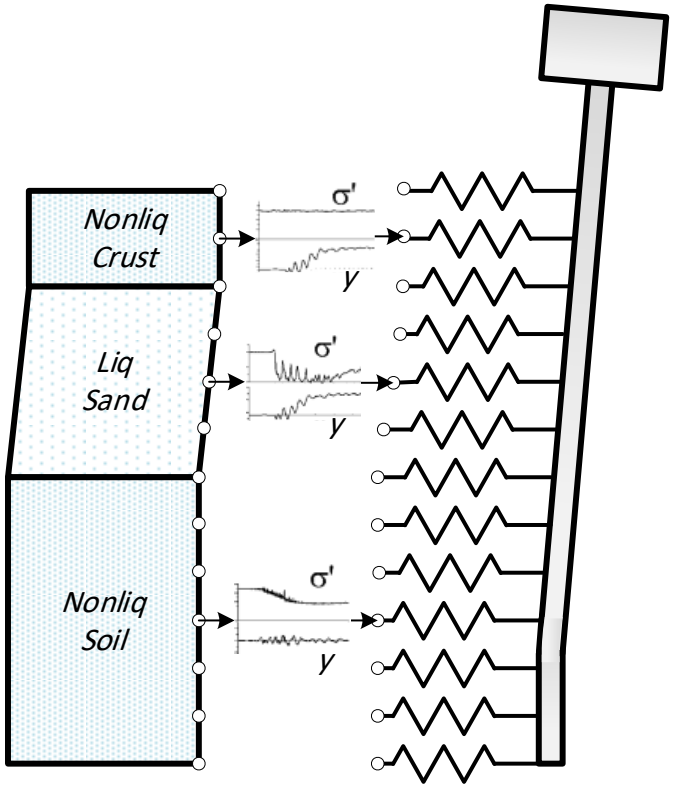

Figure 23. Schematic of the PyLiq1 material model, after Brandenberg et al. (2013)

Comparison between the centrifuge test results and the model predictions showed good agreement between the measured and predicted *p-y* responses. Brandenberg et al. (2013) stated that the cyclic mobility behavior is associated with the inverted s-shaped stress-strain curve of the material, and thus, results in an inverted s-shaped *p-y* response.

In-Situ Tests

In-situ tests such as standard penetration test (SPT), pressuremeter test (PMT), dilatometer test (DMT), and cone penetration test (CPT) are considered as fast and affordable tools for site investigation. With the increasing demand in the use of in-situ tests in geotechnical engineering, several studies have attempted to develop frameworks, based on the soil's stress-strain behavior during in-situ tests and the existing correlations in technical literature, to develop and assess p-y curves (Anderson et al., 2003; Ariannia, 2015; Briaud et al., 1983; Robertson et al., 1989; P. K. Robertson et al., 1985).

P. K. Robertson et al. (1985) proposed a *p-y* model developed directly from PMT data, based on a full-scale field test and pressuremeter tests. They suggested that the *p-y* curve for a given depth can be obtained by transferring the pressuremeter curve (stress-volume) to their soil reaction-pile deflection curve (soil pressure on unit length of the pile-displacement) by multiplying the components to pile's diameter and applying a reduction factor, α, to the pressure component. The reduction factor is suggested to be 2.0 for clays and 1.5 for sands. Robertson et al. (1989) suggested

that the *p-y* curve for both cohesive and cohesionless soils can be assumed to follow the Matlock's cubic parabola function with p_u obtained from DMT results.

Briaud et al. (1983) presented a PMT-based *p-y* model. The proposed *p-y* curve consists of two components, the front resistance curve (*Q-y*) and the friction resistance curve (*F-y*). The *Q-y* and *F-y* curves are obtained point by point from the pressuremeter curve. The following equations are presented for obtaining the front resistance curve:

$$Q = SQ \times p^* \times B$$

$$y = \frac{\Delta R}{R_0} \times R$$

where *SQ* is a coefficient related to elasticity, *B* is the pile diameter, *p** is the net pressure from pressuremeter curve, and ΔR is the change in the soil cavity radius from its initial value, R_0.
The *F-y* equation are also presented as the following equations:

$$F = SF \times B \times \chi(1+\chi) \times \frac{\Delta p^*}{\Delta \chi}$$

where *SF* is a shape factor related to elasticity, and χ is the cavity volume change ratio ($\chi = \Delta V/V_0$). The final *p-y* curve is obtained from the summation of *Q-y* and *F-y* curves. The accuracy of the proposed model was validated with several field test results from a variety of soil types and pile properties and the predictions were observed to have good agreement with field test results.

Li et al. (2018) developed a framework in which the parameters of Matlock's cubic parabola function for soft clay are determined from piezocone test (CPTu) results. The proposed *p-y* model is expressed as the following equation:

$$p = 0.5\left(\frac{N_c}{N_e} q_e D\right)\left[\frac{100y}{\left(0.215\,{}^{q_c}/_{P_a} - 1.25\right)D}\right]^{\frac{1}{3}}$$

In the equation above, N_c is the Matlock's bearing capacity factor (earlier referred as N_p), N_e is the effective cone factor, q_e is the effective cone resistance ($q_e = q_t - u_2$, with q_t and u_2 being the actual cone resistance and shoulder pore-water pressure, respectively), *D* is the pile diameter, q_c is the cone tip resistance, and P_a is the atmospheric pressure. Validation of the method with two case histories showed well predictions.

Ariannia (2015) developed a framework for computing input parameters of the *PySimple3* program directly from CPT measurements. *PySimple3* is a program in *OpenSees* which creates three-portion *p-y* curves, described in the beginning of the chapter. The inputs for *PySimple3* are the initial stiffness, K_e, the ultimate capacity, p_u, the yield resistance, p_y, and the shape factor, *C*. In the proposed framework, the soil is characterized by an index, called the soil behavior type index (I_c), expressed as the following equation:

$$I_c = \sqrt{(3.47 - \log Q_t)^2 + (\log F_t + 1.22)^2}$$

where Q_t and F_t are the normalized cone resistance and normalized friction ratio, respectively, which can be obtained from CPT measurements. Based on the value of I_c, soils are divided into three types, including sand-like ($I_c \leq 2.3$), clay like ($I_c \geq 2.7$), and intermediate ($2.3 < I_c < 2.7$). The initial stiffness, K_e, is defined as a function of shear wave velocity which is either measured directly in seismic cone penetration tests (SCPT) or obtained with appropriate CPT correlations. For sand-like behavior soils, the ultimate resistance, p_u, is determined based on the peak friction angle which can be obtained from CPT data based on the critical state soil mechanics' concept. For clay-like behavior soils, the ultimate resistance is a function of the undrained shear strength. For intermediate soils, the ultimate resistance is obtained from a linear interpolation between the upper and lower limits with respect to I_c. The yield resistance, p_y, is the soil reaction corresponding to the displacement at the end of the elastic zone. The following equation will yield p_y:

$$p_y = K_e y_y = K_e\left[2.5B\gamma_y B/(1+\nu)\right]$$

where B is the pile diameter, and γ_y is the yield strain which is obtained from the soil's stress-strain curve, and ν is the soil Poisson's ratio. Lastly, the shape factor, C, which controls the shape of the transition curve is defined as a function of the other three inputs and is expressed as the following equation:

$$C = \frac{p_y - 0.5p_u + (p_u - p_y)\ln(p_u - p_y) - (p_u - p_y)\ln(0.5p_u)}{K_e y_{50} - 0.5p_u}$$

Comparison of the proposed *p-y* curves with measured ones from five different sites showed generally good agreement.

To investigate the reliability of in-situ test results in predicting the behavior of laterally loaded piles, Anderson et al. (2003) implemented a comprehensive comparison of the *p-y* curves derived from SPT and CPT predicted soil parameters and directly derived DMT and PMT *p-y* curves with five case histories. Case histories included full-scale field test data in a variety of soil types, such as loose to dense sand, silty sand, clay, silty clay, and gravel. A software named FLPier was used to develop *p-y* curves from soil parameters that were obtained from SPT and CPT results. FLPier uses O'Neill and Murchison (1983) model for sand below the water table, Reese et al. (1974) model for sand above the water table, O'Neill and Gazioglu (1984) model for soft to medium stiff clay above the water table, Matlock (1970) model for soft to medium stiff clay below the water table, Welch (1972) and Reese and Welch (1975) models for stiff clay above the water table, and Reese et al. (1975) model for stiff clay below the water table. The input soil parameters for different soil types include internal friction angle, horizontal subgrade reaction modulus, unit weight, undrained shear strength, and soil's strain at 50% and 100% of the ultimate capacity. Some existing correlations in the literature were used to obtain the input soil parameters from SPT and CPT results (Peck et al., 1974; Robertson & Campanella, 1983; Terzaghi, 1955; Terzaghi & Peck, 1968).The dilatometer indices coupled with a cubic parabola function were used to develop the DMT-based *p-y* curves and the method proposed by P. Robertson et al. (1985) was utilized to develop the PMT-based *p-y* curves. Results of the comparison between different in-situ based *p-y* curves and field test results concluded that the cone penetration test results offer the best predictions of the field behavior. The SPT-based *p-y* curves overestimated the soil response at all

loading levels. Since the dilatometer membrane in DMT only expands 1mm, the DMT predictions were only reliable at small lateral loads. Ultimately, The PMT-based *p-y* curves offered well predictions for sand below the water table and clay above the water table, but the predictions were poor in other soil types.

Numerical Simulation

With the advancements in computational tools and numerical techniques, the demand for reliable and accurate analysis of the laterally loaded pile has increased. The application of numerical methods in capturing the interactions of laterally loaded soil-pile systems leads to more accurate predictions compared to empirical methods. As one of the results of numerical models, *p-y* curves can be derived for development and assessment of *p-y* models, as well as conducting parametric studies on the influence of different aspects of the problem.

Three-dimensional finite element (FE) models were developed by Brown and Shie (1990) to assess the plastic deformations in soil and gap formation at the soil-pile interface and to compare the derived *p-y* curves from FE analysis with the ones obtained from empirical methods. Two constitutive models were used, including an elastic-plastic Von Mises (VM) model for clay and two extended Drucker-Prager (EDP) models with different friction angles for sand. To obtain the numerical *p-y* curves, the *p* component was derived from the output bending moment data and the *y* component was used directly from the pile nodes displacements. Empirical *p-y* curves were developed using Matlock's and Reese's methods for clay and sand, respectively. Comparison between the VM model *p-y* curves and the empirical ones showed that the reduction of soil resistances near the ground surface is less in the VM model *p-y* curves. This behavior was attributed to assumption that the loading condition near the ground surface is more similar to the triaxial extension test, but the undrained shear strength used to develop empirical *p-y* curves are often obtained from unconfined and UU triaxial tests. Brown and Shie (1990) have also stated that the VM constitutive model used in their study is capable of capturing the nonlinearity of the soil and the gap formation, but it is not likely to represent the undrained loading in clay. For the two EDP models in sand, slight soil cohesions were considered to avoid the immediate failure of the soil elements behind the pile. Therefore, the comparison of the numerical and empirical results was difficult. However, the empirical *p-y* curves indicated significantly lower soil resistances at ground surface.

Using three-dimensional finite element analysis for a two-surface plasticity model, Choobbasti and Zahmatkesh (2016) computed the degradation factors for the backbone *p-y* curves in liquefiable sands. During liquefaction, piles experience significant reduction in their bearing capacities. Therefore, the backbone curve of the dynamic *p-y* curves in liquefied soils can be obtained by applying degradation factors to the non-liquefied backbone *p-y* curve. The degradation factors were computed by comparing the results of models in two cases of liquefiable and non-liquefiable sands, and then validated through a pseudo-static analysis based on centrifuge test results reported by Wilson (1998). Their results indicated that the two-surface plasticity model is capable of predicting the response of the pile in liquefiable soils and that the degradation factors are strongly dependent on the applied earthquake amplitude and sand type.

In one of the few studies of *p-y* curve method in gravelly soils, G. Yu et al. (2019) proposed a hyperbolic *p-y* function, based on 3D FE analysis in PLAXIS, with new equations for the initial stiffness and the ultimate resistance to predict the behavior of laterally loaded piles in cement-improved gravel. Static load tests were performed on drilled shafts embedded in jet-grouted gravel (in front half of the shaft) to back-calculate the model inputs for virgin and improved soil and to validate the proposed equations. The response of the pile was considered to be linear elastic in the numerical model, and the Mohr-Coulomb constitutive model was utilized for both the virgin and grouted soils. The following equations were proposed for the initial slope and the ultimate resistance:

$$k = 0.86E_s z^{-0.416}\sqrt{1.433 + 1.384\frac{R}{R_{ref}}}$$

and,

$$p_u = K_p^2 \gamma D\left[1.318 + 0.63(\frac{R}{R_{ref}})^{0.88}\right](\frac{z}{R_{ref}})^{0.5}$$

In the equations above, E_s is the virgin soil's elastic modulus, R and R_{ref} are the radii of grouted soil and the pile, respectively, z is the depth below the ground surface, γ is the soil effective unit weight, and K_p is the passive earth pressure coefficient. The results of the numerical analysis indicated that the measured and simulated *p-y* curves coincide reasonably, and the Mohr-Coulomb model is suitable for capturing the nonlinear behavior of the soil. Also, comparison between the proposed *p-y* curves and the field test results suggested well agreement.

Construction of p-y Curves from Experimental Data

Experimental methods for development of the *p-y* curves include load tests on instrumented piles. The loaded pile is attached with several strain gauges along its buried depth to capture the horizontal strain values at multiple depths when the pile is loaded. For a Euler-Bernoulli beam with constant material and cross section (i.e., constant flexural rigidity), the construction of *p-y* includes the following general steps:

Step 1: After the strain gauges data are acquired, the distribution of bending moment along the pile can be obtained using the following equation:

$$M = 2E_p I_p \frac{\varepsilon}{B}$$

where M is the bending moment values at strain gauge points, E_p is the pile's Young's modulus, I_p is the moment of inertia of the pile's cross section, B is the pile's diameter, and ε is the horizontal strain values along the pile acquired from the experimental data.

Step 2: After the values of bending moment at the strain gauge points were obtained, an appropriate function should be fitted to the values of bending moment to obtain the bending moment function of depth, *M(z)*

Step 3: The function of the deflections along the pile, *y(z)*, can be obtained by a double integration of the bending moment function with respect to depth *(z)*:

$$y = \frac{1}{E_p I_p} \iint M(z) dz dz + y_0' z + y_0$$

where y_0' and y_0 are the pile head rotation and deflection, respectively.

Step 4: The function of the soil reaction along the pile, *p(z)*, can be obtained by a double differentiation of the bending moment function with respect to depth *(z)*:

$$p = -\frac{d^2 m}{dz^2}$$

Step 5: With the obtained functions of soil reaction and pile deflection along the pile for different values of lateral load (horizontal strain values), the *p-y* curves can be developed for any given depth.

The above-described procedure may also be applied to the output bending moment data of numerical models to develop the model's *p-y* curves.

Available *p-y* Curves in LPILE

LPILE is a computer program for the analysis of deep foundations under lateral loading, developed by the structural and geotechnical engineering software company called Ensoft, Inc. This program uses the *p-y* curve method to analyze laterally loaded piles embedded in different types of soils. LPILE is widely used for both research and practical purposes. According to the results of the survey (see Appendix), LPILE is MDT's preferred software for the design of laterally loaded piles in Montana. LPILE provides models and procedures for developing short-term static and cyclic *p-y* curves in different types of soils and rocks. All models are based on experimental data gathered from studies on full-scale field tests conducted on instrumented piles. Table 4 includes a summary of the available *p-y* curves in LPILE. For each type of soil/rock material, the influence of cyclic loading and pile diameter are incorporated into the proposed models.

Figure 24 illustrates the LPILE's conceptual *p-y* curves for static and cyclic loadings. The static *p-y* curve (Figure 24a) resembles the three-portion curve discussed earlier. The initial portion of the curve is linear or nearly linear, with the slope equal to the initial reaction modulus, E_{si}, representing the *p-y* relationship for elastic small deformations. The second portion is a curve, showing the strain softening behavior of *p* with respect to *y*. The curves end at a constant value of soil reaction, called the ultimate resistance, which represents the plastic behavior of the soil-pile with increasing strains without a loss in strength.

The initial slope of the *p-y* curves is related to the slope of the soil stress-strain curve in small strains. LPILE recommends field investigation and laboratory testing of soils to obtain the stress-strain curves for each type of material (cohesive soils, cohesionless soils, rocks) with specific formulations used accordingly. The ultimate resistance of the soil-pile system in both cohesive and

cohesionless soils is associated with two different failure mechanisms, passive soil wedge failure near the ground surface and flow-around failure at great depths (Figure 25).

As shown in Figure 24b, the general assumption of LPILE is that the cyclic loading causes a loss of resistance with decreasing the *p* value, which is expressed as a function of the number of loading cycles. However, it is assumed that the cyclic loading does not affect the resistance in small deformations, and the conceptual *p-y* curves are assumed to have identical behavior in their initial portions. For cohesive soils (i.e., clays), the loss of resistance due to cyclic loading is attributed to two reasons: 1) Repeated large magnitude strains, and 2) Scouring. When the pile is subjected to cyclic lateral load in stiff clay, a gap will form between the pile and over-consolidated clay. In this situation, if free water is present, the gap will be filled with water. When the next load cycle is applied, the water inside the gap will be forced to exit and wash out clay particles. This process is called scouring and can lead to extreme impacts on the lateral resistance of the soil-pile system. Figure 26 illustrates the scouring phenomenon.

In this section, recommended procedures by LPILE for developing *p-y* curves in different soils and rocks are discussed. Each procedure includes recommendations for computing the ultimate resistance, the initial stiffness, and the relationship between the soil reaction, *p*, and the pile deflection, *y*.

Table 4. Available p-y curves for different soils and rocks in LPILE

Soil Type	Free Water	Soil Condition	Loading Condition	Recommended Soil Tests	Source
Clay	Yes	Soft	Static/Cyclic	In-situ vane shear test UU triaxial compression test Miniature vane test of samples in tube Unconfined compression test	Matlock (1970)
Clay	Yes	Stiff	Static/Cyclic	UU triaxial compression test	Reese et al. (1975)
Clay	No	Stiff	Static/Cyclic	UU triaxial compression test	Welch (1972); Reese and Welch (1975)
Sand	Yes/No	-	Static/Cyclic	Fully drained triaxial compression test	Reese et al. (1974); API (2011)
Sand	Yes	Small strain	Cyclic	-	Hanssen (2015)
Sand	Yes	Liquefied	Cyclic	-	Rollins et al. (2006)
Sand	Yes/No	Cemented (c-φ)	Static/Cyclic	Direct shear test CD triaxial compression test	Reese et al. (1974)-Revised Ismael (1990)
Rock	-	Strong	Static/Cyclic	Subsurface investigation	Reese et al. (2005)
Rock	-	Weak	Static/Cyclic	Subsurface investigation PMT for very low RQD	Reese (1997)
Rock	-	Massive	Static/Cyclic	Subsurface investigation	Liang et al. (2009)
Loess	-	Loose	Static/Cyclic	-	Johnson (2006)
Layered Soil	-	-	-	-	Georgiadis (1983)

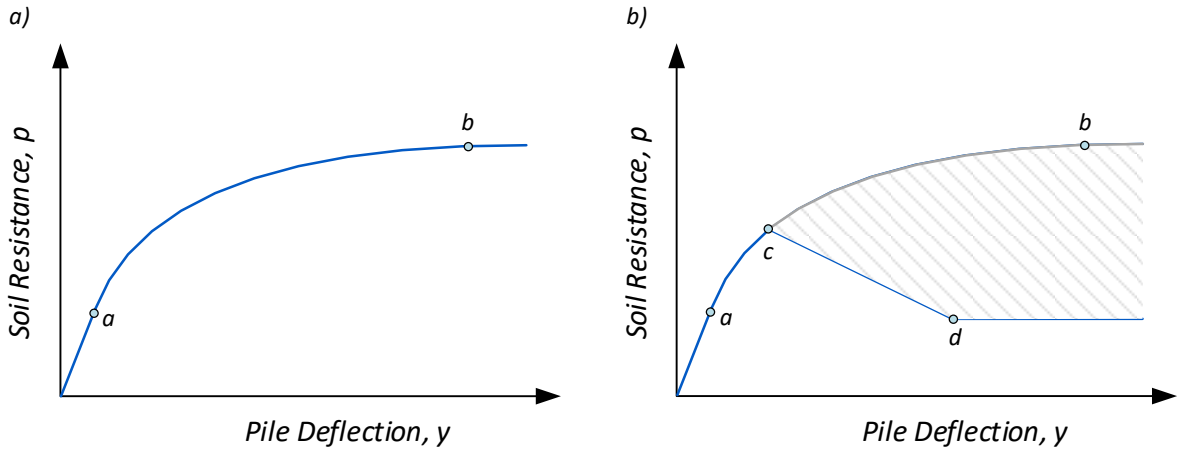

Figure 24. Conceptual p-y curves for a)static loading and b) cyclic loading, after Isenhower et al. (2019)

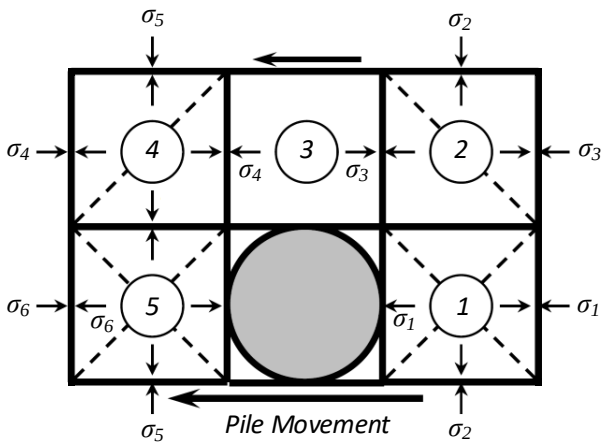

Figure 25. Illustration of the flow-around failure mode in cohesive and cohesionless soils (Isenhower et al., 2019)

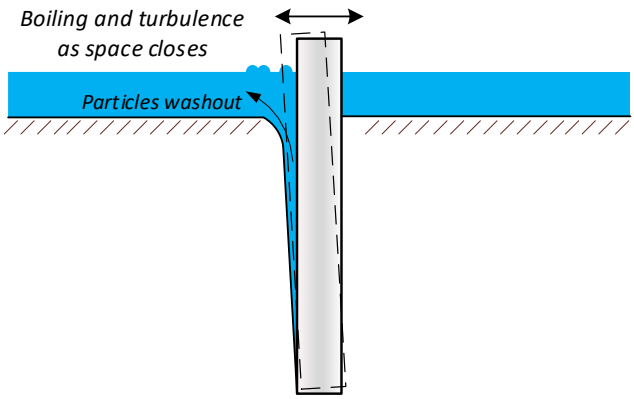

Figure 26. Scouring phenomenon in stiff clays with the presence of free water, after Isenhower et al. (2019)

p-y Curves in Cohesive Soils

LPILE utilizes the *p-y* curve models developed by Matlock (1970) for soft clays, Reese et al. (1975) for stiff clays in the presence of free water, and Reese and Welch (1975) for stiff clays without free water. These models were previously discussed in this chapter. The procedures associated with each soil and loading conditions are described here.

Soft clay-static loading p-y curve development procedure

The procedure of constructing static *p-y* curves for soft clay (Figure 16a) includes the following steps:

1. Determine the best estimate of the variations of undrained shear strength, *c*, and unit weight, γ, with depth.
2. Determine the value of the strain corresponding to the one-half of the principal stresses difference, ε_{50}. If the stress-strain curves are not obtained, the value of ε_{50} can be chosen from Table 5.

Table 5. Typical values of ε_{50} for different consistencies of clay

Clay Condition	ε_{50}
Soft	0.02
Medium	0.01
Stiff	0.005

3. The ultimate resistance, p_u, is the minimum of the values obtained from the two following equations:

$$p_u = \left[3 + \frac{\gamma'_{avg}}{c}x + \frac{J}{b}x\right]cb$$

$$p_u = 9cb$$

where

γ'_{avg} = average effective unit weight from ground surface to the depth of *p-y* curve, *x*,

J = 0.5 for soft and 0.25 for medium clays, respectively,

b = diameter of the pile

4. Compute the transition depth, x_r, by solving the two above-mentioned equations:

$$x_r = \frac{6}{\frac{\gamma'_{avg}}{c} + \frac{J}{b}} \geq 2.5b$$

5. Calculate the deflection associated with ε_{50+}:

$$y_{50} = 2.5\varepsilon_{50}b$$

6. Calculate points of the *p-y* curve from the origin to $y=8y_{50}$, using the Matlock's cubic parabola function:

$$p = 0.5p_u\left(\frac{y}{y_{50}}\right)^{1/3}$$

7. *P*-values continue to be constant beyond $y=8y_{50}$.

Soft clay-cyclic loading p-y curve development procedure

The procedure of constructing cyclic *p-y* curves for soft clay (Figure 16b) includes the following steps:

1. As shown conceptually in Figure 24b, the *p-y* curve for piles subjected to cyclic loading in soft clay doesn't degrade for small deformations. The boundary for small deformations is set to coincide with the *p*-value equal to $0.72p_u$. So, the *p-y* curve follows the same manner as the static one up to the mentioned value for *p*.

2. If the selected depth is equal or greater than the transition depth, x_r, the values of *y* corresponding to $p=0.72p_u$ are equal to $3y_{50}$. If not, *p*-values decrease linearly from $0.72p_u$ at $y=3y_{50}$ down to the values obtained from the equation below at $y=15y_{50}$:

$$p = 0.72p_u\left(\frac{x}{x_r}\right)$$

3. *p*-values continue to be constant beyond $y=15y_{50}$.

The following soil tests are recommended by LPILE for soft clays:

- In-situ vane shear test with parallel sampling for soil identification.
- Undrained-unconsolidated triaxial compression test with confining pressure equal to the overburden stress and undrained shear strength equal to one-half of the principal stresses difference.
- Miniature vane test of samples in tubes.
- Unconfined compression test.
- Tests for obtaining the total unit weight, water content, and effective unit weight.

Stiff clay-with free water-static loading p-y curve development procedure

The procedure of constructing static *p-y* curves for stiff clay in the presence of free water (Figure 17a) includes the following steps:

1. Determine the values of pile diameter, soil's effective unit weight, and undrained shear strength of clay at the desired depth.
2. Calculate the average value of the undrained shear strength over the desired depth, c_{avg}.
3. Calculate the soil resistance per unit length of the pile, p_c, from the following equations:

$$p_c = \min [p_{ct}, p_{cd}]$$

$$p_{ct} = 2c_{avg}b + \gamma' bx + 2.83c_{avg}x$$

$$p_{cd} = 11cb$$

4. Select appropriate value for the *p-y* curve shape modifying factor, A_s, as a function of normalized depth, *x/b* (Figure 27).

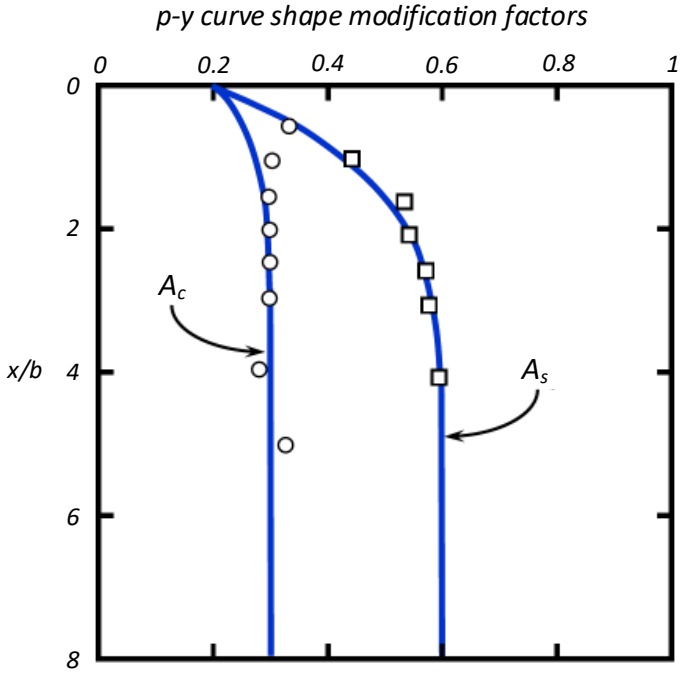

Figure 27. Shape modification factors for p-y curves in cohesive soils (Isenhower et al., 2019)

5. Create the initial linear portion, expressed as the following equation, by selecting the value of k_s from Table 6:

$$p = (k_s x)y$$

6. Compute y_{50} as:

$$y_{50} = \varepsilon_{50} b$$

7. Calculate the first parabola from $y=0$ to $y=A_s y_{50}$:

$$p = 0.5p_c(\frac{y}{y_{50}})^{0.5}$$

8. Calculate the second parabola from $y=A_s y_{50}$ to $y=6A_s y_{50}$:

$$p = 0.5p_c(\frac{y}{y_{50}})^{0.5} - 0.055p_c(\frac{y - A_S y_{50}}{A_S y_{50}})^{1.25}$$

9. Calculate the next straight-line from $y=6A_s y_{50}$ to $y=18A_s y_{50}$:

$$p = 0.5p_c\sqrt{6A_S} - 0.411p_c - \frac{0.0625}{y_{50}}p_c(y - 6A_S y_{50})$$

10. Calculate the final horizontal line:

$$p = 0.5p_c\sqrt{6A_S} - 0.411p_c - 0.75p_c A_S$$

Table 6. Typical subgrade reaction modulus values for static and cyclic loading in stiff clay

Average Undrained Shear Strength (*kPa*)	k_s **(MN/m^3)**	k_c **(MN/m^3)**
50-100	135	55
100-200	270	110
200-400	540	220

Stiff Clay-with Free Water-Cyclic Loading p-y curve development procedure

The procedure for constructing cyclic *p-y* curves for stiff clay in the presence of free water (Figure 17b) includes the following steps:

1. Determine the values of pile diameter, soil's effective unit weight, and undrained shear strength of clay at the desired depth.
2. Calculate the average value of the undrained shear strength over the desired depth, c_{avg}.
3. Calculate the soil resistance per unit length of the pile, p_c, using the same equations for static loading.
4. Select the appropriate value of A_c from Figure 27.
5. Calculate the value of y_{50} from the same equation used in static loading.
6. Calculate the value of y_p:

$$y_p = 4.1A_c y_{50}$$

7. Select the value of k_c from Table 6 and establish the initial linear portion of the curve using the equation below:

$$p = (k_c x)y$$

8. Calculate the first parabola from the intersection of the following equation to y=0.6y_p:

$$p = A_C p_c \left[1 - \left|\frac{y - 0.45y_p}{0.45y_p}\right|^{2.5}\right]$$

9. Calculate the next straight line from y=0.6y_p to y=1.8y_p:

$$p = 0.936A_C p_c - \frac{0.85}{y_{50}} p_c (y - 0.6y_p)$$

10. The final horizontal line for the p-values beyond y=1.8y_p are defined as the following equation:

$$p = 0.936A_C p_c - \frac{0.102}{y_{50}} p_c y_p$$

The following soil tests are recommended by LPILE for stiff clays with the presence of free water:

- Undrained-Unconsolidated triaxial compression test with confining pressure equal to in-situ total stresses for determining the undrained shear strength.
- Tests for obtaining unit weight.

It is worth mentioning that utilizing the above-mentioned procedure for developing cyclic *p-y* curves for stiff clays often results in overly conservative designs. This is because the reduction in clay resistance due to cyclic loading was more pronounced in the loading tests conducted by Reese et al. (1975) compared to other studies.

Stiff clay-without free water-static loading p-y curve development procedure

The procedure of constructing static *p-y* curves for stiff clay without free water (Figure 28) includes the following steps:

1. Determine the values of undrained shear strength, effective unit weight, pile diameter, and ε_{50}.
2. Calculate the average value of undrained shear strength, c_{avg}, and the average value of effective unit weight, γ'_{avg}, over the *p-y* curve depth, *x*.
3. Calculate the value of ultimate resistance based on the following equations:

$$p_u = \left[3 + \frac{\gamma'_{avg}}{c_{avg}} x + \frac{J}{b} x\right] c_{avg} b \leq 9 c_{avg} b$$

4. Obtain the value of y_{50} from the equation below:

$$y_{50} = 2.5\varepsilon_{50} b$$

5. Calculate the point of the curve from the origin to y=16y_{50}:

$$p = 0.5 p_u \left(\frac{y}{y_{50}}\right)^{0.25}$$

or

$$y = y_{50}\left[2\left(\frac{p}{p_u}\right)\right]^4$$

6. *P*-values remain constant beyond $y=16y_{50}$.

Stiff clay-without free water-cyclic loading p-y curve development procedure

The procedure of constructing cyclic *p-y* curves for stiff clay without free water (Figure 29) includes the following steps:

1. Develop the static *p-y* curve by following the previous procedure.
2. Determine the number of loading cycles, *N*, associated with the desired *p-y* curve.

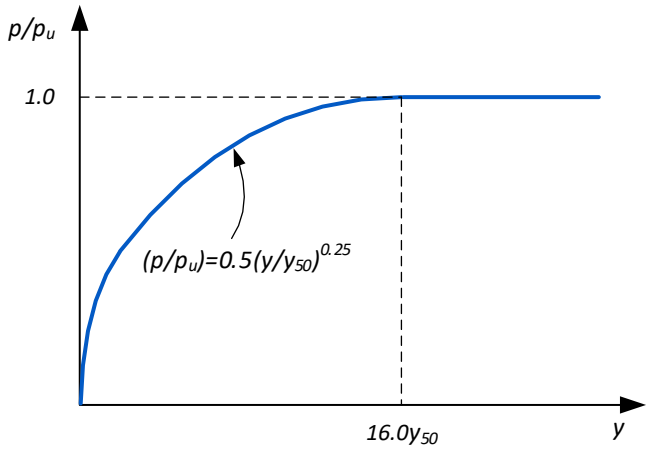

Figure 28. p-y curve in stiff clay without free water under static loading, after Reese and Welch (1975)

3. Compute the value of the parameter *C* for several values of p/p_u. *C* is a parameter for characterizing the influence of repeated loading on the deflection of the pile. The value of *C* can be obtained from the following equation:

$$C = 9.6\left(\frac{p}{p_u}\right)^4$$

4. *y*-values for cyclic loading, y_c, can be obtained from their corresponding *C*-values calculated in step 3. The equation for cyclic deflections is expressed as the following equation:

$$y_c = y_s + y_{50} C \log N$$

where y_s is the static deflection.

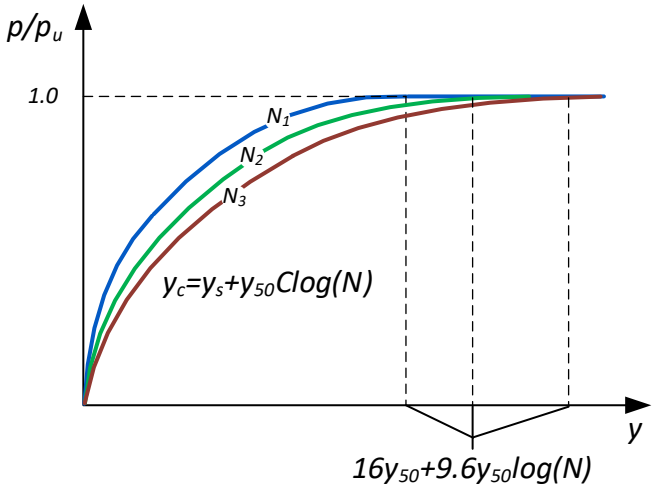

Figure 29. p-y curve in stiff clay without free water under cyclic loading, after Reese and Welch (1975)

Undrained triaxial compression tests are recommended by LPILE for stiff clays with no free water.

p-y Curves in Cohesionless Soils

The initial slope of the stress-strain curve in soils is a key parameter in p-y curve development. For sands, this parameter is a function of the confining pressure (i.e., the overburden stress) and shear stress magnitude. However, the strain fields around a laterally loaded pile are complex, making it difficult to obtain the initial stiffness of the p-y curve based solely on the mechanics of the soil. As discussed previously, failure mechanisms associated with sand are similar to those for cohesive soils. Near the ground surface, the equilibrium of internal forces of a passive soil wedge failure is assumed to obtain the ultimate resistance of the p-y curve. For greater depths below the ground surface, a flow-around failure determines the ultimate resistance.

LPILE states that insufficient data have been reported for the effects of pile diameter and cyclic loading on p-y curves in sands. However, it is evident that cyclic loading of laterally loaded piles in sand will result in permanent deflections of the pile and the formation of a gap on the rear side of the pile. It has been observed that the sand around the pile progresses toward its critical state during cyclic loading. This means that loose sand will densify, and dense sand will loosen when subjected to cyclic loading.

LPILE provides p-y curve models for piles subjected to static/cyclic lateral loads embedded in sand based on effective soil parameters (API, 2011; Reese et al., 1974) and small-strain p-y curves (Hanssen, 2015). Additionally, p-y curve models are also proposed for liquefied sand and cemented sand, which will be discussed later.

Reese et al. (1974) p-y curve development procedure for sand

The procedure of constructing *p-y* curves in sands with static/cyclic loading condition (Figure 18) includes the following steps:

1. Determine the internal friction angle, φ, unit weight (effective unit weight for below the water table and total unit weight for above the water table), and pile diameter, b, at the *p-y* curve depth, x.

2. Calculate the following parameters:

$$\alpha = {}^{\varphi}/_{2}$$

$$\beta = 45 + {}^{\varphi}/_{2}$$

$$K_0 = 0.4$$

$$K_A = tan^2(45 - {}^{\varphi}/_{2})$$

where α and β are the wedge fan spread angle and the wedge base angle in the passive soil wedge, respectively, and K_0 and K_A are the at-rest and active earth pressure coefficients, respectively.

3. Calculate the ultimate resistance, p_s, expressed as:

$$p_s = \min [p_{st}, p_{sd}]$$

$$p_{st} = \gamma x \left[\frac{K_0 x \tan\varphi \sin\beta}{\tan(\beta-\varphi)\cos\alpha} + \frac{\tan\beta}{\tan(\beta-\varphi)}(b + x\tan\beta\tan\alpha) + K_0 x \tan\beta\,(\tan\varphi\sin\beta - \tan\alpha - K_A b\right]$$

$$p_{sd} = K_A b\gamma x(tan^8\beta - 1) + K_0 b\gamma x(tan\varphi tan^4\beta)$$

4. Calculate the values of pile deflections and soil resistance associated with the points u and m, using the following equations:

$$y_u = 3b/80$$

Static loading: $p_u = A_s p_s$

Cyclic loading: $p_u = A_c p_s$

$$y_m = b/60$$

Static loading: $p_m = B_s p_s$

Cyclic loading: $p_m = B_c p_s$

The parameters A_s, A_c, B_s, and B_c can be obtained from Figure 30.

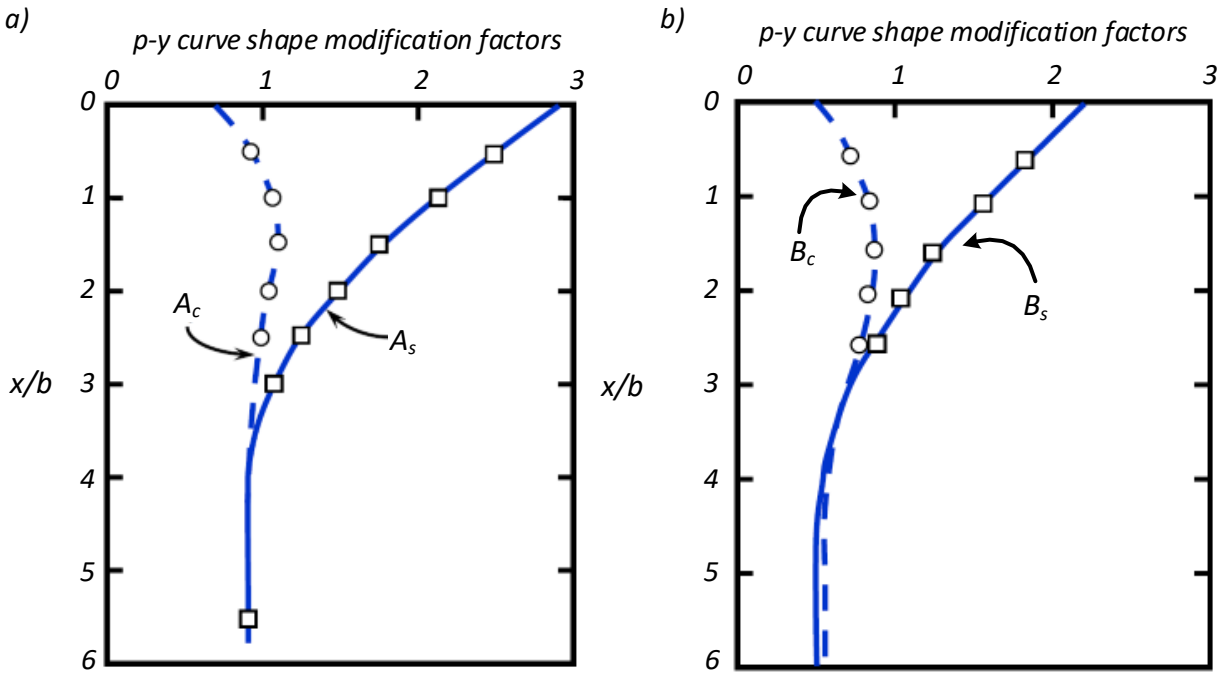

Figure 30. Shape modification factors for p-y curves in cohesionless soils (Isenhower et al., 2019)

5. The initial straight line of the curve is expressed as the equation below:

$$p = (kx)y$$

The value of the subgrade reaction modulus, *k*, can be selected based on the sand density and the position of *p-y* curve with respect to the water table from Table 7.

Table 7. Recommended values for subgrade reaction modulus in sand

Density	***k* for below the water table (MN/m^3)**	***k* for above the water table (MN/m^3)**
Loose	5.4	6.8
Medium	16.3	24.4
Dense	34.0	61.0

6. The parabolic curve should be fitted between the points *k* and *m* by calculating the slope of the second straight line, *m*, the power of the parabola, *n*, and the values of *p* and *y* for the point *k*.

$$m = \frac{p_u - p_m}{y_u - y_m}$$

$$n = \frac{p_m}{m y_m}$$

$$y_k = \left(\frac{\bar{C}}{kx}\right)^{\frac{n}{n-1}}$$

where

$$\bar{C} = \frac{p_m}{y_m{}^{1/n}}$$

and

$$p_k = (kx)y_k$$

The *p*-values along the parabola can be computed using the equation below:

$$p = \bar{C}y^{1/n}$$

If the first straight line and the parabola do not intersect at the point *k*, the *p-y* curve follows the initial straight line for all deflections. If $y_m<y_k<y_u$, the *p-y* curve follows a tri-linear path. If $y_k>y_u$, the *p-y* curve will be bi-linear.

API RP 2A procedure for sand

The API *p-y* curve procedure has been developed for the design of fixed offshore platforms in sands. The API method follows the same procedure of the Reese et al. (1974) method for obtaining the ultimate resistance. The main differences between the two models are the initial stiffness and the shape of the curves.

The *p-y* relationship proposed by API is expressed as the following equation:

$$p = Ap_u \tanh\left(\frac{kx}{Ap_u}y\right)$$

where *A* is a shape factor, obtained from:

Cyclic loading: $A = 0.9$

Static Loading: $A = \left(3 - 0.8\frac{x}{b}\right) \geq 0.9$

Fully drained triaxial compression tests are recommended by LPILE for obtaining the internal friction angle of sand.

Small strain p-y curves development procedure for sand

Conventional *p-y* curve models were not developed based on load tests on large diameter monopiles. Large diameter monopoles as the foundations of the wind turbines in sands usually undergo relatively small lateral displacements (less than 0.1% of the pile diameter) when subjected to operation loads. Hanssen (2015) proposed an overlay to the API method for small-strain *p-y* curve development in sands by correlating the initial stiffness of the curves to the maximum shear modulus value. This procedure includes a relationship between the soil reaction and the pile

deflection based on the shear modulus degradation function. The ultimate soil resistance in this model is obtained similar to the API method.

p-y Curves for Liquefied Soils

The lateral capacity of piles embedded in liquefied soil is an important factor in the design of deep foundations in liquefiable soils. Lateral spreading, a phenomenon resulting from liquefaction in sloping ground, has been the reason for the failure of deep foundations during several earthquake-induced liquefactions.

Different approaches have been utilized for deriving the *p-y* curves in liquefied soils. The first approach is to consider the liquefied layer as it has no lateral resistance. This method can be implemented in LPILE by selecting a very low value for the internal friction angle. The second approach is to consider the behavior of liquefied sand as soft clay and employ the model proposed by Matlock (1970). In this case, the residual strength of liquefied sand should be used instead of the cohesive strength of clay. However, accurate measurement of the residual strength of liquefied sand is difficult through laboratory procedures. Seed and Harder Jr (1990) examined case histories reported where major lateral spreading has occurred and concluded that the residual strength of liquefied sand is about 10 percent of the effective overburden stress.

In LPILE recommends a simplified procedure for developing *p-y* curves in liquefied sand based on the study published by Rollins et al. (2006). The method proposed by Rollins et al. (2006) is developed based on field tests on full-scale instrumented piles. Figure 31 indicates the concave-shaped *p-y* curve for liquefied sand in this model. The soil resistance for a reference pile with a diameter equal to 0.3 meters is expressed as the following equation:

$$p_{0.3} = A(By)^c \leq 15\ kN/m$$

where *A*, *B*, and *C* are functions of depth. A modifying factor, P_d, is defined for piles with smaller/greater diameters than 0.3 *m*. So, the *p-y* relationship is defined as:

$$p(y) = P_d . p_{0.3}$$

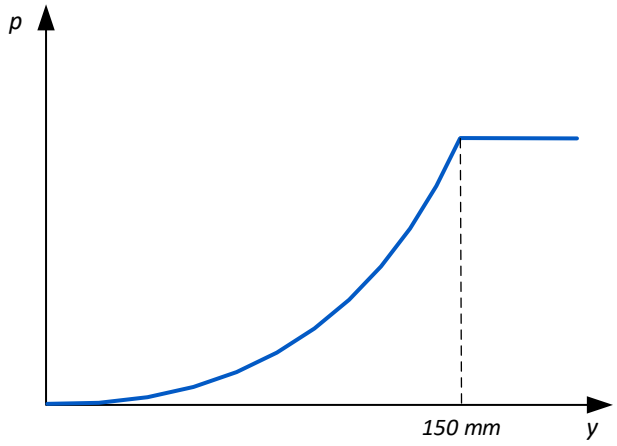

Figure 31. Example p-y curve in liquefied sand, after Rollins et al. (2006)

Note that the application of this model is limited to conditions similar to the ones in the conducted load tests, including:

- Relative density in the range of 45 to 55 percent.
- Lateral resistance per unit length of the pile smaller than 15 *kN/m* for a pile with *b=0.3 m*.
- Pile deflections less than 150 *mm*.
- Depths less than 6 meters.
- Water table close to ground surface.

p-y Curves for Cemented Soils with both Cohesion and Friction

Conventional p-y curve models are typically developed for either completely cohesive or completely cohesionless soils, as the major experiments on which these models are based were conducted in soils that can be characterized as either cohesive or cohesionless. Currently, no generally accepted procedure has been proposed for *p-y* curve development in soils with both friction and cohesion.

The revised model for developing p-y curves in cemented sand, recommended by LPILE, is the revised version of the model proposed by Reese et al. (1974) for sand included with ideas from Ismael (1990), illustrated in Figure 32.

In this model, the ultimate resistance, p_u, is derived based on the passive soil wedge failure. The active earth pressure and the side friction are assumed to be relatively small and to cancel each other. It is also assumed that the contribution of cohesion will be eliminated after the *p-y* curve reaches the peak value (point *m* in Figure 32).

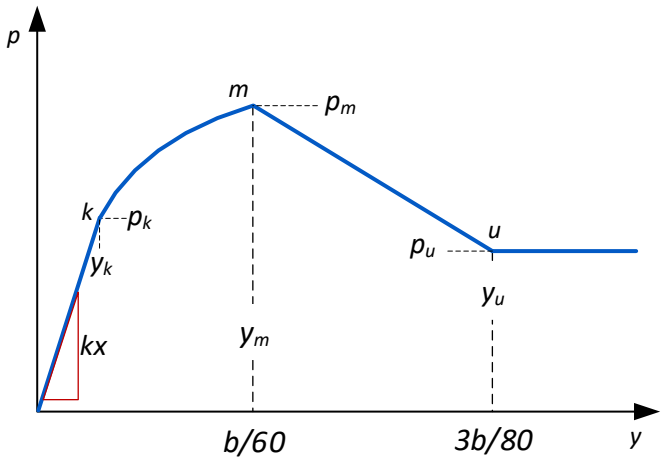

Figure 32. Characteristic shape of p-y curves in c-φ soils, after Isenhower et al. (2019)

For cemented sands, the initial slope of the curve in Figure 32, k, is the sum of k_c and k_φ, whereas for non-cemented silt, it is equal to k_φ (Figure 33).

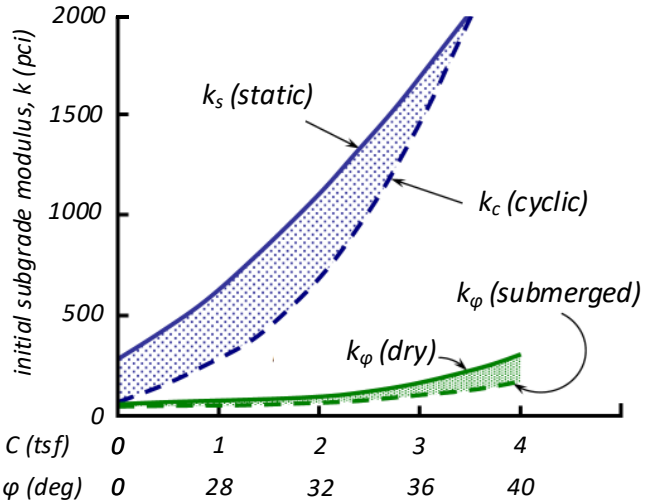

Figure 33. Subgrade reaction modulus for c-φ soils under static and cyclic loading (Isenhower et al., 2019)

Overall, the construction process of the *p-y* curve using the proposed model follows a similar procedure to the one proposed for sand, with modifying factors incorporating the simultaneous effects of cohesion and friction.

p-y Curves for Rocks

LPILE proposes two sets of criteria for *p-y* curves in rocks: one for strong rock with a compressive strength of 6.9 *MPa* or more, and another for weak rock.

The response of laterally loaded piles in rocks is significantly influenced by the secondary structure of the rock. Therefore, LPILE recommends conducting excellent subsurface investigation and intact rock sampling to determine the rock quality designation (RQD), the compressive strength of intact specimens, and if feasible, the rock mass rating (RMR). In cases where collecting intact specimens is not possible due to low RQD-values in the rock, the use of the pressuremeter test (PMT) is recommended.

In rock mechanics, intact rock is assumed to have a very brittle response to deformations, leading to a loss of strength under small deflections of the pile. However, rocks with very low to zero RQD-values are considered to be already fractured and will deform without significant loss in strength.

The procedures proposed by LPILE for developing *p-y* curves in strong and weak rocks are based on models introduced by Reese et al. (2005) and Reese (1997), respectively. Additionally, for

massive rocks, the development of *p-y* curves is based on the criterion proposed by Liang et al. (2009).

Strong rock

The proposed *p-y* curve in strong rocks by LPILE is presented in Figure 34 and includes the following considerations:

1. If the compressive strength of the rock increases with depth, the top stratum will be the controlling criterion.
2. It is assumed that cyclic loading will not cause any loss in resistance.
3. If the pile deflections are greater than 0.0004b, performing load tests is recommended.
4. If the lateral stress is greater than 0.5b×compressive strength, brittle fracture is assumed.

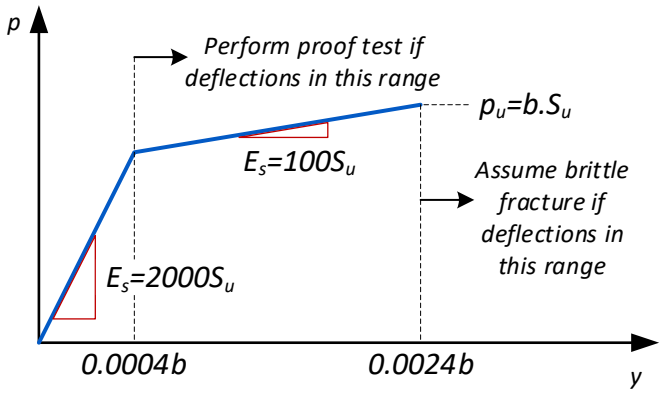

Figure 34. Characteristic shape of p-y curves in strong rocks, after Reese et al. (2005)

Weak rock

The proposed *p-y* curve in weak rocks by LPILE is presented in Figure 35 and includes the following points:

1. The ultimate resistance, p_{ur}, is expressed based on the failure of a wedge of rock at the top:

$$p_{ur} = \alpha_r q_{ur} b \left(1 + 1.4\frac{x_r}{b}\right) \quad ; \quad x_r \leq 3b$$

$$p_{ur} = 5.2\alpha_r q_{ur} b \quad ; \quad x_r \leq 3b$$

where

q_{ur}=compressive strength

α_r=strength reduction factor to account for fracturing

x_r=depth below the rock surface

b=pile diameter

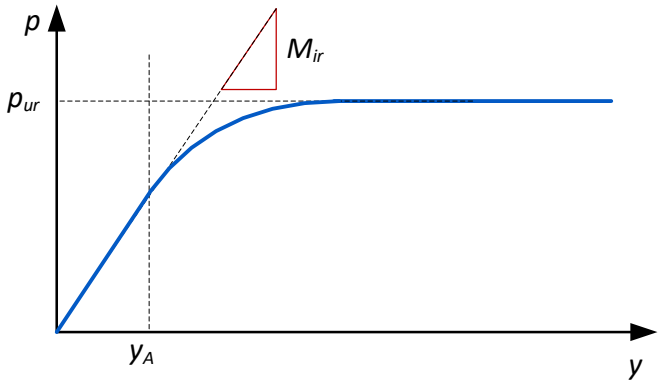

Figure 35. Characteristic shape of p-y curves in weak rocks, after Reese (1997)

The strength reduction factor, α_r, can be computed using the following equation:

$$\alpha_r = 1 - \frac{2}{3}\frac{RQD\ (\%)}{100}$$

The initial slope of the *p-y* curve, M_{ir}, is expressed as the following equation:

$$M_{ir} = K_{ir}E_{ir}$$

where

E_{ir}=the initial modulus of rock

K_{ir}=dimensionless constant

The curved portion in Figure 35 follows the equation below:

$$p = 0.5p_{ur}\left(\frac{y}{y_{rm}}\right)^{0.25} \quad , \qquad y_{rm} = \varepsilon_{rm}b$$

where ε_{rm} is a constant typically ranging from 0.0005 to 0.00005.

Also, the value of y_A is the intersection of the linear and the curve portions.

Massive rock

Based on three-dimensional finite element modeling and full-scale field load tests, Liang et al. (2009) developed a model for computing *p-y* curves for drilled shafts in mass rocks (Figure 36).

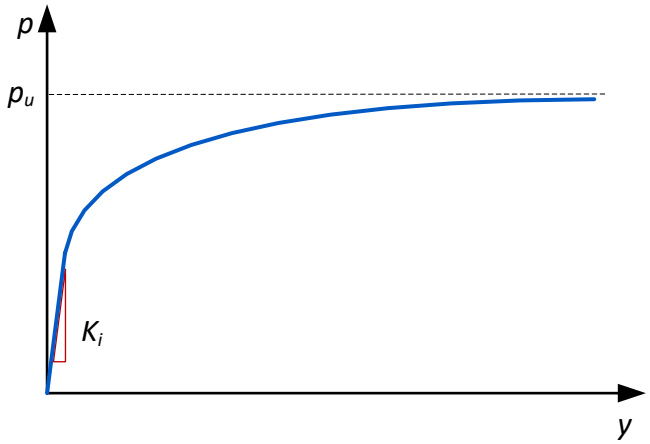

Figure 36. Characteristic shape of p-y curve in massive rocks, after Liang et al. (2009)

A hyperbolic function is assumed as the basis for the *p-y* relationship:

$$p = \frac{y}{\frac{1}{K_i} + \frac{y}{p_u}}$$

The initial slope of the curve and the ultimate resistance are calculated using the mass rock properties.

The minimum value of the ultimate resistance near the ground surface and at great depths is considered as the ultimate for the *p-y* curve. At near the ground surface, a passive wedge failure is assumed, and at great depths, the following failure mechanisms are assumed in a timely order:

1. Rock failure in tension.
2. Failure in friction between the rock and the shaft.
3. Rock failure in compression.

The initial stiffness, K_i, is expressed as the equation below:

$$K_i = E_m \left(\frac{D}{D_{ref}}\right) e^{-2\nu} \left(\frac{E_p I_p}{E_m D^4}\right)^{0.284}$$

where

E_m=modulus of the rock mass

ν=Poisson's ratio of the rock mass

D=diameter of the shaft

D_{ref}=0.3048 m

Other Recommendations in LPILE

LPILE also provides recommendations for *p-y* curves in loess soils and for layered soil profiles. Loess in a wind-blown (eolian) cohesive loose uniform soil (Terzaghi & Peck, 1968) with clastic origins, and it is mainly composed of silt-sized quartz particles and loosely arranged sand grains (Johnson, 2006). It is found in central regions of the United States, Europe, Siberia, China, and New Zealand (Bandyopadhyay, 1983). LPILE proposes a *p-y* curve procedure in loess based on the model proposed by Johnson (2006). This model is developed using load tests conducted in Kansas loess and incorporates the degradation of *p-y* curves due cyclic loading. Figure 37 illustrates the *p-y* curve model for drilled shafts in loess as presented by Johnson (2006). In this model, the ultimate resistance of the soil is correlated to the tip resistance in the cone penetration test.

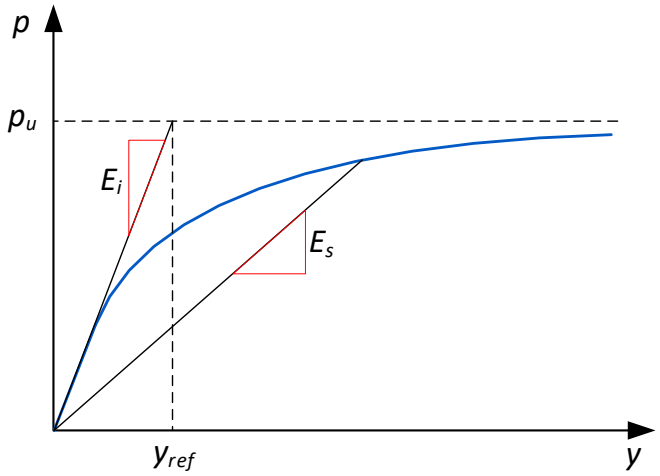

Figure 37. Generic p-y curve for drilled shafts in loess soils, after Isenhower et al. (2019)

LPILE also includes a correction procedure for layered soil profiles, which was proposed by Georgiadis (1983). This method is specifically designed for layers of soil and does not apply to rocks. It involves the use of equivalent depths of layers below the top layer. As shown in Figure 38, if the top layer has a thickness of h_1 and is underlain by a stronger soil layer, the equivalent depth would be smaller than h_1 (h_2 in Figure 38). Conversely, if the top layer is underlain by a weaker soil layer, the equivalent depth would be greater than h_1 (h_3 in Figure 38). The equivalent depths are computed by equating the integral of ultimate resistances above the underlying layer (over the equivalent depth, h_2 or h_3).

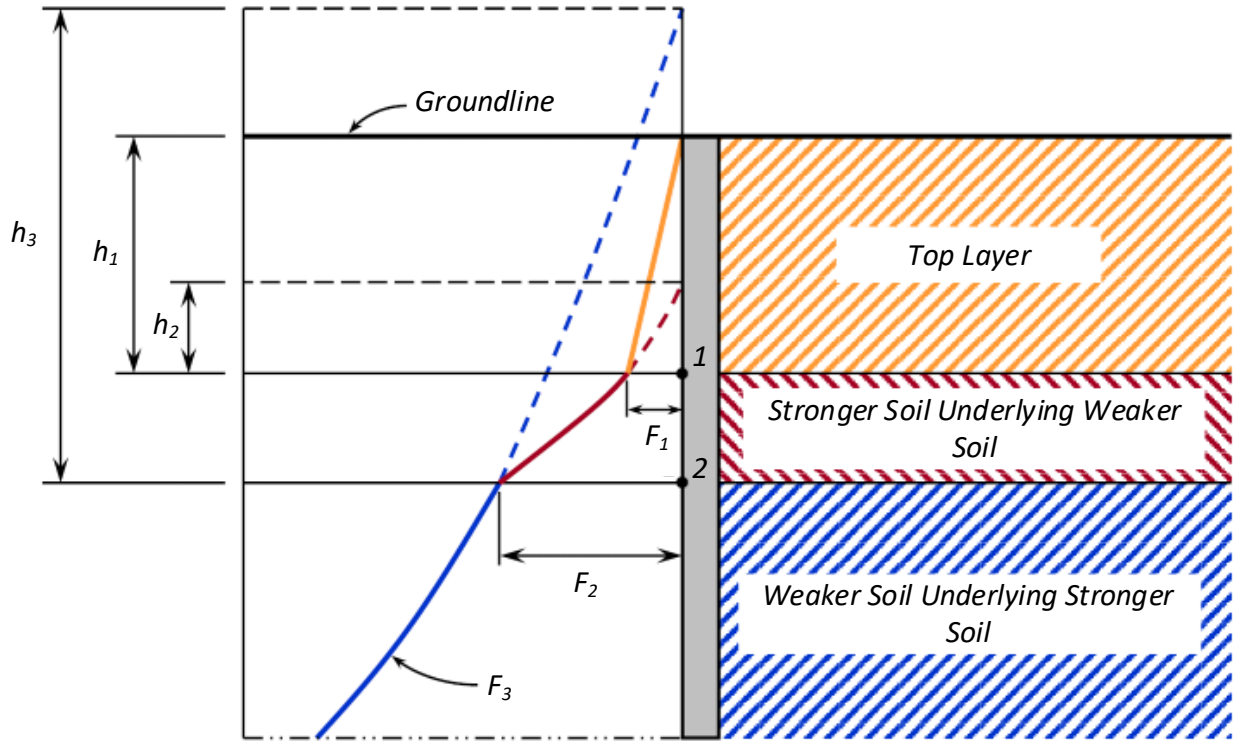

Figure 38. Illustration of the correction depth method (Isenhower et al., 2019)

Summary

The p-y curve method is the most commonly used method for the analysis of laterally loaded piles in engineering practice. This method is based on the concept of linear subgrade reaction, also known as Winkler's beam on elastic foundation theory. By modeling the soil medium as uncoupled nonlinear springs in the horizontal direction, the p-y curve method captures the interactions of the soil-pile system. Throughout the reviewed studies, it has been found that the two key parameters of p-y curves are the initial slope (initial stiffness) and the ultimate soil-pile resistance. The initial stiffness is often assumed to have a linear relationship with depth, represented by the subgrade reaction modulus, and is influenced by various soil-pile properties. The ultimate resistance, which defines the asymptote of the p-y curve at failure, is determined by equilibrium equations based on assumed failure mechanisms of the soil-pile system. Proposed p-y curve models in technical literature are categorized into hyperbolic functions, parabolic functions, and multi-portion curves consisting of curves and straight lines.

Various methodologies have been employed to study the p-y behavior of laterally loaded piles and to develop models for predicting p-y curves in different types of soils. These methodologies can be categorized into four main groups: full-scale field tests on instrumented piles, model-scale laboratory experiments (such as 1g and centrifuge testing), in-situ tests (including cone penetration tests), and numerical modeling. Full-scale field tests provide reliable p-y curves specific to unique site conditions, but they are expensive and time-consuming. Model-scale laboratory testing and

centrifuge modeling offer faster and more economical alternatives for parametric studies on different aspects of laterally loaded pile behavior. Centrifuge modeling, in particular, provides more realistic stress distribution in the soil and allows the use of smaller-scale models. In-situ tests, especially cone penetration tests, have shown promising results in predicting p-y behavior in various soil types. Additionally, numerical models using robust methods like three-dimensional finite element and finite difference analysis are capable of capturing important aspects of soil-pile interactions. However, these numerical approaches are computationally expensive and require expertise in numerical analysis, making them less practical for everyday engineering problems.

While extensive research has been conducted on sands and clays, the p-y behavior of laterally loaded piles in silts and gravels has not been fully investigated. Further studies in these soil types would enhance our understanding of pile behavior in a wider range of geological conditions.

CHAPTER 4: SOIL CONDITIONS IN MONTANA

History of Formation and Stratigraphy of the Montana Group

During much of the Late Cretaceous era, the western interior of North America hosted an epicontinental sea that stretched from the Gulf of Mexico to the Arctic Ocean, reaching widths of up to 1,000 miles in some areas. This sea was bordered along its entire length by a narrow, unstable, and frequently rising north-trending cordilleran highland. This highland acted as a barrier, separating the interior Cretaceous Seaway from the waters of the Pacific Ocean. On the eastern side of the cordilleran highland, the Rocky Mountain geosyncline could be found, while the Pacific geosyncline bordered its western side. The cordilleran highland served as the primary source of clastic material that eventually filled the Cretaceous epicontinental sea.

(Gilluly, 1963) reported that the estimated source area covered approximately 160,000 to 200,000 square miles and contributed over a million cubic miles of clastic sediment to the western interior sea. This immense volume of sediment suggests that the source area must have undergone erosion to a depth of about 5 miles. However, (Gilluly, 1963) also noted that this finding presents challenges in reconciling it with the known geology of the presumed source. This suggests the possibility of long-distance lateral transfer of material within the exposed source area.

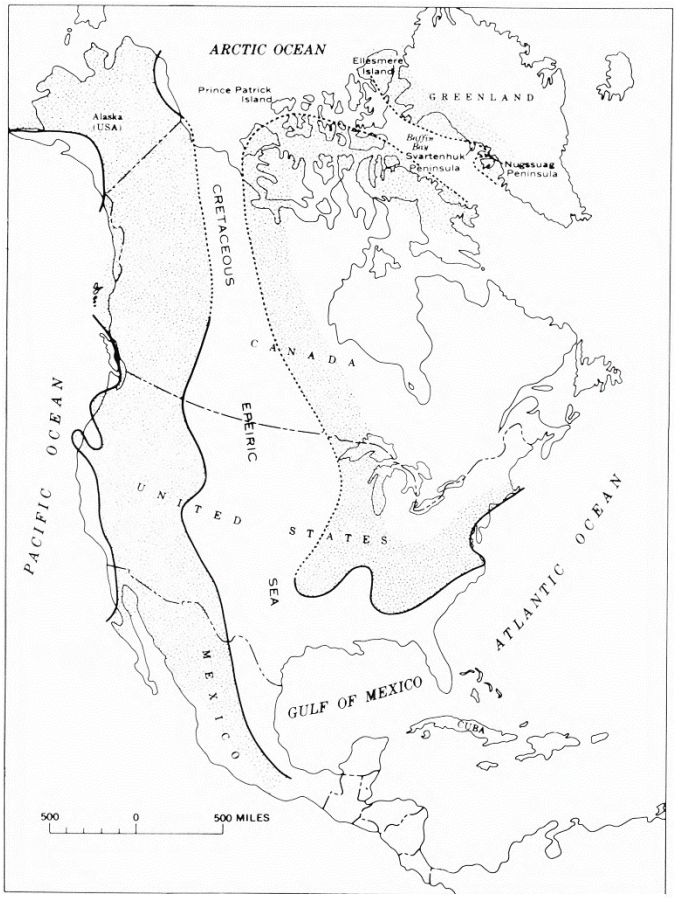

Figure 39. Distribution of land and sea in North America during late Cretaceous time, after (Gill et al., 1966)

The low-lying stable platform of the Eastern United States and Canada delineated the eastern margin of the interior sea. Although the exact location of this shoreline remains uncertain, it probably did not extend westward beyond the longitude of eastern Minnesota and Iowa.

In the Cretaceous Sea region of Montana, the majority of the deposited sediments were thought to originate from diverse petrologic provinces located along the Western Cordillera. Particularly, the Montana section of the sea witnessed a substantial influx of clastic and pyroclastic volcanic material originating from the Upper Cretaceous Elkhorn Mountains Volcanics along its western shore.

The probable distribution of land and sea in North America during the late Cretaceous period is depicted in . , illustrating the geographic position of the seaway that divided the continent into eastern and western parts.

In Montana, the formations of the Montana Group are characterized by eastward-pointing wedges of regressive deposits that comprise nonmarine and shallow-water marine strata. These wedges enclose westward-thinning wedges of fine-grained transgressive deposits, which consist of marine strata. Figure 40. Stratigraphic Diagram of Rocks of The Montana Group Between the Dearborn River and Porcupine Dome, constructed approximately perpendicular to the depositional strike from Porcupine dome to the Dearborn River in Montana, illustrates the transition from the predominantly marine section of non-calcareous shale, sandstone, and calcareous shale on the east to a range of nearshore marine, lagoonal, and fluviatile sediments. The transition eventually leads to the coarse volcanic sequence containing lava flows and welded tuffs on the West. The upper nonmarine rocks correspond to the different soil layers typically found in Montana's area, while the lower volcanic-rich rocks correspond to the gravel layer typically underlying the soil layers.

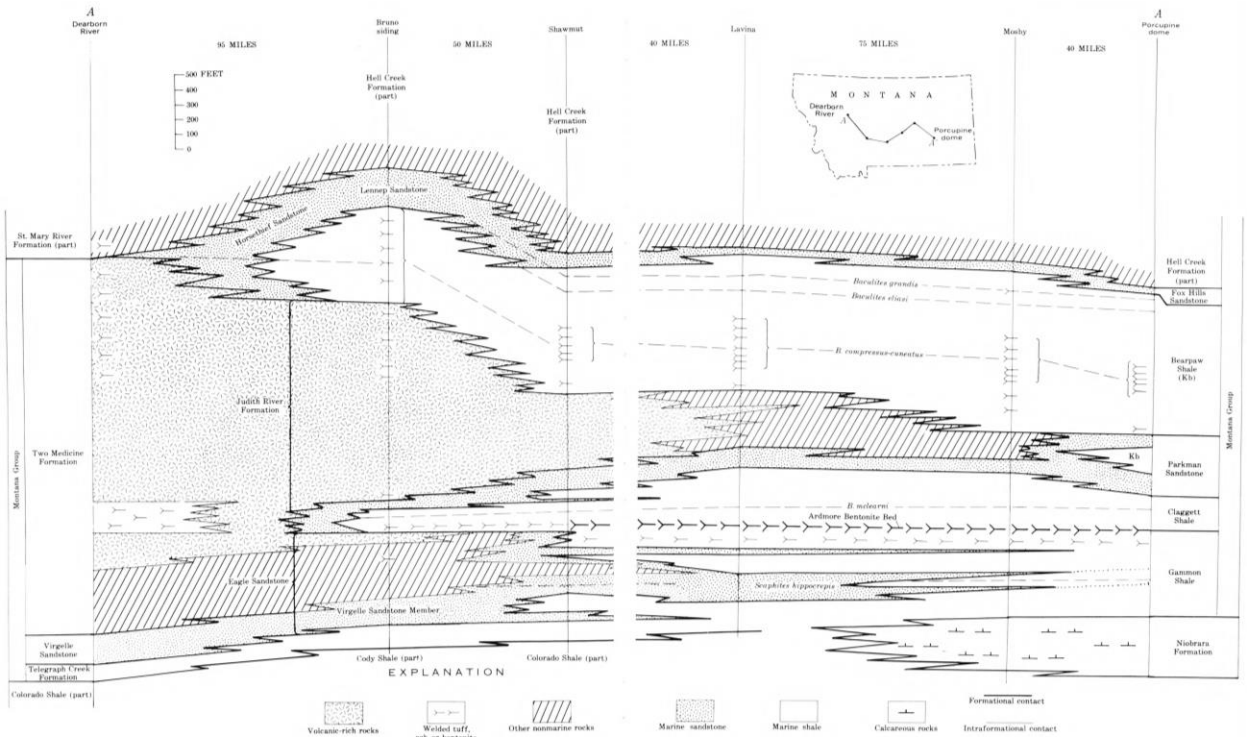

Figure 40. Stratigraphic Diagram of Rocks of The Montana Group Between the Dearborn River and Porcupine Dome (Gill & Cobban, 1973)

In the Missoula area, located on the west side of Montana state, Glacial Lake Missoula was repeatedly dammed by the Purcell Trench Lobe of the Cordilleran ice sheet during the last glaciation, raising its water level to maximum altitudes of approximately 4200 ft (1280 m). Research conducted beyond the lake basin indicates that the lake experienced multiple filling and

draining episodes during the late Pleistocene. Glacial Lake Missoula was formed during the last glaciation through the repetitive obstruction of the Clark Fork River by the Purcell Trench Lobe of the Cordilleran ice sheet, close to the current state boundary between Idaho and Montana (Breckenridge, 1989; Pardee, 1910). The lake's volume has been estimated to range from 2200 to 2600 km3, utilizing the highest shorelines, which were approximately 4200 ft (1280 m) near Missoula, Montana, and the current topography (Pardee, 1910; Smith, 2006). Glacial Lake Missoula, being a mountainous reservoir, featured several subbasins delineated by drainage basins that fed into the Clark Fork River. The northern subbasins, including the Flathead River and the lower Clark Fork River areas, held more than 75 percent of the lake's water, while the southern subbasins, encompassing the Bitterroot Valley, the Missoula Valley, and the Clark Fork River above Missoula held the remaining water (Smith, 2006). The "Lake Missoula beds" is the term Langton (1935) coined to describe deposits of glaciolacustrine silt and clay that were laid down in lake-bottom locations across the glacial Lake Missoula basin. Figure 41 illustrates the measured section and location of an optical age for the lower 11 *m* of Lake Missoula beds exposed at Rail Line (a) and for the lower 9 *m* at the Ninemile Creek section (b).

Soil Conditions in Montana

188 geotechnical investigation reports have been gathered and reviewed to identify and classify soil types in Montana. The reviewed reports include a total of 352 SPT and CPT soundings conducted in 15 counties, comprising 322 SPTs and 30 CPTs. The distribution of SPT/CPT soundings across Montana is illustrated in Figure 42.

Based on the number of in-situ tests and the variation of soil types in different parts of the state, six regions are considered for presenting soil conditions: East, North, South, Northwest, West, and Southwest (Figure 43). Figure 44 to Figure 49 present the average distribution of different soil types in different areas.

Data from the East region included 17 SPT/CPT soundings, with 11 soundings in Miles City and 6 soundings in Fairview and Bainville. As shown in Figure 44, the upper layer of soil profiles on the East side consists primarily of low plasticity clay (CL) accounting for over 50% of the total depths. Additionally, high plasticity clays (CH) have been observed, forming approximately 25% of the soil profiles. In Miles City, the middle layer is composed of silty sands, followed by a CH layer. Conversely, in Fairview and Bainville, the middle layer comprises the CH layer.

On the North side of Montana, only one SPT data from Havre was available. The result of this single SPT sounding indicated that the upper layer consists of 44% of CL followed by 56% silty sand (Figure 45).

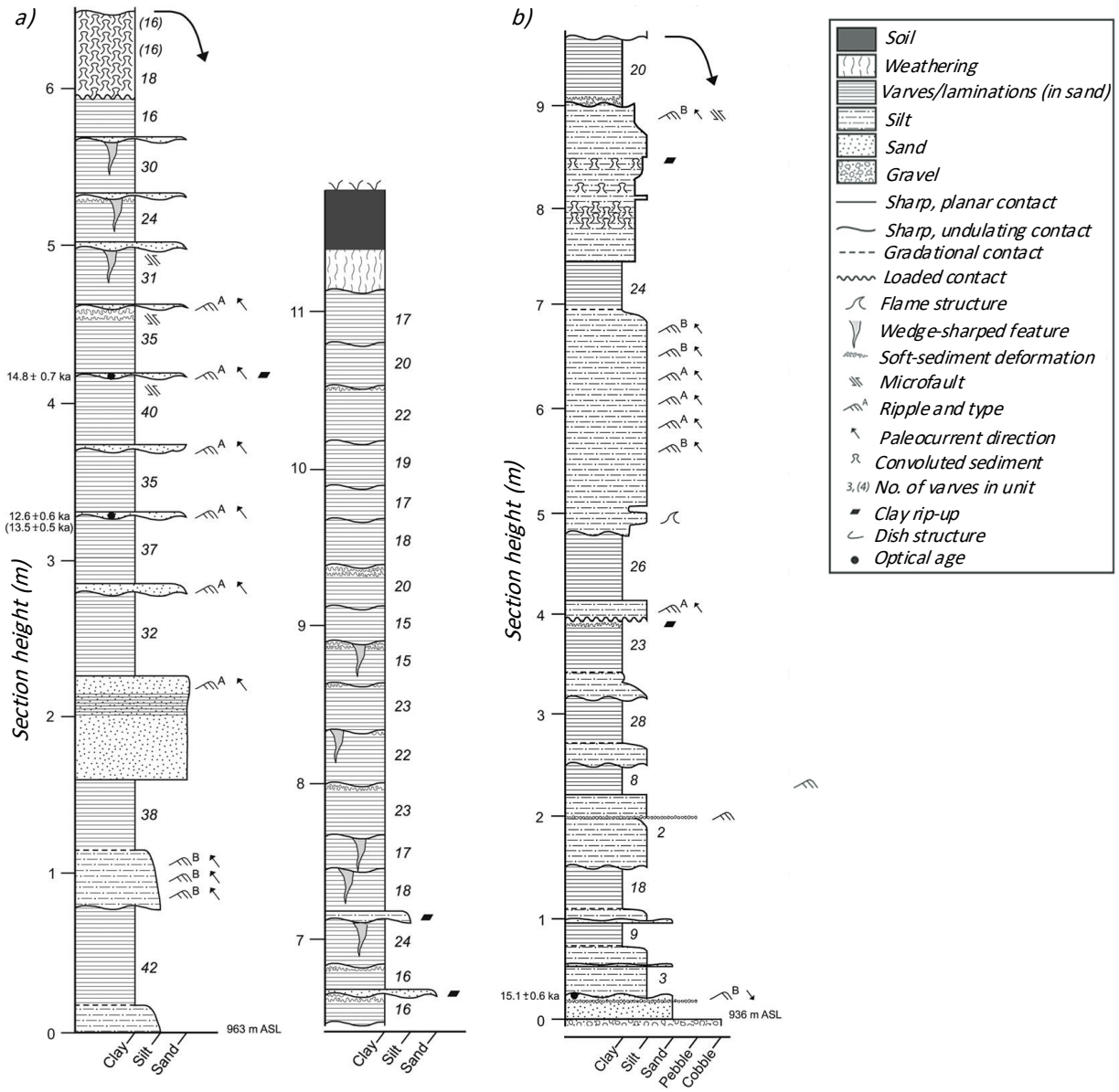

Figure 41. Stratigraphic logs of Lake Missoula beds, a) Rail Line, and b) Ninemile Creek (Hanson et al., 2012)

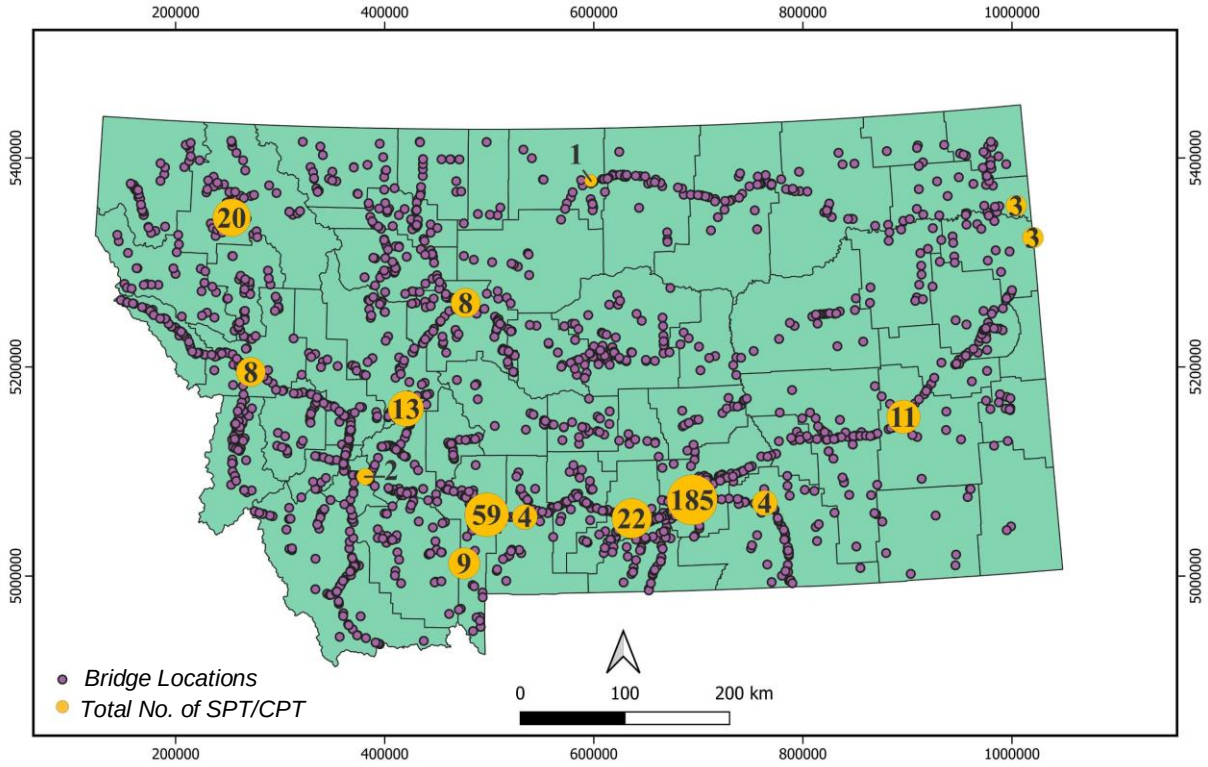

Figure 42. Distribution of in-site tests in Montana from the reviewed geotechnical investigation reports

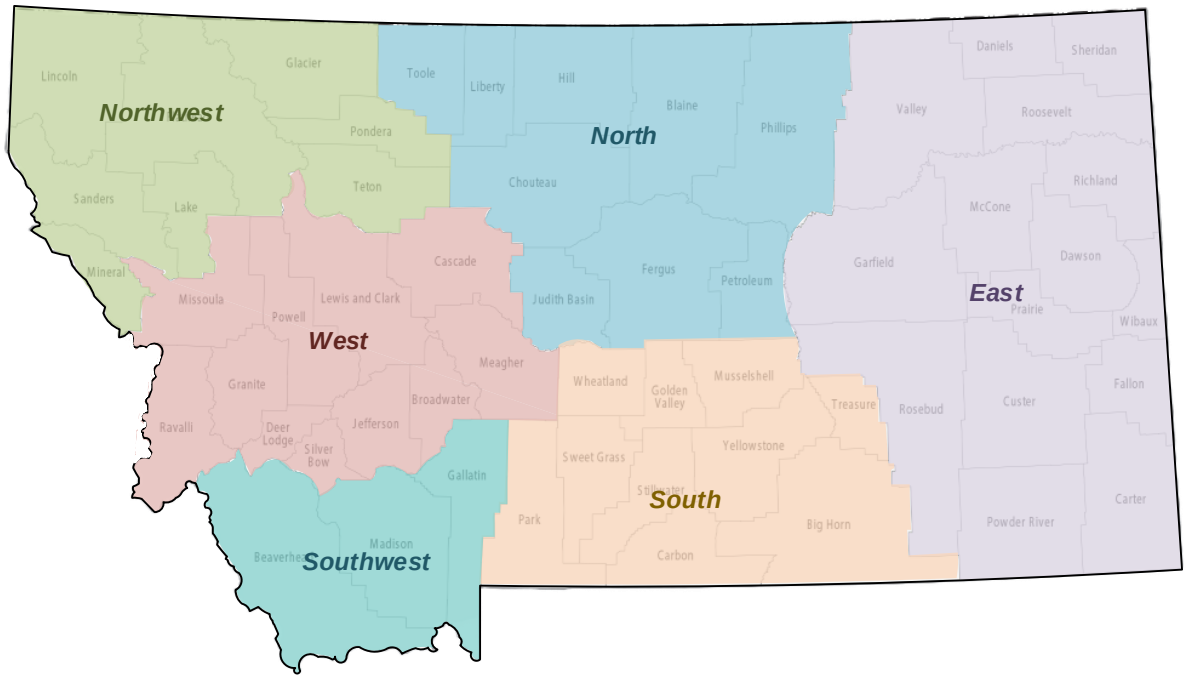

Figure 43. Division of Montana based on the available geotechnical investigation reports

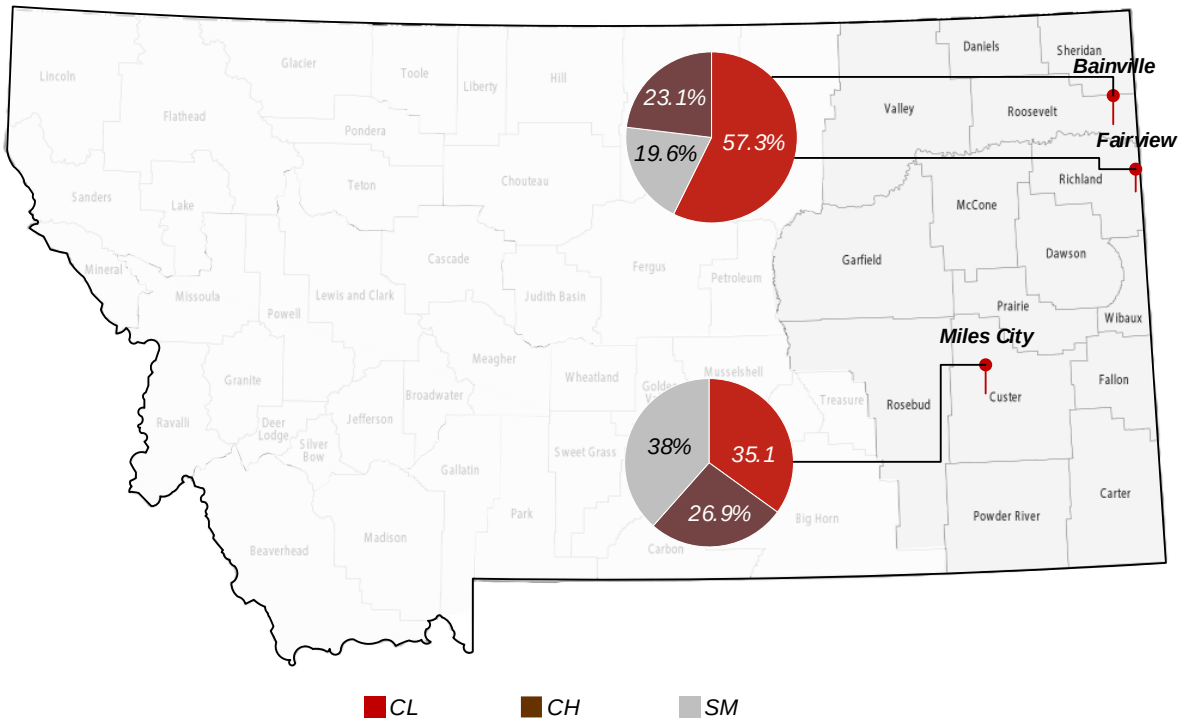

Figure 44. Average soil profiles in the East of Montana

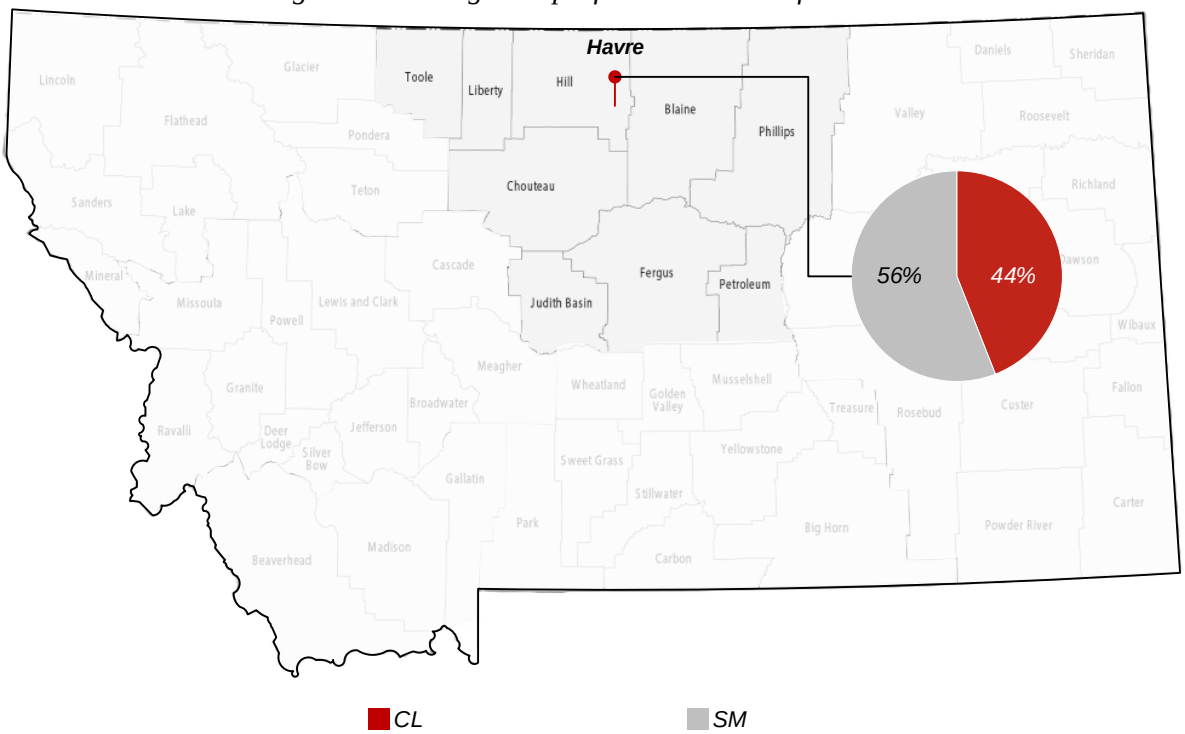

Figure 45. Average soil profile in the North of Montana

Data from the Northwest region included 20 SPT/CPT soundings in Kalispell. The average soil profile in Kalispell showed a variety of soil types, including low plasticity clay, low plasticity silt, silty sand, silty gravel, clayey gravel, and small amounts of poorly graded gravel (Figure 47).

In the West region, data were collected from 8 soundings in Missoula, 8 soundings in Great Falls, and 13 soundings in Helena. In Great Falls, the average soil profile contained more than 50 percent of high plasticity clays in the upper layers, underlain by silty and poorly graded gravels. In Helena, the upper layers were mostly made of low plasticity clays with sand and silt. Below the upper layer of the soil profiles in Helena, high plasticity clayey silts (MH) were observed, which formed about 30% of the average soil profile. The layer of MH was followed by clayey sands and low plasticity sandy silts (Figure 48).

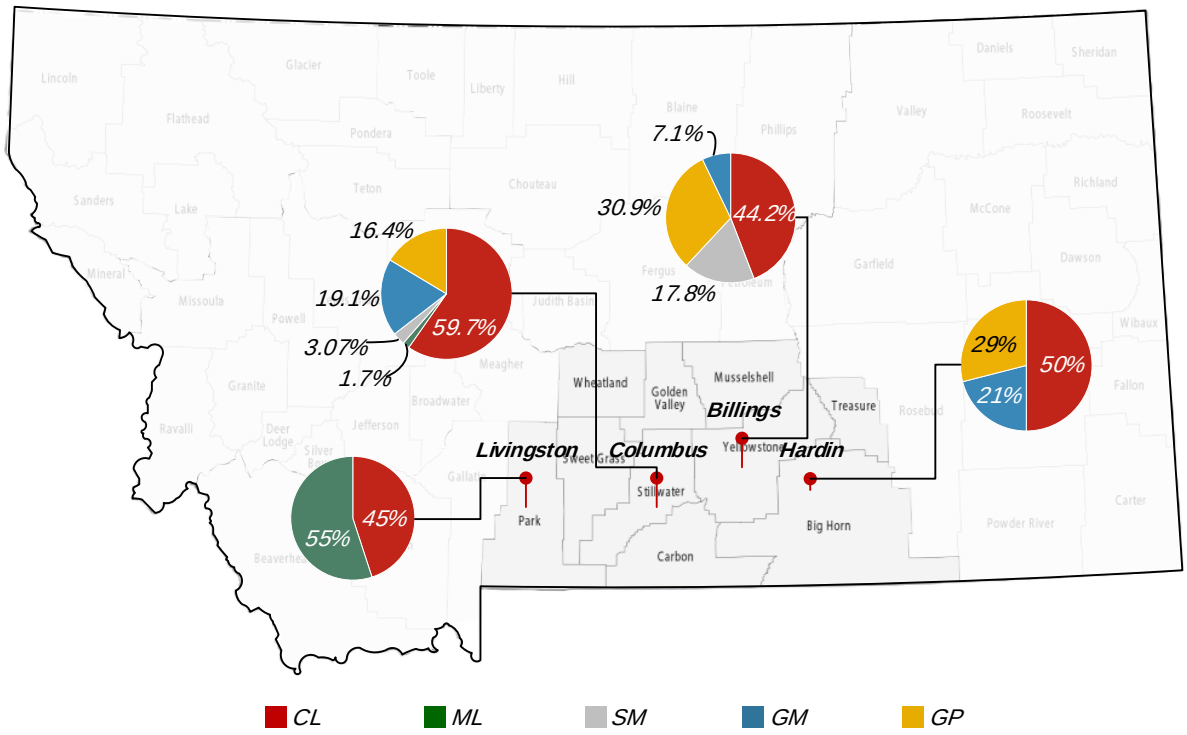

Figure 46. Average soil profiles in the South of Montana

As presented in Figure 48, considerable amounts of low plasticity silts with small contents of clay were observed as the top layer in Missoula. The middle layer of the average soil profile in Missoula is mostly formed of clayey gravel (GC) and the down layer contains about 30% of poorly graded gravel with silt and clay contents.

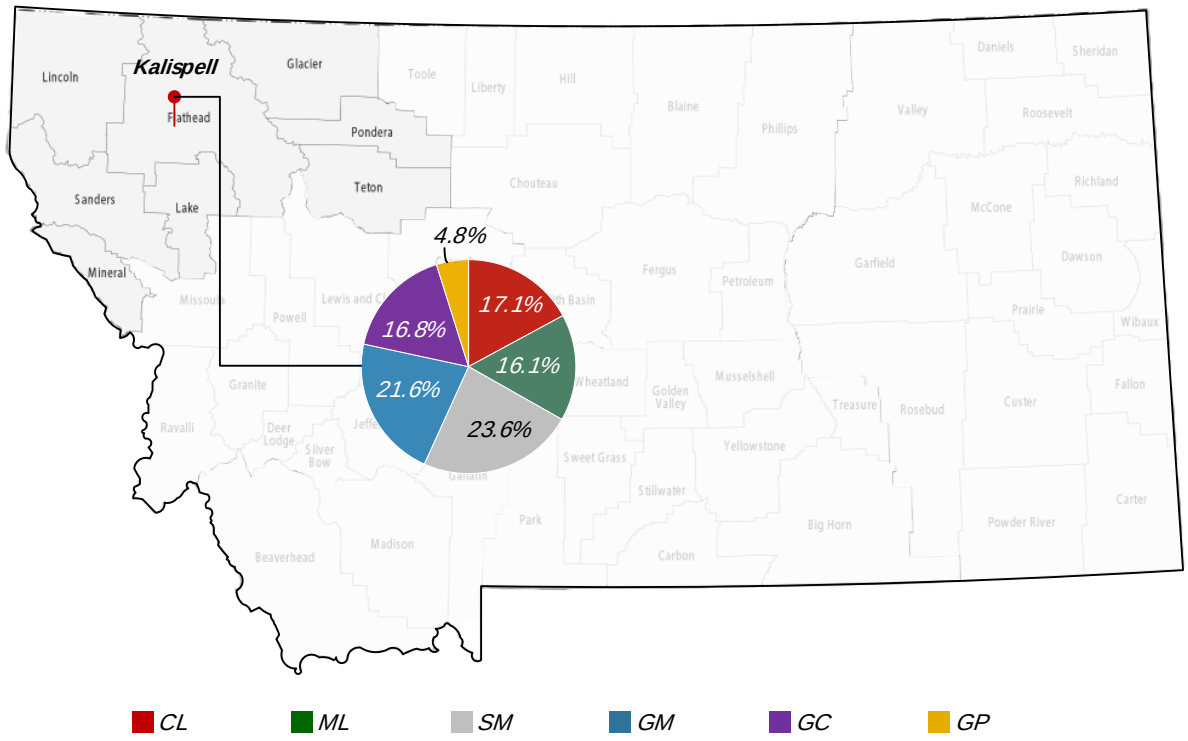

Figure 47. Average soil profiles in the Northwest of Montana

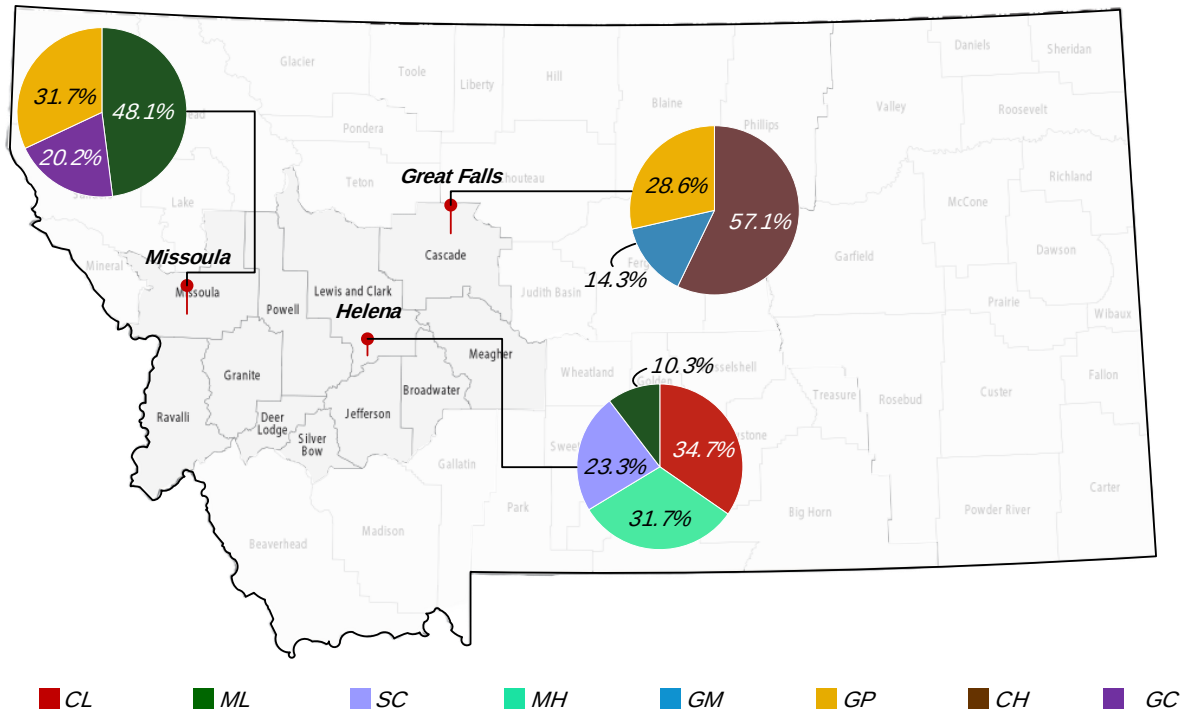

Figure 48. Average soil profiles in the West of Montana

Finally, the reports from the Southwest region include 59 SPT/CPT soundings in Bozeman, and 9 soundings in Big Sky. As shown in Figure 49, the average soil profiles in both cities contain large amounts of lean clay with silt and sand contents as the upper layer. The upper layer in Bozeman is underlain by poorly graded gravel and small amounts of low plasticity silt and clayey gravel. In Big Sky, the upper layer is followed by weathered shale, up to 26.7% of the average soil profile.

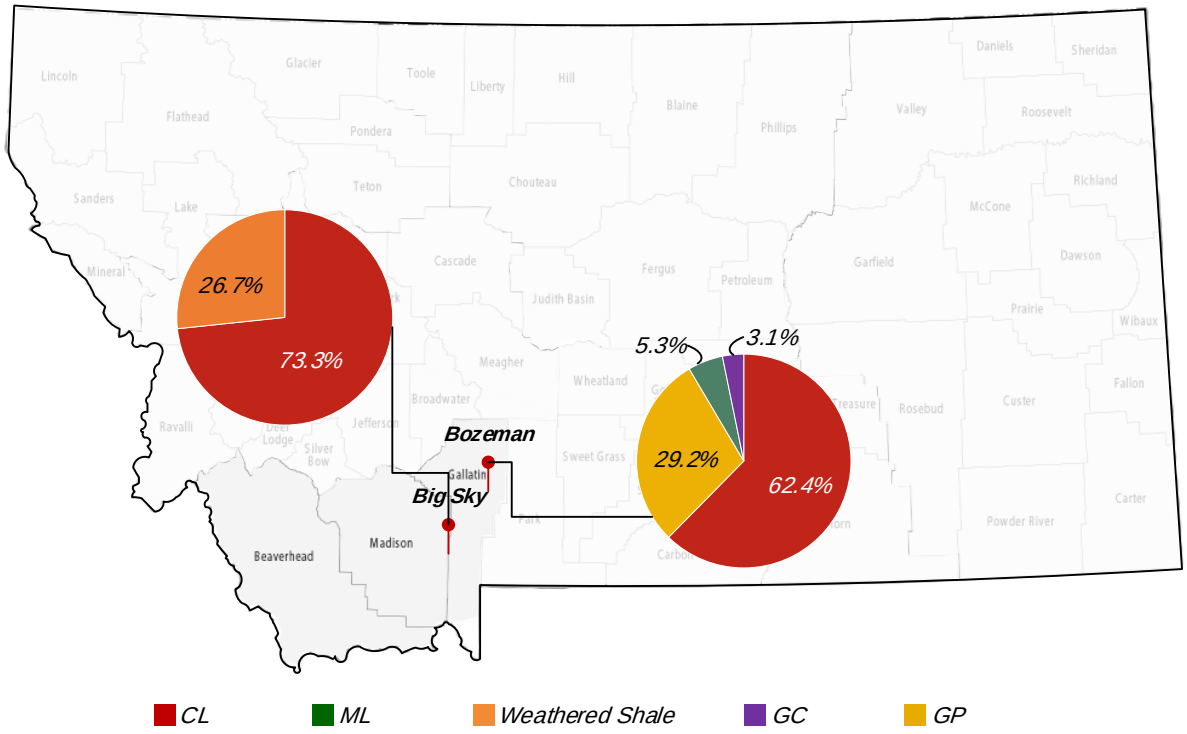

Figure 49. Average soil profiles in the Southwest of Montana

Summary of the soil conditions in Montana

An extensive dataset of 188 geotechnical investigation reports, comprising 352 SPT/CPT soundings, was gathered, and carefully processed to assess the soil conditions in Montana. Although further reports are required for a comprehensive classification of soil types, the available geotechnical investigation reports provide a summary of the soil conditions in Montana, which can be outlined as follows:

- Montana, being a large state, exhibits a wide range of soil types with significant variations observed across its regions.
- The dominant surface layer in Montana is composed of low plasticity lean clay (CL) with varying contents of silt and sand. The CL layer is commonly found to extend down to 20 ft from the ground surface.

- Significant quantities of low plasticity silts (ML), and silt contents in gravelly, clayey, and sandy soils have been frequently observed in the West and South regions of Montana. A plasticity index (PI-value) of 5 has been reported for the ML layers in Livingston, Missoula, and Kalispell.
- High plasticity clays have been observed mostly on the East side of Montana.
- Deeper layers of the average soil profiles in different regions have been frequently observed to contain gravelly soils with silt and clay contents.
- The depths of the bedrock and the water table showed to be highly variable in different cities.

Summary and Conclusion

Pile foundations that support various structures, such as highway bridges, offshore platforms, marine platforms, and wind turbines, are subjected to both static and cyclic lateral loads, as well as axial loads and overturning moments. Analyzing the behavior of laterally loaded piles is a complex geotechnical engineering problem due to the interactions between the piles and the surrounding soil. This complexity arises from the interdependence of the pile's behavior and the response of the soil.

There are four main categories of methods for the analysis of laterally loaded piles. The first category is the ultimate limit state (ULS) methods, where the soil-pile system is assumed to be at its failure state, and its capacity is derived accordingly. The conventional static approach, as well as the Blum, Brinch-Hansen, and Broms methods, fall under this category. However, these methods have some limitations, including over-conservative designs and the lack of consideration for pile deflections in the working load range.

The second category is the discrete load-transfer approach, commonly known as the p-y curve method. This method is based on Winkler's beam on elastic foundation theory and models the soil medium as a series of discrete linear elastic springs. The p-y curve method incorporates the nonlinear behavior of the soil into the model springs, defining the relationship between pile lateral deflection and soil reaction at different depths below the ground surface. Various methods are used to develop p-y curves in different soil types, including full-scale field tests, model-scale laboratory experiments, in-situ test frameworks, and continuum-based approaches.

Full-scale field tests on instrumented piles are the most accurate method for developing site-specific p-y curves. However, they are expensive and time-consuming. Model-scale tests and in-situ tests, such as cone penetration tests and pressuremeter tests, offer faster and more economical alternatives to develop p-y curves. Three-dimensional numerical methods, like finite element and finite difference analysis, are also used to model the complex behavior of laterally loaded piles, but they are computationally expensive and may not be suitable for practical engineering applications.

In Chapter 4, the soil conditions in Montana are discussed. The Montana group was formed from sediments deposited in the Cretaceous Sea during the Cretaceous era. The region received significant amounts of clastic and pyroclastic volcanic materials from the Elkhorn Mountains volcanics along its western shores. Glacial Lake Missoula in the Missoula area was repeatedly formed and drained during the last glaciation, depositing glaciolacustrine silt and clay in lake-bottom locations.

Over 180 geotechnical investigation reports were reviewed to identify soil type variations across Montana. The data set included more than 350 SPT/CPT soundings from 15 different counties. The state was divided into six regions based on the quantity of data points and soil type variations. Various soil types were encountered, including lean clay, low and high plasticity silts, gravelly soils, silty and clayey sands, and high plasticity clay. The most common surface layer was low

plasticity clay with some sand and silt content. Low plasticity silty soils with a PI-value equal to 5 were commonly found in the South and West regions. Silty and clayey sands were mostly present in middle layers, while poorly graded gravel with clay and silt contents was common at greater depths. High plasticity clay was observed only on the East side of Montana. Due to the high variation of soil types, further geotechnical investigations are needed for a comprehensive understanding of soil conditions in Montana.

References

Achmus, M., Abdel-Rahman, K., & Peralta, P. (2005). On the design of monopile foundations with respect to static and quasi-static cyclic loading. *European Wind Energy Association: Brussels, Belgium*.

Anderson, J., Townsend, F., & Grajales, B. (2003). Case history evaluation of laterally loaded piles. *Journal of geotechnical and geoenvironmental engineering*, *129*(3), 187-196.

API (2011). Geotechnical and foundation design considerations, API Washington, DC.

Ariannia, S. S. (2015). *Determination of py Curves by Direct Use of Cone Penetration Test (CPT) Data*. University of California, Los Angeles.

Ashour, M., Norris, G., & Pilling, P. (1998). Lateral loading of a pile in layered soil using the strain wedge model. *Journal of geotechnical and geoenvironmental engineering*, *124*(4), 303-315.

Bandyopadhyay, S. (1983). *Geotechnical evaluation of loessial soils in Kansas*.

Banerjee, P., & Davies, T. (1978). The behaviour of axially and laterally loaded single piles embedded in nonhomogeneous soils. *Geotechnique*, *28*(3), 309-326.

Barton, Y., Finn, W., Parry, R., & Towhata, I. (1983). Lateral pile response and py curves from centrifuge tests. Offshore Technology Conference,

Basu, D., Salgado, R., & Prezzi, M. (2009). A continuum-based model for analysis of laterally loaded piles in layered soils. *Geotechnique*, *59*(2), 127-140.

Blum, H. (1932). *Wirtschaftliche dalbenformen und deren berechnung*. Verlag nicht ermittelbar.

Brandenberg, S. J., Boulanger, R. W., Kutter, B. L., & Chang, D. (2005). Behavior of pile foundations in laterally spreading ground during centrifuge tests. *Journal of geotechnical and geoenvironmental engineering*, *131*(11), 1378-1391.

Brandenberg, S. J., Zhao, M., Boulanger, R. W., & Wilson, D. W. (2013). p-y plasticity model for nonlinear dynamic analysis of piles in liquefiable soil. *Journal of geotechnical and geoenvironmental engineering*, *139*(8), 1262-1274.

Brant, L., & Ling, H. I. (2007). Centrifuge modeling of piles subjected to lateral loads. Soil Stress-Strain Behavior: Measurement, Modeling and Analysis: A Collection of Papers of the Geotechnical Symposium in Rome, March 16–17, 2006,

Breckenridge, R. M. (1989). Lower glacial lakes Missoula and Clark Fork ice dams. *Glacial Lake Missoula and the Channeled Scabland Missoula, Montana to Portland, Oregon, July 20–26, 1989*, *310*, 13-21.

Briaud, J. L., Smith, T., & Meyer, B. (1983). Using the pressuremeter curve to design laterally loaded piles. Offshore Technology Conference,

Broms, B. B. (1964a). Lateral resistance of piles in cohesionless soils. *Journal of the soil mechanics and foundations division*, *90*(3), 123-156.

Broms, B. B. (1964b). Lateral resistance of piles in cohesive soils. *Journal of the soil mechanics and foundations division*, *90*(2), 27-63.

Brown, D. A., & Shie, C.-F. (1990). Three dimensional finite element model of laterally loaded piles. *Computers and Geotechnics*, *10*(1), 59-79.

Brown, D. A., SHIE, C.-F., & KUMAR, M. (1989). Py curves for laterally loaded piles derived from three-dimensional finite element model. International symposium on numerical models in geomechanics. 3 (NUMOG III),

Budhu, M., & Davies, T. G. (1988). Analysis of laterally loaded piles in soft clays. *Journal of Geotechnical Engineering*, *114*(1), 21-39.

Choo, Y. W., & Kim, D. (2016). Experimental development of the p-y relationship for large-diameter offshore monopiles in sands: Centrifuge tests. *Journal of geotechnical and geoenvironmental engineering*, *142*(1), 04015058.

Choobbasti, A. J., & Zahmatkesh, A. (2016). Computation of degradation factors of py curves in liquefiable soils for analysis of piles using three-dimensional finite-element model. *Soil Dynamics and Earthquake Engineering*, *89*, 61-74.

Coyle, H. M., & Reese, L. C. (1966). Load transfer for axially loaded piles in clay. *Journal of the soil mechanics and foundations division*, *92*(2), 1-26.

Dyson, G., & Randolph, M. (2001). Monotonic lateral loading of piles in calcareous sand. *Journal of geotechnical and geoenvironmental engineering*, *127*(4), 346-352.

EVANS JR, L. T. (1982). *Simplified analysis of laterally loaded piles*. University of California, Berkeley.

Georgiadis, M. (1983). Development of py curves for layered soils. Geotechnical practice in offshore engineering,

Ghayoomi, M., Ghadirianniari, S., Khosravi, A., & Mirshekari, M. (2018). Seismic behavior of pile-supported systems in unsaturated sand. *Soil Dynamics and Earthquake Engineering*, *112*, 162-173.

Gill, J., Cobban, W., & Kier, P. (1966). The Red Bird section of the Upper Cretaceous Pierre Shale in Wyoming, with a section on a new echinoid from the Cretaceous Pierre Shale of eastern Wyoming (No. 393-A). *A1–A73*.

Gill, J. R., & Cobban, W. A. (1973). *Stratigraphy and geologic history of the Montana Group and equivalent rocks, Montana, Wyoming, and North and South Dakota* (Vol. 776). US Government Printing Office.

Gilluly, J. (1963). The tectonic evolution of the western United States: Seventeenth William Smith lecture. *Quarterly Journal of the Geological Society*, *119*(1-4), 133-174.

González, L., Abdoun, T., & Dobry, R. (2009). Effect of soil permeability on centrifuge modeling of pile response to lateral spreading. *Journal of geotechnical and geoenvironmental engineering*, *135*(1), 62-73.

Gupta, B. K., & Basu, D. (2020). Computationally efficient three-dimensional continuum-based model for nonlinear analysis of laterally loaded piles. *Journal of Engineering Mechanics*, *146*(2), 04019117.

Haiderali, A., Cilingir, U., & Madabhushi, G. (2013). Lateral and axial capacity of monopiles for offshore wind turbines. *Indian Geotechnical Journal*, *43*, 181-194.

Hansen, J. B. (1961). The ultimate resistance of rigid piles against transversal forces. *Bulletin 12, Danish Geotech. Institute*, 1-9.

Hanson, M. A., Lian, O. B., & Clague, J. J. (2012). The sequence and timing of large late Pleistocene floods from glacial Lake Missoula. *Quaternary Science Reviews*, *31*, 67-81.

Hanssen, S. (2015). Small strain overlay to the API py curves for sand. Frontiers in Offshore Geotechnics III: Proceedings of the 3rd International Symposium on Frontiers in Offshore Geotechnics (ISFOG 2015),

Haouari, H., & Bouafia, A. (2020). A centrifuge modelling and finite element analysis of laterally loaded single piles in sand with focus on p–y curves. *Periodica Polytechnica Civil Engineering*, *64*(4), 1064-1074.

Helmers, M. J. (1997). *Use of ultimate load theories for design of drilled shaft sound wall foundations* Virginia Tech].

Isenhower, W., et al. (2019). LPILE v2019 user's manual: a program for the analysis of deep foundations under lateral loading, Austin, TX, USA: Ensoft Inc.

Ismael, N. F. (1990). Behavior of laterally loaded bored piles in cemented sands. *Journal of Geotechnical Engineering*, *116*(11), 1678-1699.

Janbu, N. (1963). Soil compressibility as determined by oedometer and triaxial tests. Proc. European Conf. SMFE, Wiesbaden, 1963,

Johnson, R. (2006). *Soil characterization and py curve development for loess* University of Kansas].

Klinkvort, R. T., Leth, C. T., & Hededal, O. (2010). Centrifuge modelling of a laterally cyclic loaded pile. *Physical Modelling in Geotechnics*, *7*, 959-964.

Langton, C. M. (1935). Geology of the northeastern part of the Idaho batholith and adjacent region in Montana. *The Journal of Geology*, *43*(1), 27-60.

Lee, M., Bae, K.-T., Lee, I.-W., & Yoo, M. (2019). Cyclic py curves of monopiles in dense dry sand using centrifuge model tests. *Applied Sciences*, *9*(8), 1641.

Li, H., Liu, S., Tong, L., Wang, K., & Ha, S. (2018). Estimating p-y Curves for Clays by CPTU Method: Framework and Empirical Study. *International Journal of Geomechanics*, *18*(12), 04018165.

Liang, R., Yang, K., & Nusairat, J. (2009). p-y Criterion for Rock Mass. *Journal of geotechnical and geoenvironmental engineering*, *135*(1), 26-36.

Matlock, H. (1970). Correlation for design of laterally loaded piles in soft clay. Offshore technology conference,

McClelland, B., & Focht, J. (1956). Soil modulus for laterally loaded piles. *Journal of the soil mechanics and foundations division*, *82*(4), 1081-1081-1081-1022.

McKenna, F., Scott, M. H., & Fenves, G. L. (2010). Nonlinear finite-element analysis software architecture using object composition. *Journal of Computing in Civil Engineering*, *24*(1), 95-107.

Mindlin, R. D. (1936). Force at a point in the interior of a semi-infinite solid. *physics*, *7*(5), 195-202.

Mokwa, R. L., Duncan, J. M., & Helmers, M. J. (2000). Development of py curves for partly saturated silts and clays. In *New Technological and Design Developments in Deep Foundations* (pp. 224-239).

Ng, C. W., & Zhang, L. M. (2001). Three-dimensional analysis of performance of laterally loaded sleeved piles in sloping ground. *Journal of geotechnical and geoenvironmental engineering*, *127*(6), 499-509.

Norris, G. (1986). Theoretically based BEF laterally loaded pile analysis. Proceedings of the 3rd international conference on numerical methods in offshore piling,

O'Neill, M. W., & Murchison, J. M. (1983). *An evaluation of py relationships in sands*. University of Houston.

O'Neill, M., & Gazioglu, S. (1984). Evaluation of p–y relationships in cohesive soils. *Proceedings of a Analysis and Design of Pile Foundations, ASCE Geotechnical Engineering Division*, 192-213.

Pardee, J. T. (1910). The glacial lake Missoula. *The Journal of Geology*, *18*(4), 376-386.

Peck, R., Hanson, W., & Thornburn, T. (1974). Foundation Engineering‖ John Wiley & Sons. *Inc, New York*.

Poulos, H. G., & Davis, E. H. (1980). *Pile foundation analysis and design* (Vol. 397). Wiley New York.

Price, A. B. (2018). *Cyclic strength and cone penetration resistance for mixtures of silica silt and kaolin*. University of California, Davis.

Randolph, M. F. (1981). The response of flexible piles to lateral loading. *Geotechnique*, *31*(2), 247-259.

Reese, L. C. (1997). Analysis of laterally loaded piles in weak rock. *Journal of geotechnical and geoenvironmental engineering*, *123*(11), 1010-1017.

Reese, L. C., Cox, W. R., & Koop, F. D. (1974). Analysis of laterally loaded piles in sand. Offshore Technology Conference,

Reese, L. C., Cox, W. R., & Koop, F. D. (1975). Field testing and analysis of laterally loaded piles om stiff clay. Offshore technology conference,

Reese, L. C., Isenhower, W. M., & Wang, S.-T. (2005). *Analysis and design of shallow and deep foundations* (Vol. 10). John Wiley & Sons.

Reese, L. C., & Welch, R. C. (1975). Lateral loading of deep foundations in stiff clay. *Journal of the Geotechnical engineering division*, *101*(7), 633-649.

Robertson, P., Campanella, R., Brown, P., Grof, I., & Hughes, J. (1985). Design of axially and laterally loaded piles using in situ tests: A case history. *Canadian Geotechnical Journal*, *22*(4), 518-527.

Robertson, P. K., & Campanella, R. (1983). Interpretation of cone penetration tests. Part I: Sand. *Canadian Geotechnical Journal*, *20*(4), 718-733.

Robertson, P. K., Davies, M. P., & Campanella, R. G. (1989). *Design of laterally loaded driven piles using the flat dilatometer*. ASTM International.

Robertson, P. K., Hughes, J. M., Campanella, R. G., Brown, P., & McKeown, S. (1985). Design of laterally loaded piles using the pressuremeter. The pressuremeter and its marine applications: Second International Symposium,

Rollins, K. M., Hales, L. J., Ashford, S. A., & Camp, I., William M. (2006). PY curves for large diameter shafts in liquefied sand from blast liquefaction tests. In *Seismic Performance and Simulation of Pile Foundations in Liquefied and Laterally Spreading Ground* (pp. 11-23).

Ruigrok, J. (2010). Laterally loaded piles, models and measurements.

Seed, R. and L. Harder Jr (1990). SPT-based Analysis of Cyclic Pore Pressure Generation and Undrained Residual Strength": Proc., HB Seed Memorial Symp., Vol. 2, BiTech Publishing, Vancouver, BC, Canada.

Smith, L. N. (2006). Stratigraphic evidence for multiple drainings of glacial Lake Missoula along the Clark Fork River, Montana, USA. *Quaternary Research*, *66*(2), 311-322.

Tak Kim, B., Kim, N.-K., Jin Lee, W., & Su Kim, Y. (2004). Experimental load–transfer curves of laterally loaded piles in Nak-Dong River sand. *Journal of geotechnical and geoenvironmental engineering*, *130*(4), 416-425.

Terzaghi, K. (1955). Evalution of conefficients of subgrade reaction. *Geotechnique*, *5*(4), 297-326.

Terzaghi, K., & Peck, R. B. (1968). *Soil Mechanics in Engineering Practice: 2d Ed*. J. Wiley.

Tokimatsu, K., & Suzuki, H. (2004). Pore water pressure response around pile and its effects on py behavior during soil liquefaction. *Soils and Foundations*, *44*(6), 101-110.

Trochanis, A. M., Bielak, J., & Christiano, P. (1991). Three-dimensional nonlinear study of piles. *Journal of Geotechnical Engineering*, *117*(3), 429-447.

Verruijt, A., & Kooijman, A. (1989). Laterally loaded piles in a layered elastic medium. *Geotechnique*, *39*(1), 39-49.

Welch, R. C. (1972). *Lateral load behavior of drilled shafts*. The University of Texas at Austin.

Wilson, D., Boulanger, R., & Kutter, B. (1997). Soil-pile-superstructure interaction at soft or liquefiable soils sites. *Centrifuge Data Rep. for CSP2: UCD/CGMDR-97/03, Univ. of California, Davis, CA.*

Wilson, D. W. (1998). *Soil-pile-superstructure interaction in liquefying sand and soft clay* (Vol. 1998). University of California, Davis America.

Winkler, E. (1867). *Die Lehre von der Elasticitaet und Festigkeit: mit besonderer Rücksicht auf ihre Anwendung in der Technik, für polytechnische Schulen, Bauakademien, Ingenieure, Maschinenbauer, Architecten, etc*. H. Dominicus.

Xu, L.-Y., Cai, F., Wang, G.-X., & Ugai, K. (2013). Nonlinear analysis of laterally loaded single piles in sand using modified strain wedge model. *Computers and Geotechnics*, *51*, 60-71.

Yoo, M.-T., Choi, J.-I., Han, J.-T., & Kim, M.-M. (2013). Dynamic py curves for dry sand from centrifuge tests. *Journal of earthquake engineering*, *17*(7), 1082-1102.

Yu, G., Gong, W., Chen, M., Dai, G., & Liu, Y. (2019). Prediction and analysis of behaviour of laterally loaded single piles in improved gravel soil. *International Journal of Civil Engineering*, *17*, 809-822.

Yu, H., Peng, S., & Zhao, Q. (2019). Field tests of the response of single pile subjected to lateral load in gravel soil sloping ground. *Geotechnical and Geological Engineering*, *37*, 2659-2674.

APPENDIX A: Montana Department of Transportation Survey

The purpose of this study is to prioritize soil conditions in Montana for which laterally loaded pile behavior is not well known. This questionnaire asks about the availability of any data (e.g., Cone Penetration Test (CPT)/Standard Penetration Tests (SPT)), and insights on soil types in Montana, common methods of the determination of soil properties/parameters (CPT vs. SPT), preferred design methods for laterally loaded piles, and the availability of full-scale field tests data on laterally loaded piles. If available, a member of the research team from MSU will be sent to MDT to collect available data that would be useful for the study. Your response will be anonymous, and your participation is entirely voluntary. If there are items you do not feel comfortable answering, please skip them. Thank you for your cooperation.

1- Are there any specific soil types that are unique to Montana and require special consideration in construction?

Answer 1: Missoula silts and Milk River silt deposits.

Answer 2: We are primarily interested in glacial lake silts, such as the Glacial Lake Missoula silts of Western Montana. We are also interested in fine grained intermediate geomaterials, such as the Cretaceous and Tertiary shales and claystone of Eastern Montana.

2- Which type of in-situ testing method is more common to determine soil properties/parameters in Montana?

□ Standard Penetration Test (SPT)

□ Cone Penetration Test (CPT)

□ Dilatometer Test (DMT)

□ Pressure Meter Test (PMT)

□ Others (specify):

MDT Response: SPT is the most common method. CPT is used fairly often. PMT has been used on a limited basis.

3- If available, please fill in the following table with the MDT's data on in-situ test results with location, test method, and the number of tests.

No.	*Location*	*Test Method*	*No. of Tests*
1			
2			
3			

4			
5			
6			
7			
8			
9			
10			
11			
12			
13			
14			
15			

MDT Response: Without an exhaustive search this is difficult to determine. This information will be transmitted separately.

4- Are there any challenges or limitations with respect to soil investigation and characterization in Montana?

MDT Response: Montana is a large state with a wide variety of subsurface conditions. Many of our river valleys have dense cobbles and boulders. Other locations have highly plastic, under-consolidated soil. We are limited primarily by the lack of *p-y* curves to accurately model the less common geomaterial types, such as silts and shales.

5- Does MDT have any available data on Seismic Cone Penetration Test (SCPT) and/or Piezocone Penetration Test (CPTu)? If so, please provide the number and the soil type associated with each test.

MDT Response: For SCPT there is no data. For CPTu there is some data.

6- Has there been any encounters with problematic soil, such as swelling soils or collapsible soils, in Montana? If so, please mention the soil type and the data available on it.

MDT Response: Montana is a large and varied state, and the complexity of its geology is well known. Swelling soils, collapsible soils, organic soils, and corrosive soils have all been noted occasionally, though these are not widely distributed at typical deep foundation depths. We anticipate that the two material types mentioned above are sufficiently different from the preprogrammed L-Pile P-y curve parameters to merit closer scrutiny.

7- Please provide an estimate of the breakdown of pile types used in Montana.

MDT Response:

- Driven Piles

  - Steel pipe piles 70%-81%
  - Steel H-piles 10%-25%
  - Timber piles 0-1%
  - Pre-cast concrete piles 0
- Drilled Shafts
  - Cast-in-place concrete piles 5%-9%
- Others (specify) 0

8- What is the MDT's general approach for designing laterally loaded piles?

□ Subgrade Reaction Approach (*p-y* Curve Method, Strain Wedge Method)

□ Ultimate Limit State Approach (Brinch Hansen's Method, Blum Method, Brom's Method)

□ Continuum Method (Boundary Element Method)

□ Others (specify):

MDT Response: We generally apply the *p-y* curve method used in Ensoft's L-Pile program for designing laterally loaded piles. We perform an Ultimate Limit State method as a check for reasonableness.

9- Can you provide us with any documents that summarize the design process of laterally loaded pile foundations in transportation infrastructure projects in Montana?

MDT Response: The operating manual of L-Pile and A-Pile would be the best guide for our design process. Also, the AASHTO design guide would be the other source. Also, MDT Geotechnical Manual is available here: https://www.mdt.mt.gov/publications/manuals.aspx. Lateral loading is discussed on 16.4.2.13. We follow the latest LRFD guidance from FHWA.

10- What is MDT's preferred p-y curve for each soil type?

Soil Type	*Method*
Clay	
Non-plastic intermediate soil (Silt)	
Gravel	
Sand	
Low-plasticity intermediate soil (Silt with small amounts of clay)	
Layered soil	

MDT Response: In general, the *p-y* methods are divided into two soil types. Sand or clay, whichever is the dominate grain size gradation. The entire soil layer is lumped into that dominate soil type. Furthermore, Clays and silts are treated as clays. Thinly layered soils are treated as clays, thicker layers (>1-3') are treated as separate layers. Gravels and sands are treated as sands.

11- What is the most common pile-head connection type in Montana transportation infrastructures?

□ Fixed Headed

□ Free Headed

□ Both options are common

MDT Response: Both options are common.

12- How does MDT verify and validate the design of a laterally loaded pile prior to construction?

MDT Response: A PDA is used for the axial load and no direct method is used to verify the lateral load capabilities. In one instance, a full-scale instrumented test pile was laterally loaded prior to construction, to verify a design. Instrumented test piles have been loaded axially on several occasions, including drilled shafts with Osterberg cells. Generally, we rely on hand calculated checks of L-Pile prior to construction.

13- How does MDT account for uncertainties or variations in soil properties when designing laterally loaded piles?

MDT Response: By over designing the piles. We change load and resistance factors to achieve to a more conservative design. This conservatism increases the expense of the design, which is what we hope to optimize by using more appropriate *p-y* curve.